

# DRAFT

## TURBINE ROTOR MATERIAL DESIGN PHASE II

FINAL REPORT  
SwRI<sup>®</sup> Project No. 18.2676

*Prepared by*

Southwest Research Institute  
GE Aircraft Engines  
Honeywell  
Pratt & Whitney  
Rolls-Royce Corporation

*Prepared for*

Federal Aviation Administration  
Grant No. 99-G-016

November 2005



**SOUTHWEST RESEARCH INSTITUTE<sup>®</sup>**  
SAN ANTONIO                      HOUSTON                      WASHINGTON, DC

# **TURBINE ROTOR MATERIAL DESIGN PHASE II**

**FINAL REPORT  
SwRI<sup>®</sup> Project No. 18.2676**

*Prepared by*

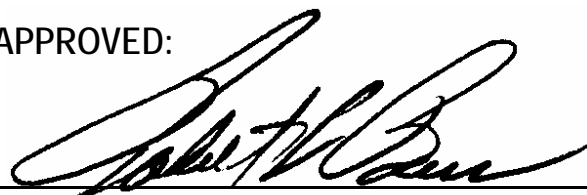
**Southwest Research Institute  
GE Aircraft Engines  
Honeywell  
Pratt & Whitney  
Rolls-Royce Corporation**

*Prepared for*

**Federal Aviation Administration  
Grant No. 99-G-016**

**November 2005**

APPROVED:



---

**Dr. Robert L. Bass III  
Vice President, Mechanical and Materials Engineering Division**

**DOT/FAA/AR-xx/xx**

Office of Aviation Research  
Washington, D.C. 20591

# **Turbine Rotor Material Design - Phase II**

November 2005

Final Report

This document is available to the public through the National  
Technical Information Service (NTIS), Springfield, Virginia 22161.



U.S. Department of Transportation  
**Federal Aviation Administration**

## **NOTICE**

This document is disseminated under the sponsorship of the U.S. Department of Transportation in the interest of information exchange. The United States Government assumes no liability for the contents or use thereof. The United States Government does not endorse products or manufacturers. Trade or manufacturer's names appear herein solely because they are considered essential to the objective of this report. This document does not constitute FAA certification policy. Consult your local FAA aircraft certification office as to its use.

This report is available at the Federal Aviation Administration William J. Hughes Technical Center's Full-Text Technical Reports page: [actlibrary.tc.faa.gov](http://actlibrary.tc.faa.gov) in Adobe Acrobat portable document format (PDF).

1. Report No. DOT/FAA/(AR)-xx/xx		2. Government Accession No.		3. Recipient's Catalog No.	
4. Title and Subtitle TURBINE ROTOR MATERIAL DESIGN—PHASE II				5. Report Date November 2005	
				6. Performing Organization Code	
7. Author(s) R. C. McClung*      Y.-D. Lee*      J. A. Tschopp <sup>†</sup> S. K. Srivatsa <sup>†</sup> G. R. Leverant*      C. J. Waldhart*      M. A. Jameel <sup>††</sup> M. P. Enright*      H. R. Millwater**      D. J. Lehmann <sup>†††</sup> L. Huyse*      S. H. K. Fitch***      J. P. Dubke <sup>††††</sup>				8. Performing Organization Report No. 18-2676	
9. Performing Organization Name and Address * Southwest Research Institute <sup>®</sup> 6220 Culebra Road San Antonio, TX 78238  ** University of Texas at San Antonio 6900 North Loop 1604 West San Antonio, TX 78249  *** Mustard Seed Software 1634 Brandywine Drive Charlottesville, VA 22901				10. Work Unit No. (TRAIS)	
				† GE Aircraft Engines 1 Neumann Way Cincinnati, OH 45215	
				†† Honeywell 111 South 34 <sup>th</sup> Street Phoenix, AZ 85072	
				††† Pratt & Whitney 400 Main Street East Hartford, CT 06108	
				†††† Rolls-Royce Corporation 2001 South Tibbs Avenue Indianapolis, IN 46241	
12. Sponsoring Agency Name and Address U.S. Department of Transportation Federal Aviation Administration Office of Aviation Research Washington, DC 20591				13. Type of Report and Period Covered Final Report	
				14. Sponsoring Agency Code ANE-110	
15. Supplementary Notes The FAA William J. Hughes Technical Center Technical Monitor was Joseph Wilson.					
16. Abstract The aircraft engine industry is working with the FAA to develop an enhanced life management process, based on probabilistic damage tolerance principles, to address the threat of material or manufacturing anomalies in high-energy rotating components, and the process is documented in current and planned versions of FAA Advisory Circular (AC) 33.14. An integrated team of Southwest Research Institute, GE Aircraft Engines, Pratt & Whitney, Honeywell, and Rolls-Royce Corporation has developed enhanced predictive tool capability and supplementary material/anomaly behavior characterization and modeling to support and enhance the process and the AC. Sensitivity studies were performed to guide a planned update of the hard alpha (HA) anomaly distributions. A computer code was developed to describe the diffusion of nitrogen or oxygen in titanium from an inclusion during melting and heat treatment. A DEFORM <sup>TM</sup> forging microcode was validated experimentally and used to study cracking of HA anomalies during forging. Ultrasonic inspection methods were evaluated at billet and forging stages. The influence of elevated oxygen on Ti-17 was evaluated with tensile and fatigue tests. Spin pit and coupon experiments were conducted to study the fatigue behavior of embedded HA. Vacuum fatigue crack growth (FCG) data were generated for three nickel alloys and Ti-6242. Thermo-mechanical FCG behavior was studied in IN-718. A literature survey was conducted on the stability and significance of surface residual stresses in fatigue. New DARWIN <sup>®</sup> versions were developed to address anomalies associated with surface damage in 3D components and different types of inherent anomalies (including large numbers of 3D anomalies and non-negligible crack formation lives). Enhancements in probabilistic methods and many other new DARWIN capabilities were developed to improve the overall efficiency and accuracy of the risk assessment computations. The partner engine companies verified the accuracy and usability of DARWIN. A three-day DARWIN training workshop was conducted. An infrastructure was developed to support code licensing and distribution for users employing DARWIN for official FAA and company purposes.					
17. Key Words Aircraft Gas Turbine Engines, Disks, Rotors, Low Cycle Fatigue, Crack Growth, Probabilistic Damage Tolerance, Risk Assessment, Forging, Non-Destructive Evaluation, Titanium Hard Alpha			18. Distribution Statement		
19. Security Classif. (of this report) Unclassified		20. Security Classif. (of this page) Unclassified		21. No. of Pages 621	22. Price

## ACKNOWLEDGEMENTS

Successful completion of this large, multidisciplinary research project would not have been possible without the significant contributions and assistance of many different people. Some are named as authors on this report, and many others deserve special mention.

Special appreciation is extended to the Federal Aviation Administration (FAA) employees and consultants who provided sustained support, encouragement, and guidance throughout the program. Heartfelt thanks goes to Tim Mouzakis of the Engine and Propeller Directorate in the New England Regional Office, Bruce Fenton (now retired) and Joe Wilson of the William J. Hughes Technical Center, and FAA Consultants Jon Bartos and Nick Provenzano.

The entire program was motivated and guided by the Rotor Integrity Sub-Committee (RISC) of the Aerospace Industries Association (AIA), capably led by chairman Bill Knowles of Honeywell Engines, Systems, and Services.

Direct leadership was provided by the industry Steering Committee comprising representatives from the four partner companies: GE Aircraft Engines (GEAE), Honeywell, Pratt & Whitney (P&W), and Rolls-Royce Corp (RRC). Current members are chair Darryl Lehmann (P&W), Jon Tschopp (GEAE), Ahsan Jameel (Honeywell), and Jon Dubke (RRC). Previous members during the term of this program include Nichola Howard and Gary Mihlbachler (GEAE)—both former chairs, Sandeep Muju (Honeywell), and Geoff Ward and Doug Herrmann, both from RRC.

Jon Tschopp (GEAE) provided leadership on the hard alpha anomaly distribution task (§2.1 and Appendix A), and Masamichi Hongoh (P&W) performed some supporting sensitivity studies.

Tony Giamei (United Technologies Research Center / Belcan) and Ernesto Gutierrez-Miravete (Rensselaer Polytechnic Institute) developed the GROW code and completed code validation testing (§2.2 and Appendix B). Masamichi Hongoh (P&W) prepared the GROW code development plan and provided code testing.

Shesh Srivatsa (GEAE) led the modeling of hard alpha deformation during forging, including validation of the DEFORM™ microcode (§3.1 and Appendix C) and investigation of strain to cause cracking (§3.3 and Appendix F). Jon Bartos (now retired) and Andy Woodfield (both GEAE) led the supporting metallography effort, and Mike Keller (GEAE) conducted the seeded forging UT inspections (§3.2 and Appendix E).

John Schirra (P&W) contributed to the validation work on DEFORM for bulk residual stresses (§3.4).

Andy Woodfield (GEAE) led the investigation of elevated oxygen effects on titanium alloys (§4.1 and Appendix G).

Peter McKeighan (SwRI) led the fatigue testing of coupon specimens from the seeded forgings (§4.2 and Appendix H).

Peter Laz (formerly of SwRI) performed the analytical investigations of potential thermal residual stress effects on fatigue crack formation and growth from synthetic hard alpha seeds (§4.3 and Appendix I).

Darryl Lehmann (P&W) provided leadership for the spin tests of titanium disks with hard alpha inclusions (§4.4 and Appendix J). Paul Wawrzonek (Test Devices Inc.) conducted the spin tests, Jeff Umbach, Dave Raulerson, and Karl Gruca (P&W) completed UT inspections of the spin disks, and Hongyang Bao (P&W) led the fractographic assessments. Brent Barber (P&W) conducted vacuum crack growth testing of the Ti 6-4 spin disk material. Umbach, Raulerson, and Gruca also performed UT inspections of material containing nickel anomalies (§4.6 and Appendix L).

Yancy Gill, Dennis Chamblee, Jim Hartman, and Sandeep Muju (Honeywell) performed and evaluated vacuum fatigue crack growth tests (§4.5 and Appendix K), along with Barney Lawless at GEAE. Jack Telesman (NASA Glenn Research Center) is thanked for providing U720 specimen material and corresponding air fatigue crack growth data.

Barney Lawless (GEAE) conducted the IN718 thermomechanical fatigue crack growth test program (§4.7 and Appendix M), and Bob VanStone (GEAE) provided testing support.

Yi-Der Lee (SwRI) developed the Flight\_Life fracture mechanics module and all corresponding stress intensity factor solutions (§4.8 and Appendix N), with additional guidance from Craig McClung and Graham Chell (both SwRI). SwRI student employees Nairan Normand and Paul Green provided assistance with the generation of FADD-3D reference solutions to support new weight function K solutions.

Craig McClung (SwRI) performed the literature survey of the stability and significance of residual stresses in fatigue (§4.9 and Appendix O).

DARWIN development (§5 and Appendices P, Q, R, S, T, U, and V) during TRMD-II was led first by Harry Millwater (formerly at SwRI) and then by Mike Enright (SwRI), with substantial support from Luc Huyse (SwRI). Chris Waldhart (SwRI) led DARWIN testing and validation activities, and SwRI student employees Hector Flores, Jeff Magnusson, and David Anderson provided assistance with these activities. Simeon Fitch (Mustard Seed Software) performed all graphical user interface development for DARWIN.

Harry Millwater and his students provided additional DARWIN support in his current position at the University of Texas at San Antonio (UTSA): student Faiyazmehadi Momin developed a link between finite element software and DARWIN such that additional random variables can be considered, and Wes Osborn developed and verified probabilistic sensitivity equations (Appendix T) for implementation into DARWIN. University of Texas at Austin student Sridhar Guduru developed a PERL language-based Darwin verification program called SCOUT.

Paul Roth (GEAE) provided guidance on the reliability analysis of materials with multiple anomalies (Appendix P). Michael Gorelik and Dan Greving (both Honeywell) reviewed probabilistic methodologies.

Steve Schrantz (GEAE) provided additional DARWIN code development support.

The partner companies provided extensive evaluation and testing of new DARWIN releases throughout the program. Ting-Chieh Chang was the GEAE lead, and Darryl Lehmann was the P&W lead. Doug Hermann, Geoff Ward, and Jon Dubke performed validation studies at RRC. Eddie Perez-Ruberte, Kim Kington, Waled Hassan, Harry Kington, Dan Greving, Sandeep Muju, and Ahsan Jameel were DARWIN evaluators at Honeywell.

Mike Enright (SwRI) managed the development and presentation of the DARWIN short course (§6.2), and also managed the DARWIN industrialization activities (§7). SwRI student employee Hector Flores developed the interactive video tutorial of the DARWIN GUI.

Birdie Matthews (SwRI) provided superlative clerical assistance in preparing this large final report, and Patty Soriano and Roxanne Kerr (both SwRI) provided significant clerical support throughout the program. Gerry Leverant is thanked for his careful peer review of the final report.

Gerry Leverant served as the TRMD-II program manager and principal investigator at SwRI from the beginning of the program in March 1999 through his retirement in February 2003, and Craig McClung filled those roles for the remaining months of the program.

## TABLE OF CONTENTS

	Page
EXECUTIVE SUMMARY	xvii
1. INTRODUCTION	1-1
1.1 Background	1-1
1.2 Organization of Research	1-2
1.3 Industry Vision	1-3
2. ANOMALY DISTRIBUTIONS	2-1
2.1 Titanium Hard Alpha Anomaly Distribution Updates	2-1
2.2 Definition of Stealth Anomalies	2-3
2.2.1 GROW Code Development	2-3
2.2.2 Studies on Stealth Anomaly Region and Triple Melt Processing	2-4
2.2.3 Conclusions	2-5
3. EFFECT OF FORGING ON ANOMALY MORPHOLOGY AND BULK RESIDUAL STRESSES	3-1
3.1 Validation of DEFORM™ Microcode	3-1
3.1.1 Seed Polishing Procedure	3-1
3.1.2 Microcode Validation	3-2
3.1.3 Regression Analysis	3-5
3.1.4 Validation of the Regression Equations	3-5
3.1.5 Comparison of Direct and Regression Approaches	3-8
3.2 Ultrasonic Inspection of Forgings	3-8
3.2.1 Documentation of Previous Inspections	3-8
3.2.2 New Inspection Results	3-9
3.3 Processing Conditions Needed to Crack Hard Alpha Anomalies	3-11
3.3.1 Strain to Crack Hard Alpha	3-11
3.3.2 Cracking Strain vs. Forging Strain	3-12
3.3.3 Cracking During Billet Conversion and Component Forging	3-14
3.3.4 Anomaly Orientation	3-14
3.4 Monitor Development of SFTC Code for Bulk Residual Stress	3-15

## TABLE OF CONTENTS (cont.)

		Page
4.	CRACK NUCLEATION AND GROWTH DATA AND MONITORING	4-1
4.1	Mechanical Properties of Titanium with Elevated Oxygen	4-1
4.2	Fatigue Testing of Forged Coupons with Hard Alpha Anomalies	4-3
	4.2.1 Material and Procedures	4-4
	4.2.2 Results and Analysis	4-4
4.3	Residual Stresses Associated with Hard Alpha	4-6
	4.3.1 Review of Experimental Results from TRMD-I	4-7
	4.3.2 Measurement of Thermal Expansion Coefficient	4-7
	4.3.3 Analysis of Residual Stresses In and Around HA Defects	4-7
	4.3.4 Fracture Strength Modeling	4-8
	4.3.5 Fatigue Modeling	4-8
4.4	Spin Pit Tests of Titanium Rotors Containing HA Anomalies	4-9
	4.4.1 Pre-Test Analysis	4-9
	4.4.2 Test Setup and Test Plan	4-9
	4.4.3 Test Results	4-10
4.5	Vacuum Fatigue Crack Growth Testing	4-12
	4.5.1 Materials and Test Procedures	4-13
	4.5.2 Results	4-13
4.6	Nickel Anomaly Fatigue Testing	4-16
	4.6.1 Additional UT Inspection of Inco718 Mults	4-17
	4.6.2 UT Inspection of Inco718 Forgings	4-18
4.7	Thermo-Mechanical Fatigue Crack Growth Testing	4-19
4.8	Enhancement of Flight_Life Module	4-21
	4.8.1 Stress Intensity Factor Solutions	4-21
	4.8.2 Other Flight_Life Enhancements	4-25
4.9	Stability and Significance of Residual Stresses in Fatigue	4-25
	4.9.1 Literature Survey	4-26
	4.9.2 Observations and Conclusions	4-27

## TABLE OF CONTENTS (cont.)

		Page
5.	PROBABILISTIC INTEGRATION DESIGN CODE AND DEVELOPMENT	5-1
5.1	Enhancement of DARWIN for Surface Anomalies	5-1
	5.1.1 User Specified Surface Damage (1D Analysis)	5-2
	5.1.2 3D Finite Element-Based Surface Damage (3D Analysis)	5-2
5.2	Enhancement of DARWIN for General Inherent Anomalies	5-3
	5.2.1 Probabilistic Approach	5-3
	5.2.2 Adaptive Optimal Sampling Methodology	5-3
	5.2.3 User-Supplied Crack Formation Module	5-4
	5.2.4 3D Anomalies	5-4
5.3	General DARWIN Enhancements	5-5
	5.3.1 Probabilistic Methods	5-5
	5.3.2 Zone Discretization	5-6
	5.3.3 Inspection	5-8
	5.3.4 Mission Mixing	5-9
	5.3.5 Stress Conversion	5-9
	5.3.6 Stress Processing Enhancements	5-10
	5.3.7 Data Management Enhancements	5-10
	5.3.8 PC/Linux Versions of DARWIN	5-11
	5.3.9 Parallel Processing Capability	5-11
	5.3.10 Influence of Finite Element-Based Random Variables	5-11
5.4	Graphical User Interface (GUI)	5-11
	5.4.1 Visualization and Polynomial Fitting of Stress Gradients	5-12
	5.4.2 Report Generation	5-12
	5.4.3 GUI Directed Execution of Risk Assessment Code	5-12
	5.4.4 Additional Enhancements	5-13
5.5	DARWIN Electronic Help System	5-15
5.6	OEM Evaluation of Darwin	5-16
	5.6.1 Quantitative Verification	5-16
	5.6.2 Qualitative Evaluation	5-19
	5.6.3 OEM Review Comments	5-19

## TABLE OF CONTENTS (cont.)

	Page
6. TECHNOLOGY TRANSFER	6-1
6.1 Progress Reports and Review Meetings	6-1
6.2 DARWIN Training Workshops	6-1
6.3 Conference Presentations and Journal Articles	6-2
6.4 Technology Transfer to Other Government Agencies	6-3
7. INDUSTRIALIZATION OF DARWIN SOFTWARE	7-1
7.1 Automated Software Verification	7-1
7.2 Software Revision Management	7-1
7.3 Internet Distribution of DARWIN	7-2
7.3.1 Internet Distribution of Software	7-2
7.3.2 Electronic Distribution of Manuals	7-2
7.3.3 Resources for New Users	7-2
7.4 User Support	7-2
7.4.1 Live User Support	7-3
7.4.2 Video Tutorials	7-3
7.4.3 Automated Bug Tracking Software	7-3
7.5 Software Licensing	7-3
7.5.1 Software License Agreement	7-3
7.5.2 Registered Trademark	7-3
7.5.3 Commercial Licensing Activity	7-4
8. SUMMARY AND CONCLUSIONS	8-1
9. REFERENCES	9-1

## TABLE OF CONTENTS (cont.)

### APPENDICES

- A—Supporting Studies for Titanium Hard Alpha Anomaly Distribution Updates
- B—GROW Code Development, Validation, and Parametric Studies
- C—Validation of DEFORM™ Microcode
- D—Summary of Engine Company Inspection Results for Seeded and CBS Mults, Pancakes, and Disk Forgings from TRMD Phase I Program
- E—Ultrasonic Inspection of Forgings
- F—Deformation Strain Needed to Crack Hard Alpha Anomalies
- G—Sensitivity of Ti-17 to an Oxygen-Stabilized Hard Alpha
- H—Fatigue Testing of Forged Coupons with Embedded Hard Alpha Anomalies
- I—Effects of Residual Stresses Caused by Differential Thermal Expansion In and Around Hard Alpha Particles in Titanium Alloys
- J—Spin Pit Tests of Titanium Rotors Containing Natural and Seeded HA Anomalies
- K—Vacuum Fatigue Crack Growth Testing
- L—Inspection of Nickel Anomalies
- M—Thermo-Mechanical Fatigue Crack Growth Testing
- N—Development of New Weight Function Stress Intensity Factor Solutions
- O—Literature Survey on the Stability and Significance of Residual Stresses During Fatigue
- P—Risk Assessment for Large Numbers of Inherent Material Anomalies
- Q—Adaptive Optimal Sampling Methodology for Multiple Anomalies
- R—Confidence Bounds
- S—Importance Sampling Techniques
- T—Probabilistic Sensitivities
- U—Optimal Sampling for Zones
- V—Efficient Conditional Failure Analysis
- W—List of Publications and Presentations During "Turbine Rotor Material Design, Phase II" Grant

## LIST OF FIGURES

Figure	Page
1-1 The Rotor Integrity Sub-Committee Vision for an Enhanced Rotor Life Management Process Based on Damage Tolerance	1-4
2-1 Classifications of "Stealth" Anomalies	2-3
2-2 Stealth Region Predicted for Given Temperature Exposure	2-4
2-3 Core Width as a Function of Initial Particle Size and Concentration for a Representative Exposure History	2-5
2-4 Comparison of JETQC Data to Predicted Core vs. Core Plus Diffusion Zone Size Neglecting Pure Beta Phase	2-6
3-1 Typical Ultrasonic Inspection Data for One Seed	3-2
3-2 Typical Analysis and Metallographic Data for One Seed	3-3
3-3 Comparison of Measured Deformed Diffusion Zone Size with Predictions from the Direct Application of the Microcode	3-4
3-4 Comparison of Measured Deformed Hard Alpha Size with Predictions from the Direct Application of the Microcode	3-4
3-5 Comparison of Regression Equation Prediction with Microcode Prediction for the Deformation Strain in the Diffusion Zone	3-6
3-6 Comparison of Regression Equation Prediction with Microcode Prediction for the Deformation Strain in the Hard Alpha	3-6
3-7 Comparison of Measured Deformed Diffusion Zone Size with Regression Equation Predictions	3-7
3-8 Comparison of Measured Deformed Hard Alpha Size with Regression Equation Predictions	3-7
3-9 Hard Alpha Ultrasonic Response in Billets vs. Subsequent Forgings	3-10
3-10 Contours of Strain-to-Cracking as a Function of (Left) Strain Rate and Temperature (Right) Temperature and Damage	3-12

## LIST OF FIGURES (cont.)

Figure	Page
3-11 Contours of HA Damage as a Function of (Left) Strain Rate and Temperature (Right) Temperature and Macro Strain	3-13
3-12 Representative Damage Contours in SB1 - SB3	3-13
3-13 Surface Stresses Predicted Accurately for As-Quenched Condition	3-16
3-14 Surface Stresses Predicted Accurately for Stress Relieved Condition	3-16
3-15 Sub-Surface Stresses Predicted Accurately for As-Quenched Condition	3-17
3-16 Internal Stresses Predicted Accurately for Quenched/Rough Machined Condition	3-17
3-17 Prediction of Influence of Cooldown Rates	3-18
3-18 Prediction of Influence of Geometry Effects on Local Cooldown	3-18
4-1 Effect of Oxygen Additions on Tensile Properties	4-2
4-2 Effect of Oxygen Additions on Dwell Fatigue Properties: Stress to Give a 2000 Cycle Dwell Fatigue Life	4-2
4-3 Fracture Surfaces of Specimen SB3-25C (Cluster with Diffusion Zone)	4-5
4-4 Comparison of Predicted FCG Lifetime and Actual Total Fatigue Test Lifetime for Forged Coupons with Hard Alpha Anomalies	4-6
4-5 Disk SB6 Fracture Surface at Inclusion with Scanning Directions Identified	4-12
4-6 Vacuum FCG Results for P&W and Honeywell Ti-6242 Materials at 600°F	4-14
4-7 Vacuum FCG Results for Waspaloy at $R = 0.05$ and Three Different Temperatures	4-15
4-8 Effect of Environment (Air versus Vacuum) on Fatigue Crack Growth Rates in Waspaloy at 500°F, $R = 0.05$	4-15
4-9 Vacuum FCG Results for IN-718 at $R = 0$ and Four Different Temperatures	4-16
4-10 C-Scan Images for Mults 804085-3X and 904618-5A1	4-18
4-11 C-Scan Images for Mults 8045395X and 804618-5A	4-19

## LIST OF FIGURES (cont.)

Figure		Page
4-12	Comparison of Experimental Lifetimes with Predictions Based on the Conventional Stress Rainflow Method for IN-718, René 95, and René 88DT Subjected to TMF Histories	4-21
5-1	3D Surface Damage Analysis Capability Linked Directly to a 3D Finite Element Model	5-2
5-2	Architecture Linking the User-Supplied Crack Formation Module to DARWIN	5-5
5-3	Illustration of Zone Refinement Capability	5-7
5-4	Illustration of the Element Subdivision Technique	5-8
5-5	Illustration of the Onion Skin Capability	5-8
5-6	Visualization and Polynomial Fitting of Bivariant Stress Gradients	5-12
5-7	Illustration of GUI Report Generation Capability	5-13
5-8	Illustration of Crack Growth Visualization Capability	5-14
5-9	The DARWIN Electronic Help System in Web Browser Format	5-15
5-10	Illustration of OEM Verification of DARWIN for Inherent Anomalies	5-17
5-11	Illustration of OEM Verification of Flight_Life Module	5-17
5-12	Illustration of OEM Verification of Induced Anomalies, Comparing DARWIN Life Predictions to Experimental Results	5-18

## LIST OF TABLES

Table		Page
2-1	Summary of HA Distribution Process Studies	2-2
4-1	Summary of Vacuum FCG Test Conditions	4-13
4-2	Production UT Inspection Results for Ni Billet Indications	4-17
4-3	Maximum UT Response for Billet and Pancake Indications	4-19
4-4	Summary of New or Enhanced SIF Solutions Developed During TRMD-II	4-22
5-1	Summary of DARWIN Enhancements Developed Under TRMD-II	5-1
5-2	Summary of 3D Element Types Supported in DARWIN	5-3

## LIST OF ACRONYMS

1D	one-dimensional
2D	two-dimensional
3D	three-dimensional
AC	Advisory Circular
AE	acoustic emission
AFRL	Air Force Research Laboratory
AIA	Aerospace Industries Association
A/P	actual-to-predicted life
API	application program interface
BWF	bivariant weight function
CBS	Contaminated Billet Study
CC	corner crack
CFA	conditional failure analysis
CFM	Crack Formation Module
cpm	cycles per minute
CTE	coefficient of thermal expansion
CVS	Concurrent Version System
DARPA	Defense Advanced Research Projects Agency
DARWIN	Design Assessment of Reliability With INspection
DSTO	Defence Science and Technology Organisation
DZ	diffusion zone
EDM	electro-discharge machining
ETC	Engine Titanium Consortium
FAA	Federal Aviation Administration
FBH	flat-bottom hole
FCG	fatigue crack growth
FEM	finite element method
FPI	fluorescent penetrant inspection
GE	General Electric
GEAE	GE Aircraft Engines
GE-CR&D	GE Corporate Research and Development
GUI	graphical user interface
HA	hard alpha
HIP	hot isostatically pressed
JETQC	Jet Engine Titanium Quality Committee
LCF	low-cycle fatigue
NDE	nondestructive evaluation
OEM	original equipment manufacturer

## LIST OF ACRONYMS (cont.)

P&W	Pratt & Whitney
PD	potential drop
PDF	portable document format
PDS	probabilistic design system
PM	powder metallurgy
POD	probability of detection
RISC	Rotor Integrity Sub-Committee
RS	residual stress
SB	seeded billet
SC	surface crack
SCOUT	SCanning Outfile Utility
SC(T)	surface crack tension
SEM	Scanning Electron Microscope
SENBH	single edge notch button head
SFTC	Scientific Forming Technologies Corporation
SIF	stress intensity factor
SwRI	Southwest Research Institute
TMF	thermo-mechanical fatigue
TRMD	Turbine Rotor Material Design
UT	ultrasonic
UWF	univariant weight function
VAR	Vacuum Arc Remelting
WF	weight function
XML	Extensible Markup Language

## EXECUTIVE SUMMARY

The aircraft engine industry is currently working with the FAA to develop an enhanced life management process, based on probabilistic damage tolerance principles, to address the threat of material or manufacturing anomalies in high-energy rotating components. This process for hard alpha (HA) anomalies in titanium rotors is documented in FAA Advisory Circular (AC) 33.14-1, and future revisions to AC 33.14 will address other materials and anomaly types. A multi-year research program titled “Turbine Rotor Material Design—Phase II” (TRMD-II) addressed shortfalls in the data and technology required to support and enhance the AC and its implementation. The integrated TRMD-II team, comprising Southwest Research Institute<sup>®</sup>, GE Aircraft Engines, Pratt & Whitney, Honeywell, and Rolls-Royce Corporation, developed enhanced predictive tool capability and supplementary material/anomaly behavior characterization and modeling. Major TRMD-II accomplishments include the following:

Sensitivity studies were performed to guide a planned update by RISC of the AC 33.14-1 HA anomaly distributions. These studies incorporated TRMD-generated technology as well as new data and insights from OEM experience to identify variables with the most significant impact.

To better understand the evolution of HA anomalies and predict the maximum expected sizes of undetected anomalies, a computer code was developed and calibrated to describe the diffusion of nitrogen or oxygen in titanium from an inclusion during metal forming and heat treatment.

Detailed NDE and metallography were performed on forgings with seeded or natural HA anomalies to validate the DEFORM<sup>™</sup> forging microcode. Measurements of core and diffusion zone (DZ) sizes in the forgings compared favorably with microcode predictions. The microcode was also used to characterize the conditions associated with cracking of HA anomalies during forging. Studies of representative forging shapes indicated that ingot-to-billet conversion and component forging would, under common processing conditions, crack all HA anomalies with nitrogen content greater than 4% (the lowest HA N content evaluated).

Ultrasonic inspections performed on natural and seeded HA anomalies in final forged shapes indicated that multizone methods detected anomalies more effectively than conventional methods, and synthetic and natural HA inclusions were easier to detect in billets than in forgings.

Tensile and fatigue tests were performed on high oxygen seeded Ti-17. Results indicated only a small impact of elevated oxygen on tensile and dwell fatigue properties, a slightly higher impact than for Ti-6-4, but a much smaller impact than for Ti-6-2-4-2.

Experiments were conducted to understand the fatigue behavior of embedded HA. Fatigue tests were performed on coupons machined from seeded forgings. The total fatigue life observed was always nearly at least twice as long the calculated FCG life, based on the assumptions that crack nucleation life was zero and the initial crack size was equal to the core plus DZ size. Spin pit tests were performed with material from TRMD-I forgings containing natural and synthetic HA anomalies. Flight Life analyses indicated that initial crack sizes more nearly corresponded to core sizes than DZ sizes. The thermal expansion coefficient of bulk HA with different nitrogen contents was measured, and the results employed to evaluate the potential effects of thermally-induced residual stresses on fatigue crack behavior at synthetic HA inclusions.

Some damage tolerance issues for nickel-based superalloys were briefly explored. Thermo-mechanical FCG data for IN 718 were generated to evaluate simple stress rainflow analysis methods. Several Waspaloy mults with sonic indications were obtained, inspected, forged, re-inspected, and selected for machining into coupon specimens for future fatigue testing. Vacuum FCG data were generated for two nickel alloys (IN 718 and Waspaloy) and a powder metallurgy nickel alloy (Udimet 720), plus one titanium alloy (coarse-grained Ti-6-2-4-2).

A survey was conducted of the scientific literature on the stability and significance of surface residual stresses in fatigue, based on a comprehensive bibliography of over 300 citations.

New DARWIN<sup>®</sup> versions were developed to address anomalies associated with surface damage (4.x and 5.x), as well as different types of inherent anomalies in other materials (6.0). DARWIN 5.x introduced a sophisticated 3D GUI that enables the user to visualize and then slice a fully 3D finite element model at a chosen surface crack location to create a 2D model for fracture mechanics analysis. New Version 6.0 capabilities address other types of inherent material anomalies including risk assessment equations for large numbers of anomalies, user-supplied crack formation modules, and 3D modeling of anomalies and associated production inspections.

Enhancements in probabilistic methods were developed to improve the overall efficiency and accuracy of the risk assessment computations, including enhanced importance sampling, optimal allocation of Monte Carlo samples, probabilistic confidence bounds, probabilistic sensitivities, conditional failure analysis methods, and an adaptive optimal sampling methodology.

Many other new DARWIN capabilities were developed and implemented, including zone discretization methods; enhanced inspection capabilities; mission mixing; an enhanced ANS2NEU module; a searchable electronic help system; and computational efficiency improvements such as enhanced stress processing, restart capability, a new XML database system, PC and Linux versions, and parallel and batch processing. The graphical user interface was enhanced significantly to support all new features as well as expanded visualization and report generation. Twelve new or enhanced stress intensity factor (SIF) solutions were developed for the Flight\_Life fracture mechanics module, including a new bivariate weight function SIF formulation and novel strategies to improve computational speed.

The partner engine companies participated in substantial review efforts to verify the accuracy and usability of DARWIN, including quantitative comparisons with experimental data, field experience, and internal company software; Alpha/Beta version evaluation to identify bugs and needed enhancements; and assessment of practical DARWIN use for design and certification.

A three-day DARWIN training workshop was conducted near the end of the program. Over forty technical papers were presented and/or published at conferences and in archival journals. Royalty-free DARWIN licenses were provided to several other U. S. Government agencies.

At the request of the industry and FAA, an infrastructure was developed for software configuration management, code licensing and distribution, and support for users employing DARWIN for official FAA and company purposes. License fees collected by SwRI are exclusively used to enhance DARWIN for the benefit of engine manufacturers and the FAA.

## 1. INTRODUCTION.

### 1.1 BACKGROUND.

The traditional design practice for high-energy aircraft gas turbine rotors, the so-called “safe-life” method, implicitly assumes that all material or manufacturing conditions that may influence the fatigue life of a rotor have been captured in laboratory coupon and full-scale component fatigue testing. In addition, the final design is usually based conservatively on minimum properties. This methodology provides a structured approach for design and life management that ensures high levels of safety. However, industry experience has shown that certain material and manufacturing anomalies can potentially degrade the structural integrity of high-energy rotors. These anomalies generally occur very rarely and, therefore, are not typically present in laboratory test articles. However, on those rare occasions when anomalies are present in manufactured products in service, they represent a significant departure from the assumed nominal conditions, and they can result in incidents such as the Sioux City accident in 1989 [1].

As a result of Sioux City, the Federal Aviation Administration (FAA) requested that industry, through the Aerospace Industries Association (AIA) Rotor Integrity Sub-Committee (RISC), review available techniques to determine whether a damage tolerance approach could be introduced to produce a reduction in the rate of uncontained rotor events. The industry working group concluded that additional enhancements to the conventional rotor life management methodology could be developed that explicitly addressed anomalous conditions. During the development of this probabilistic damage tolerance approach, it became apparent to RISC that the capabilities and effectiveness of the emerging technology could be significantly enhanced by further research and development. In early 1995, Southwest Research Institute (SwRI), in partnership with four major U.S. engine manufacturers (GE Aircraft Engines, Honeywell, Pratt & Whitney, and Rolls-Royce Corporation) and with guidance from RISC, proposed a multiple-year R&D program and was awarded an FAA grant to address identified shortfalls in technology and data. This program, titled “Turbine Rotor Material Design” (TRMD), developed enhanced predictive tool capability and supplementary material/anomaly behavior characterization and modeling with a particular focus on hard alpha anomalies in titanium rotors.

One of the key outcomes of that work was a probabilistic damage tolerance computer code called DARWIN<sup>®</sup> (Design Assessment of Reliability With INspection). DARWIN integrates finite element models and stress analysis results, a new fracture mechanics module for low-cycle fatigue (LCF) called Flight\_Life, material anomaly data, probability of anomaly detection, and uncertain inspection schedules with a user-friendly graphical user interface (GUI) to determine the probability-of-fracture of a rotor disk as a function of operating cycles with and without inspections. Other major accomplishments under the TRMD grant included the generation of fatigue crack growth (FCG) data in vacuum for three titanium rotor alloys [2], experimental and analytical characterization of the constitutive and damage properties of bulk titanium hard alpha (HA) [3, 4], experimental characterization of HA cracking in titanium alloy matrix material under monotonic and cyclic loading [5], development of a forging microcode capable of predicting the fracture and change of location and shape of HA during reduction from ingot to billet and from billet to final forged shape, forging experiments to validate the microcode, development of advanced probabilistic methods for risk assessment of components with rare inherent material anomalies [6], and validation of DARWIN against industry experience.

Further details are available in the comprehensive TRMD Final Report [7]. The DARWIN code developed under this program received an R&D 100 Award from *R&D Magazine* as one of the 100 most technologically significant new products of the year in 2000.

An incident at Pensacola, Florida in 1996 called special attention to surface anomalies induced by manufacturing activities. With guidance from the FAA, RISC began to apply and extend the insights and methods developed for inherent material anomalies in titanium rotors to the broader problem of induced surface anomalies in all rotor materials. SwRI, in continuing collaboration with the industry, proposed and was awarded a second FAA grant (“Turbine Rotor Material Design – Phase II”). This program began to address the surface anomaly challenge while completing the titanium hard alpha work.

## 1.2 ORGANIZATION OF RESEARCH.

The TRMD-II grant was organized into six major tasks.

One task focused on the supporting technology for the derivation of titanium hard alpha anomaly distributions. Sensitivity studies were performed to support a planned update of the HA anomaly distribution included in FAA Advisory Circular 33.14, incorporating new TRMD-generated technology (vacuum FCG data, the HA forging microcode, and the spin pit and coupon HA fatigue tests) as well as new data and insights from original equipment manufacturer (OEM) experience in order to identify the variables with the most significant impact on the resulting distributions. In order to better understand the evolution and predict the size of hard alpha anomalies, a mathematical model and computer code were also developed and validated to describe the diffusion of nitrogen or oxygen in titanium from an inclusion during metal forming and heat treatment.

A second task addressed the effects of forging and heat treatment on hard alpha anomaly morphology and residual stresses. Detailed nondestructive evaluation (NDE) and metallography were performed on the forgings with seeded or natural HA anomalies produced in TRMD-Phase I in order to validate the HA forging microcode developed in TRMD-I. The HA microcode was also used to assess the influence of nitrogen content, temperature, strain, and strain rate on the orientation, deformation, and cracking of HA anomalies during the forging operation. The relative detectability of hard alpha in billets vs. forgings was evaluated. The development of the DEFORM<sup>TM</sup> forging analysis software to predict bulk residual stresses was evaluated.

A third task generated experimental data and analytical models for various crack nucleation and growth phenomena. Vacuum FCG data were generated at representative temperatures and stress ratios for one titanium rotor alloy (coarse-grained Ti-6-2-4-2), two nickel rotor alloys (IN 718 and Waspaloy), and a powder metallurgy nickel alloy (Udimet 720). The coefficient of thermal expansion of bulk HA with different nitrogen contents was measured experimentally, and the results were employed in detailed stress, damage, and fracture mechanics analyses to evaluate the potential effects of thermally-induced residual stresses on fatigue crack initiation and growth at HA inclusions. Spin pit tests and coupon fatigue tests were performed with material from the TRMD-Phase I forgings containing natural and synthetic HA anomalies, conducting post-test fractography and metallography, and comparing test lives with Flight\_Life analyses. Tensile and fatigue tests were performed on high oxygen seeded Ti-17 in order to

evaluate the potential impact of elevated oxygen on tensile and dwell fatigue properties. Thermo-mechanical FCG data for IN 718 were generated with diagnostic stress-temperature histories and used to evaluate simple stress rainflow analysis methods employing isothermal data from the temperature at the maximum stress time point. A robust new weight function (WF) stress intensity factor (SIF) formulation was developed to accommodate general bivariant stress distributions on the crack plane, and highly accurate new WF SIF solutions were developed for select crack geometries under univariant and bivariant stressing using state-of-the-art 3D boundary element analysis to generate the reference solutions.

A fourth task emphasized the further development of the methodologies and software for reliability calculations in a design context. Advanced probabilistic methods were developed to improve the efficiency and accuracy of risk assessment computations. An importance sampling technique and associated confidence bounds were developed that significantly improve the risk computation speed (roughly two orders of magnitude faster than Monte Carlo simulation). A method was developed to assign Monte Carlo samples to zones based on relative risk that dramatically reduces the total number of samples (and associated computation time) required to predict risk for a specified level of accuracy. A sophisticated 3D graphical user interface was developed for DARWIN that enables the user to load and visualize a fully 3D finite element model and stress results, select a surface crack location, slice the 3D model along the principal stress plane at that location, re-mesh the slice to create a two-dimensional (2D) stress model, build a 2D fracture mechanics model on the cut plane, and extract the necessary input for the 2D fracture mechanics life calculation. New DARWIN versions were developed to implement these and other technology advances in a computer program that can easily be used by engine companies for design and certification purposes. Versions 4.x introduced simple 1D surface damage capabilities, Versions 5.x introduced full 3D surface damage features, and Version 6.0 introduced generalized capabilities for inherent anomalies. Each DARWIN version was validated against engine company experience.

A fifth task formalized the technology transfer process through meetings, reports, training workshops, publications, and presentations. A sixth task facilitated technology transfer into industrial production contexts. At the request of the industry and FAA, an infrastructure was developed for formal software configuration management, code licensing and distribution, and user support for engine companies to employ DARWIN for official FAA and company purposes. This infrastructure includes a source code repository, automated software verification procedures, bug-tracking software, user manuals, an on-line help system, and a web site.

This document is a comprehensive final report of all the investigations conducted and results obtained under the TRMD-II grant. The main body of the report is a summary of the major activities and the key results from the program. The details of the various investigations and results are contained in a series of appendices.

### 1.3 INDUSTRY VISION.

The broad RISC vision for enhanced life management of high-energy rotors is summarized in figure 1-1. Here damage tolerance is implemented as a supplement to the existing safe life methodologies. The RISC vision embraces both inherent anomalies introduced during production of the rotor materials and induced surface anomalies introduced during

manufacturing or maintenance of the rotors themselves. All rotor materials are addressed—titanium alloys, conventional cast and wrought nickel alloys, and advanced nickel alloys employing powder metallurgy technologies. The red check mark adjacent to the titanium hard alpha box indicates that the methods and supporting technologies to address that threat have been developed and are now formally defined in FAA Advisory Circular 33.14-1. Current RISC activities are focused on induced manufacturing anomalies, and a corresponding revision to AC 33.14 is forthcoming. Some preparatory work is also underway in RISC to address inherent anomalies in nickel alloys, with further modifications to AC 33.14 anticipated in future years.

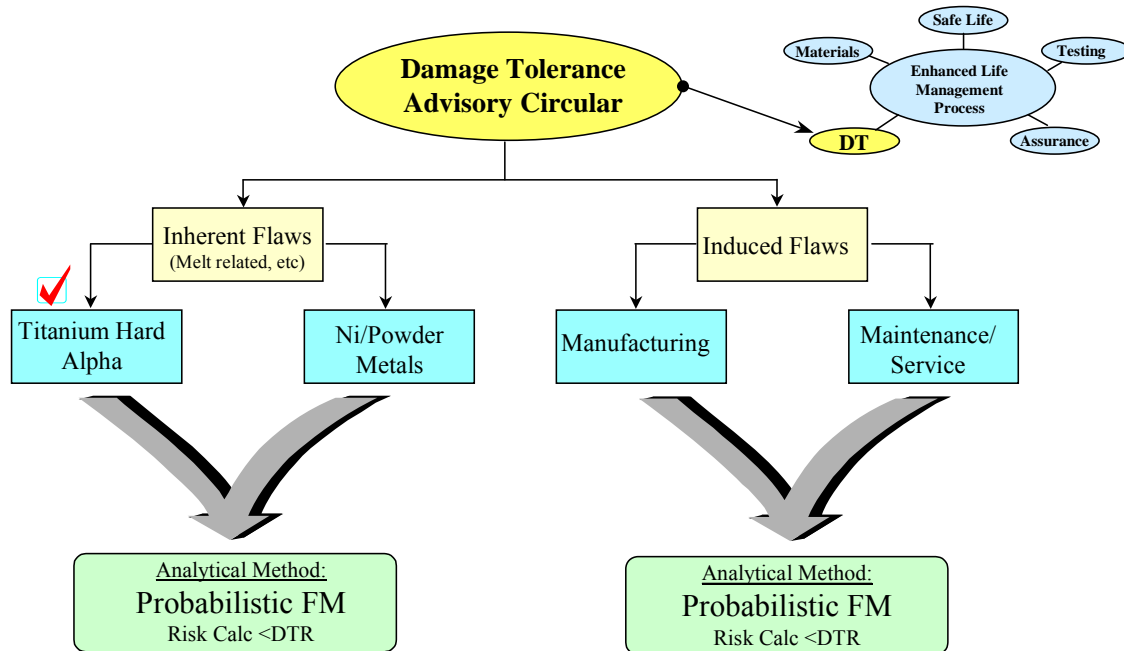


FIGURE 1-1. THE ROTOR INTEGRITY SUB-COMMITTEE VISION FOR AN ENHANCED ROTOR LIFE MANAGEMENT PROCESS BASED ON DAMAGE TOLERANCE

The TRMD grants have closely mirrored this incremental realization of the RISC vision. TRMD-I focused exclusively on supporting the implementation and planned updating of AC 33.14 for titanium hard alpha anomalies, and some TRMD-II activities were dedicated to the completion of those objectives. The primary focus of TRMD-II was to support the development and implementation of probabilistic damage tolerance methods for induced surface anomalies at bolt holes, corresponding with ongoing revisions to AC 33.14 within RISC. Other TRMD-II activities explored technology issues relevant to new and anticipated RISC efforts to address inherent material anomalies in a variety of nickel materials.

## 2. ANOMALY DISTRIBUTIONS.

### 2.1 TITANIUM HARD ALPHA ANOMALY DISTRIBUTION UPDATES.

Development of anomaly distributions for hard alpha (HA) in titanium disk alloys was initiated by RISC in 1991. The Jet Engine Titanium Quality Committee (JETQC) had gathered data between 1990 and 1993 representing HA finds in billet and bar that had been ultrasonically inspected. While the available data were limited, they served as the basis for an extensive analysis performed by RISC to develop HA anomaly distributions that are applicable to Ti-64, Ti-6242, and Ti-17. The final distributions were set based upon calibration to actual field experience and associated assumptions. The analysis process and its results have been summarized elsewhere [8].

Since the development of the original HA distributions, several advancements in technology and available data have made it both possible and desirable to update the original HA anomaly distributions. For example, vacuum fatigue crack growth data have been generated to characterize more accurately the growth rates of embedded cracks in titanium disk alloys, additional anomaly data from field finds have accumulated, and the DEFORM™ microcode has been developed to model anomaly deformation and damage during the forging process.

A plan to update the HA anomaly distributions was accepted by RISC in October 2001. The first phase of this plan, performed within TRMD-II, was to perform sensitivity studies on the model elements used to construct the HA distributions and determine which elements should be included in a revised derivation process. These studies included (1) variability in crack growth behavior, (2) variability in crack aspect ratio, (3) impact of vacuum crack growth data, (4) DEFORM micro-code impact on original billet and forging hard alpha deformation modeling assumptions, (5) possible alloy and melt practice bias, (6) impact of alternate approach to estimating the ingot distribution, (7) impact of effective inclusion size assumption, and (8) the impact of five additional years of JETQC HA data.

In the second phase of the plan, which was not part of TRMD-II, RISC will make decisions on which revised model elements will be incorporated into the updated HA anomaly distributions and/or lifing practice based on the results of these sensitivity studies. The second phase will be funded by the RISC membership. This report includes only the results of the first phase. Ultimately, RISC will formulate and calibrate revised HA distributions to be incorporated into a future revision of AC 33.14 on damage tolerance for titanium rotor components.

Table 2.1 summarizes all of the eight HA distribution studies and the preliminary conclusions on whether a studied effect should be included in the new derivation process for updated hard alpha anomaly distributions. Further details are available in Appendix A.

TABLE 2-1. SUMMARY OF HA DISTRIBUTION PROCESS STUDIES.

#	Study	Objective	Preliminary Conclusion
1	<i>Crack growth scatter</i>	Quantify the impact of expected material and analytical scatter on component POF predictions.	Negligible impact on POF predictions, but should be considered for technical completeness. <i>INCLUDE.</i>
2	<i>Crack aspect ratio</i>	Quantify the impact of crack aspect ratio on component POF predictions.	Negligible impact on POF predictions. <i>DO NOT INCLUDE.</i>
3	<i>Titanium vacuum crack growth data</i>	Quantify the impact of vacuum crack growth data on predicted POF for actual components.	Impact not large, but should be considered for technical accuracy and precedence. <i>INCLUDE.</i>
4	<i>HA deformation model</i>	Evaluate the impact of the new DEFORM™ HA micro-code on the construction of the HA distribution.	Negligible impact on POF predictions. <i>DO NOT INCLUDE.</i>
5	<i>Titanium melt practice</i>	Study the relative differences between titanium melt practices and alloys and their impact on component POF.	Results suggest this is not significant. <i>DO NOT INCLUDE.</i>
6	<i>Alternative approach to estimate ingot distribution</i>	Evaluate impact of alternative approaches to estimating the initial ingot distribution shape on correlation to component field experience.	Results suggest this may be significant. <i>INCLUDE.</i>
7	<i>Inclusion size, core vs. core+DZ</i>	Study the impact on component POF results due to the assumed initial crack location in the part (surface vs. subsurface).	Results suggest this may be significant. <i>POSSIBLY INCLUDE.</i>
8	<i>Five additional years of JETQC data</i>	Use five years additional JETQC data to study the impact of change in rate of 3VAR HA (post-2000) vs. vintage from '90 (1990-1996).	Results suggest this may be significant. <i>INCLUDE.</i>

## 2.2 DEFINITION OF STEALTH ANOMALIES.

Historically, a number of rotor disk fracture and cracking events have originated from embedded anomalies, which, although they were substantial in size, were undetected by production inspections. These anomalies have been called “stealth” anomalies due to their ability to evade inspection detection; i.e., the reflected signal is small relative to the inclusion size. Recent studies into the mechanisms and physics of sonic detection have led to a new understanding of what constitutes a stealth anomaly.

“Stealth” anomalies basically consist of three types (figure 2-1) in two categories. The first category is comprised of those anomalies whose sonic signal response is minimized. One type is due to anomaly orientation unfavorable to the path of the sonic signal. The other type is due to sonic signal scattering associated with extreme surface irregularities. The second category of “stealth” anomaly are those types which are ductile and well bonded making them less likely to have cracking and voiding during ingot and billet conversion. The lack of cracking and voiding combined with similarity in elastic modulus and density to the parent alloy renders them indistinguishable from the parent alloy for sonic detection. These anomalies frequently are created from a smaller material irregularity reacting chemically with the surrounding parent alloy to form a zone of material that is substantially weaker in tensile and fatigue capability than base metal. These areas are known as reaction zones, commonly gamma or gamma prime depleted zones in nickel alloys, and diffusion zones in titanium alloys. Hard alpha (HA) nuggets with concentrations of nitrogen or oxygen in titanium characteristically have diffusion zones associated with them. In some instances, the nitrogen nugget can be fully processed out, leaving behind only a residual diffusion zone that is very similar in acoustic response to the parent alloy.

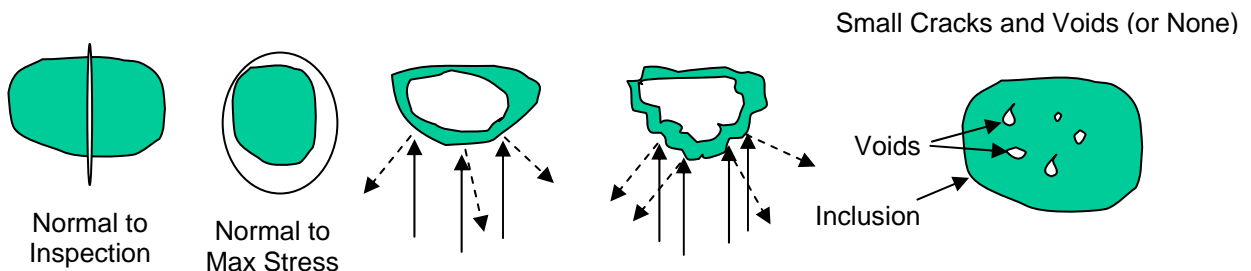


FIGURE 2-1. CLASSIFICATIONS OF “STEALTH” ANOMALIES

### 2.2.1 GROW Code Development.

The GROW code, consisting of a set of UNIX scripts and FORTRAN codes, was developed to assist suppliers and users of titanium base alloys in better understanding the dissolution history of nitride and oxide inclusions in molten and solid titanium alloys under various combinations of exposure temperature and time. The code was developed with the intention of allowing users to predict the formation of “stealth” anomalies, which can go undetected by NDE and may be harmful to fatigue life.

The GROW code takes thermal cycles associated with melting / metal forming and heat treatment as input. Calculations are based on a finite difference method, using temperature

integrated over time to accumulate the growth of the diffusion-affected zone. Concentration profiles are predicted as well as the extent of the various layers surrounding the inclusion. The diffusion process is assumed to follow the standard diffusion equation, which is complicated by the presence of multiple phases, each with its own set of characteristic physical/chemical properties. Since the instantaneous locations of the various phase interfaces depend on the instantaneous value of the nitrogen or oxygen concentration, the mathematical problem becomes nonlinear, and a numerical approach is most appropriate.

The code and user manual are available through the DARWIN web site. Detailed information about the GROW code and its calibration/validation is provided in Appendix B.

### 2.2.2 Studies on Stealth Anomaly Region and Triple Melt Processing.

Multiple studies were conducted to assess the formation of stealth anomalies and predictions relative to sizes measured in the JETQC data. A study was carried out to determine the shape of the stealth anomaly region in size and concentration space at fixed temperature and exposure time. The stealth region, as illustrated in figure 2-2, is hyperbolic in shape. The branch at small size and high concentration is bounded, but the branch at large size and low concentration is unbounded (for fixed exposure temperature and time.) At lower temperatures, stealth anomalies are not created, because the original inclusion is preserved due to low diffusivity. At higher temperatures, more dissolution occurs. Whether the stealth anomaly disappears depends on the exact combination of temperature and time selected.

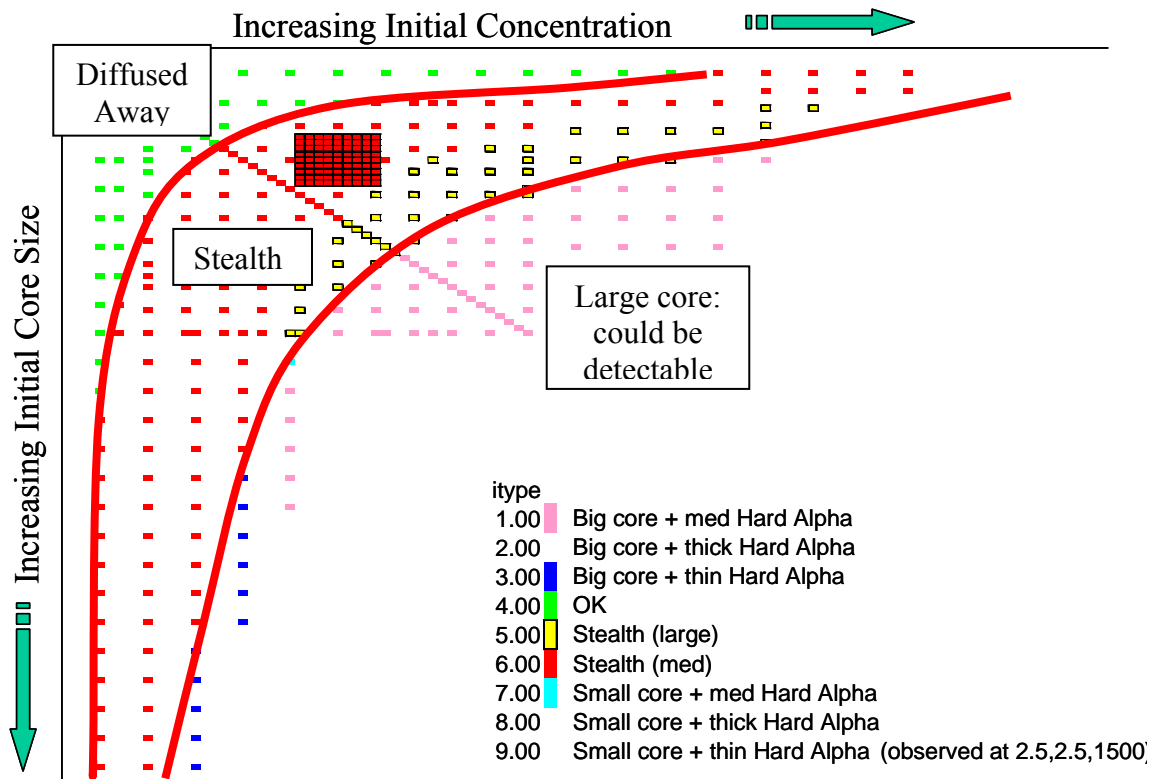


FIGURE 2-2. STEALTH REGION PREDICTED FOR GIVEN TEMPERATURE EXPOSURE

A systematic set of seventy cases was run to determine, for a given temperature history, the residual core width vs. initial particle size and nitrogen concentration. As the core width approaches zero (figure 2-3), the anomalies can reach a point where they may not be detectable and are classified as stealth anomalies.

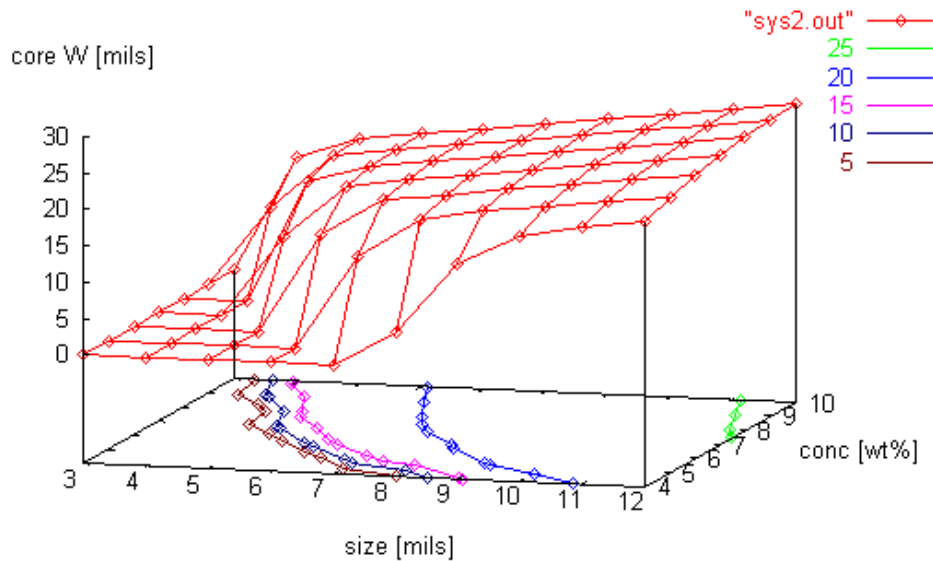


FIGURE 2-3. CORE WIDTH AS A FUNCTION OF INITIAL PARTICLE SIZE AND CONCENTRATION FOR A REPRESENTATIVE EXPOSURE HISTORY

The original JETQC data for the core and the core plus diffusion zone sizes are based on 3XVAR (Vacuum Arc Remelting) billet and bar finds. The data were used to derive the HA relative size distribution in the ingot, which includes the core and the diffusion zone sizes. A Monte Carlo simulation was run with forty randomly generated core sizes in the ingot to validate the relative core to core plus diffusion zone sizes predictions from the GROW code for a representative 3XVAR process to the JETQC data. The diffusion zone size included the nitrated beta phase and the alpha plus beta phase. If the pure beta phase is neglected, which is less than 1 wt % of nitrogen at 1400°C, the GROW code prediction compares well with the JETQC data (as shown in figure 2-4), particularly for core sizes greater than 20 mils.

### 2.2.3 Conclusions.

The GROW code development has helped to improve the understanding of the formation of “stealth” anomalies formed by the diffusion of nitrogen or oxygen inclusions in titanium during the melt processing. The code predicts concentration profiles as a function of the thermal exposure history. The GROW code has been successfully validated to provide acceptable predictions relative to available literature data for a series of dissolution experiments. These validation exercises have indicated a dependence on temperature, likely due to increasing convection with temperature, which can have a second order effect of increasing the rates of diffusion relative to predictions. Thus the predictions can be expected to set an upper limit regarding the amount of nitride or oxide remaining for a given anomaly and temperature history.

### Post 3XVAR DZ Size Distribution

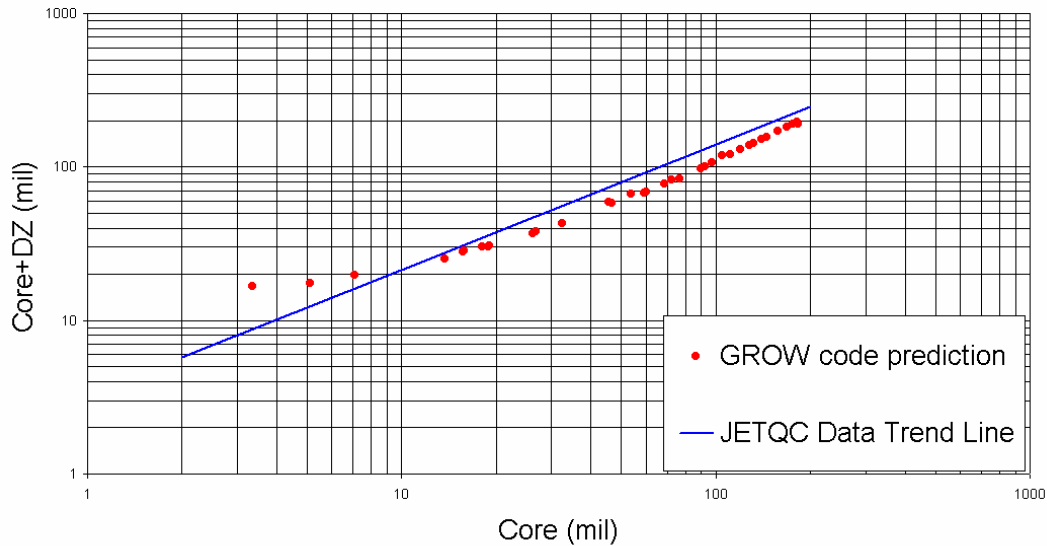


FIGURE 2-4. COMPARISON OF JETQC DATA TO PREDICTED CORE VS. CORE PLUS DIFFUSION ZONE SIZE NEGLECTING PURE BETA PHASE

Parametric studies have demonstrated that the GROW code can provide useful information about the effect of the melting process on the resulting core and the diffusion zone sizes. For a given melt process and initial anomaly size distribution, the maximum expected sizes of stealth anomalies can be predicted. This can be useful for material producers to optimize the melt temperature hold time and convection to minimize the number of potential anomalies remaining.

Comparisons of predictions to JETQC data have indicated close agreement between predictions for a random input set and measurements for the core and diffusion zone size relationship. This gives increased confidence in the code predictions as well as in the applicability of the shape of the anomaly distributions originally developed for engine rotor life prediction based on a limited data set of anomaly finds.

### 3. EFFECT OF FORGING ON ANOMALY MORPHOLOGY AND BULK RESIDUAL STRESSES.

#### 3.1 VALIDATION OF DEFORM™ MICROCODE.

The hard alpha anomaly distribution developed by RISC [8] was based on certain assumptions regarding the geometrical changes experienced by a HA anomaly when an ingot is converted to a billet and subsequently to an aircraft engine rotating disk forging. To test the validity of these assumptions, a finite element method (FEM) based deformation microcode was developed to predict the change in shape and orientation of HA anomalies during the metal forming processes. The microcode simulates the interaction and deformation among the HA inclusion, nitrogen diffusion zone (DZ), and parent material during the forming process, and the degradation of the strength of the HA particle due to fracture using a continuum damage mechanics constitutive model. The information from the microcode could be used to establish the nature of the anomalies that would be interrogated by ultrasonic NDE methods during the billet and disk forging inspections and to assess the assumptions made with respect to the flaw size used in fracture mechanics analyses.

In the TRMD Phase I program, the microcode was developed and tested. This microcode was an add-on to the commercial macro-deformation forging analysis code DEFORM, which was developed by Scientific Forming Technologies Corporation (SFTC). Necessary constitutive property data for the HA and DZ material were determined experimentally. Forging experiments were conducted to generate data for microcode validation. Preliminary validation was performed using data from the constitutive property tests and one forging. The microcode was demonstrated through application to typical Rolls-Royce disk geometries. Further details were provided in the TRMD-I Final Report [7].

In TRMD-II, 28 of the 44 seeds from the TRMD-I forging experiments were cut up for microcode validation. Improved regression equations were developed based on the calculated relationships between anomaly deformation and forging macro strain. The observed deformation in the forging experiments was compared with predictions based on direct application of the microcode or the regression equations. A detailed report of this activity is available in Appendix C. For convenience, a brief summary follows.

##### 3.1.1 Seed Polishing Procedure.

Seeds from pancake forgings of seeded billet (SB) SB1, SB3, and SB4 were located using ultrasonic C-scan and time of flight measurements to approximate the depth of the seed from the surface. Once located, wire electro-discharge machining (EDM) was used to remove a cube of material about 0.75" x 0.75" x 0.75" around the seed(s) while maintaining the original orientation from the forging.

After the seeds were removed, high-resolution 25 MHz ultrasonic inspections were made from each side of the cubed blocks (figure 3-1). In addition, a B-scan was taken from the direction in which the seed was to be polished. This is also the direction from which the indication was located in the forging. The depth and location of the seeds in each cube was then reported to the metallography group, which used the information to quickly polish to the seed and to estimate equal distance for the selected number of polish steps (typically ten).

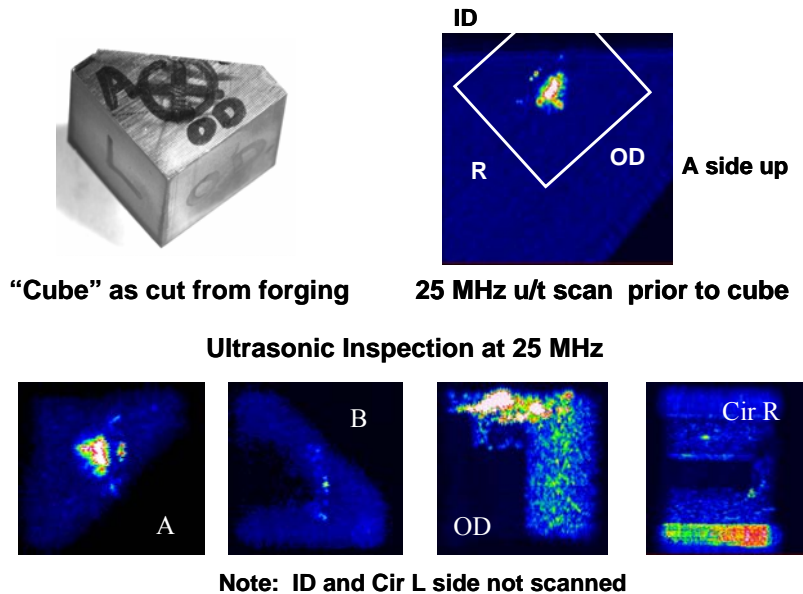


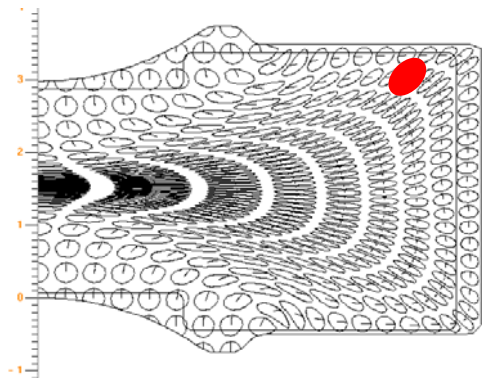
FIGURE 3-1. TYPICAL ULTRASONIC INSPECTION DATA FOR ONE SEED

Incremental grinding and polishing of each cube was performed in 40 mil steps until the DZ and core was first revealed or a depth of 200 mils was reached. Thereafter, finish polishing, etching, photography, and microprobe analysis for nitrogen content was performed at 30 mil increments through the seed. The overall dimensions of HA seeds and DZ in axial, radial and hoop directions were measured from the seed polish images. The measured values were recorded for the largest dimensions of the HA and the DZ in the three directions. Since the microcode cannot predict cracking and voiding, overall seed dimensions were used to validate the predictions, and it was not possible to validate all the details of inclusion damage.

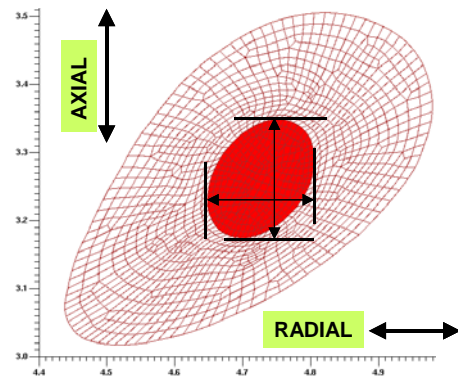
### 3.1.2 Microcode Validation.

The validation of microcode predictions consisted of comparing the predicted overall deformed shapes of the seed and DZ with the corresponding measured shape, as shown in figure 3-2. Microcode validation was done in two ways: by direct application of the microcode, and by application of regression equations derived from the microcode, as described further below.

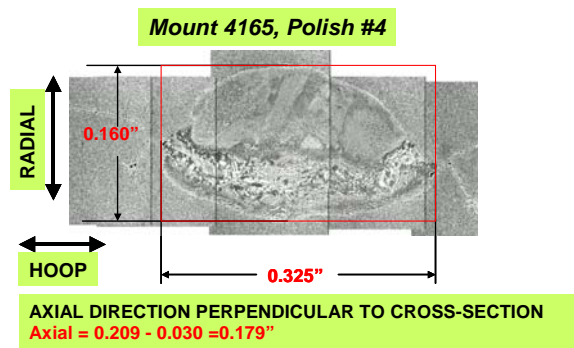
Figure 3-3 shows a comparison of measured deformed DZ size with that predicted by the direct application of the microcode for the six seeds in forging SB1. Figure 3-4 shows a similar comparison for the deformed hard alpha size. Data are in all three directions: hoop, axial, radial. The agreement between measurements and predictions was good for the radial and axial deformation. The hoop deformation was over-predicted due to the 2D axisymmetric assumption in the analysis.



MICROVOLUME LOCATION IN THE FORGING



PREDICTED MICROVOLUME DEFORMATION



POLISHED SECTION WITH THE LARGEST DIMENSIONS OF THE SEED

FIGURE 3-2. TYPICAL ANALYSIS AND METALLOGRAPHIC DATA FOR ONE SEED

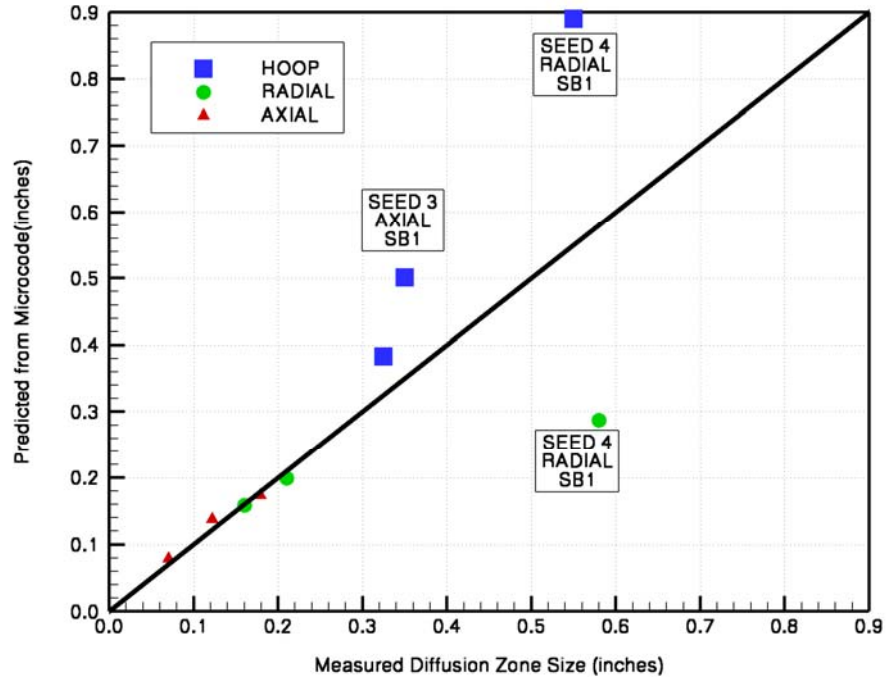


FIGURE 3-3. COMPARISON OF MEASURED DEFORMED DIFFUSION ZONE SIZE WITH PREDICTIONS FROM THE DIRECT APPLICATION OF THE MICROCODE

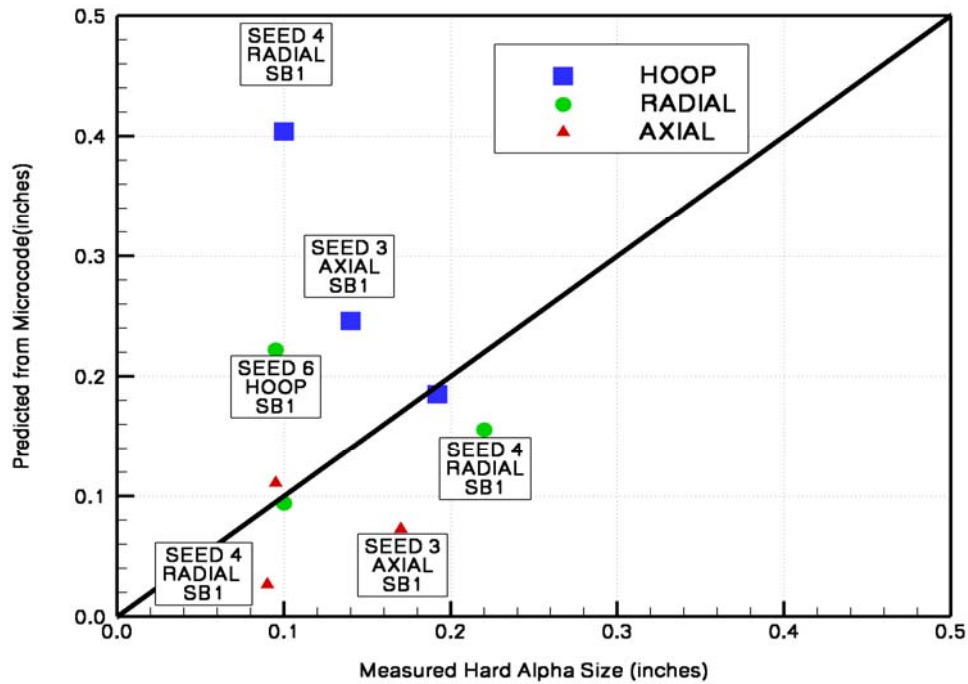


FIGURE 3-4. COMPARISON OF MEASURED DEFORMED HARD ALPHA SIZE WITH PREDICTIONS FROM THE DIRECT APPLICATION OF THE MICROCODE

### 3.1.3 Regression Analysis.

The deformation microcode is based on a 2D axisymmetric or plane strain model. In order to more accurately establish the shape of the HA anomaly and the DZ, regression relationships were generated between the HA and DZ deformation and the forging macro-strain, and then these relationships were utilized to approximate 3D anomaly deformation in a forging.

Parametric studies were first performed with the microcode to evaluate the relative importance of different variables for anomaly deformation. Hard alpha and diffusion zone nitrogen content, forging temperature, strain rate, and macro strain were found to be the most significant variables, while the aspect ratio of the inclusion, the ratio of DZ size to particle size, and the hydrostatic pressure were found to be relatively insignificant variables.

A new regression analysis was conducted in TRMD-II to obtain the inclusion strain and the DZ strain as a function of the variables investigated, where both the individual variables and their products were included in the regression equations. The resulting regression quality was much higher than in the TRMD-I regressions.

Figures 3-5 and 3-6 show a comparison of the values calculated from the regression equations with the microcode predictions used to generate the regression equations, showing that the regression equations provided an accurate representation of the data generated by the microcode.

### 3.1.4 Validation of the Regression Equations.

The overall dimensions of the HA seeds and the DZ in the axial, radial, and hoop directions were also predicted by application of the regression equations. The regression equations were applied to all the seeds in the synthetically seeded forgings SB1 – SB4. Temperature, strain and strain-rate histories at each of the seed locations were obtained from the model of the forging process using the point-tracking feature in DEFORM. Average values of strain, strain-rate, and temperature over the process were used in the regression equations.

Figure 3-7 shows a comparison of the measured deformed DZ size with that predicted by the regression equations, and figure 3-8 shows a similar comparison for the deformed hard alpha size. Data were provided in all three directions (hoop, axial, radial) from all seeds that were cut up. Overall, the agreement between measurements and predictions was good. The DZ flows smoothly like the base material, but with a higher flow stress, and therefore, the predictions matched the measurements well. The flow of HA is discontinuous (depending on when failure occurs with accumulated damage/strain) and therefore, the agreement between the measurements and predictions for HA was not as good as for the DZ.

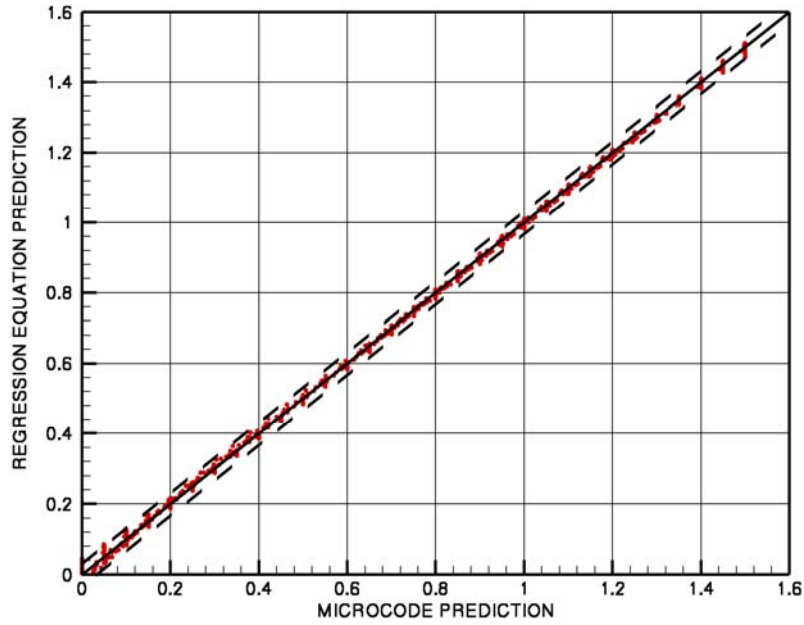


FIGURE 3-5. COMPARISON OF REGRESSION EQUATION PREDICTION WITH MICROCODE PREDICTION FOR THE DEFORMATION STRAIN IN THE DIFFUSION ZONE

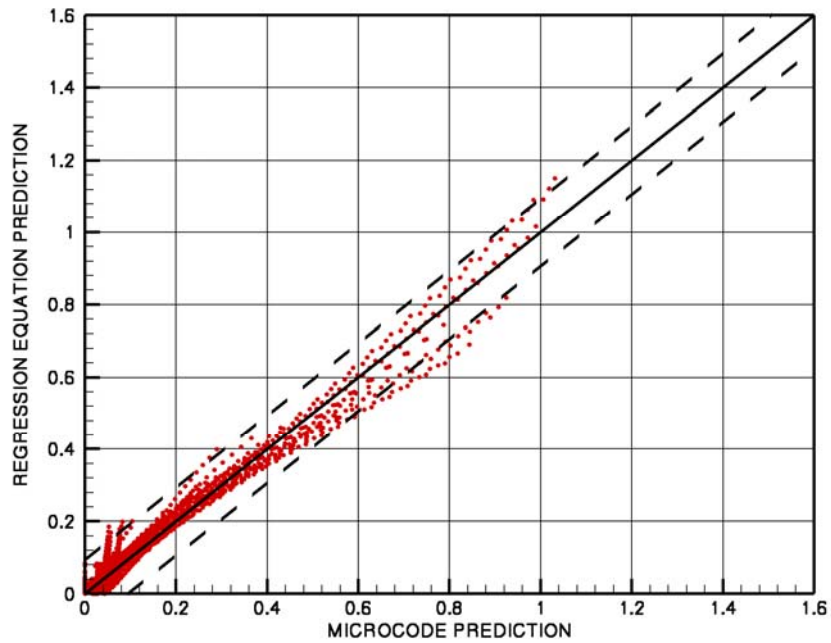


FIGURE 3-6. COMPARISON OF REGRESSION EQUATION PREDICTION WITH MICROCODE PREDICTION FOR THE DEFORMATION STRAIN IN THE HARD ALPHA

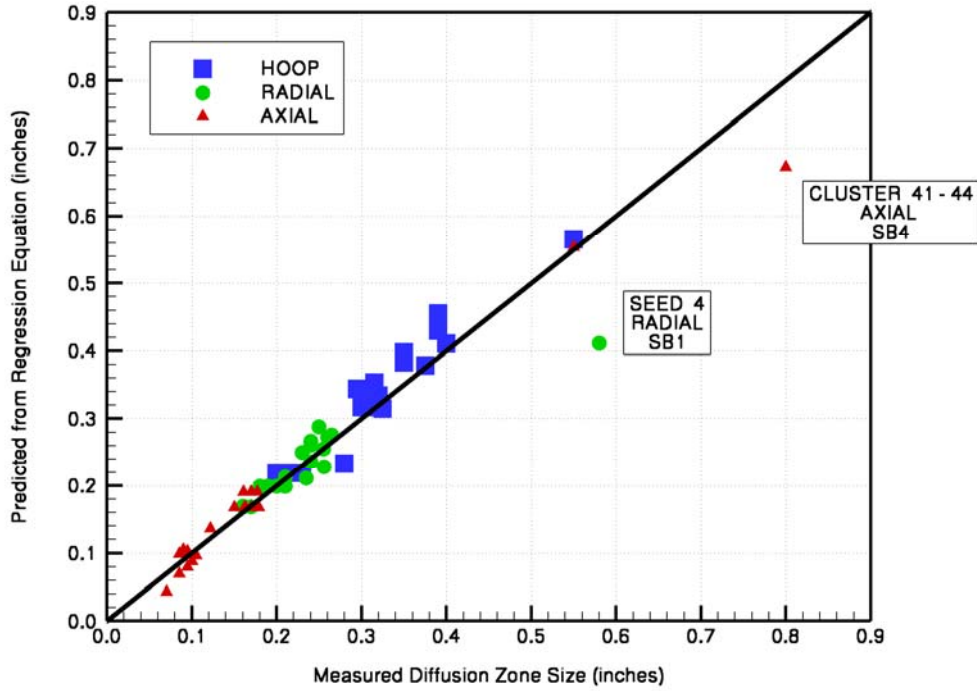


FIGURE 3-7. COMPARISON OF MEASURED DEFORMED DIFFUSION ZONE SIZE WITH REGRESSION EQUATION PREDICTIONS

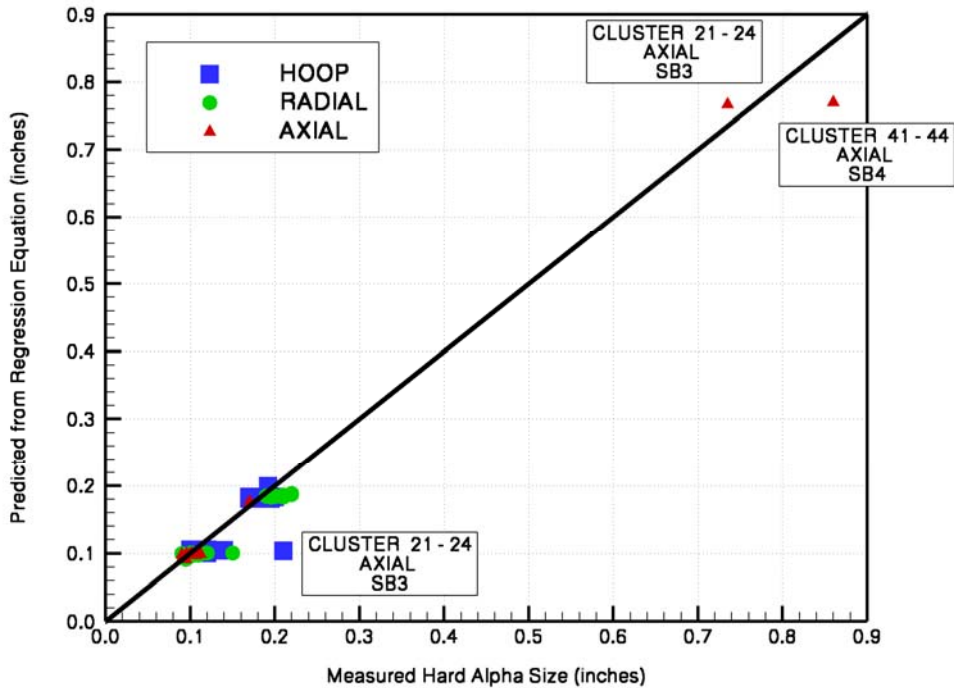


FIGURE 3-8. COMPARISON OF MEASURED DEFORMED HARD ALPHA SIZE WITH REGRESSION EQUATION PREDICTIONS

### 3.1.5 Comparison of Direct and Regression Approaches.

The overall predicted deformed shapes have been compared with measurements without looking at the details of fragmentation and voiding. In some cases, the predictions from a direct application of the microcode were in better agreement with the measurements. In other cases, the regression equations were better.

The microcode treats the seed as being 2D axisymmetric, a ring anomaly over 360 degrees. As a result, the microcode over-predicts hoop deformation and under-predicts radial and axial deformation. The actual deformation is 3D and cannot be accurately predicted by 2D methods.

The regression equations use the individual strain components scaled appropriately. Because the regression equations do not force the anomaly to be a full 360 degrees, they capture the 3D behavior more accurately than the microcode itself. The discontinuity between cracked and non-cracked conditions is like a step function and is difficult to fit with regression.

The application of the microcode to each individual seed is more involved, and the use of the regression equations is the preferred way of predicting seed behavior. Overall, the results from the regression equations are satisfactory.

A sensitivity analysis was performed to assess the error bounds in the predictions due to uncertainties in the input variables in the regression equations. The DZ deformation was over-predicted on average by ~3 % with a standard deviation of ~10%, and the HA deformation was under-predicted on average by ~5 % with a standard deviation of ~8 %.

## 3.2 ULTRASONIC INSPECTION OF FORGINGS.

### 3.2.1 Documentation of Previous Inspections.

During the TRMD Phase I program, forging experiments were conducted to evaluate the relative detectability of hard alpha (HA) inclusions in billets vs. forgings. These forgings included dogbone and backflow parts that were forged at Schlosser Forge Company using hot-die techniques, and pancake and engine disks that were forged at Pratt & Whitney Georgia using isothermal press forging.

The Engine Titanium Consortium (ETC) provided inspection results for the RMI CBS billets. Initial TRMD-I program plans only called for GE inspections of the seeded billets, pancakes, and disks, and the CBS pancakes and disks. These inspection results were included in the TRMD-I final report. However, where permitted within the task schedule, Honeywell, P&W Florida, P&W Georgia, and Rolls-Royce Corporation also voluntarily performed additional inspections of the pancake and disk forgings as program enhancements using company funding. The full compilation of inspection results from the different companies includes a combination of production and laboratory inspections, as well as standard ultrasonic, multizone, and shear wave inspections.

Since these supplementary inspections were not in the initial program plan and conclusions from ETC had not been received at the time, it was agreed to only include the planned GE inspections in the TRMD-I final report. After further consideration, the TRMD Steering Committee has

agreed to document all of the inspection results under the TRMD Phase II program to preserve these additional results for future reference by the industry team. These results are tabulated in Appendix D. Conclusions regarding this data are being deferred to the ETC.

### 3.2.2 New Inspection Results.

TRMD Phase II ultrasonic NDE efforts examined both conventional and multizone inspection techniques on natural and seeded anomalies in the final forging shapes. Inspection in the billet and intermediate forging shapes was conducted in TRMD-I. The purpose of this study was to examine the effects of material processing on the location in the forging and ultrasonic response of synthetic and natural HA anomalies, to compare the inspection sensitivity of conventional and multizone procedures, and to compare the inspection sensitivity in billets versus forgings. A detailed report on this study is provided in Appendix E. A short summary is provided below.

#### 3.2.2.1 Procedures.

Forgings identified as SB-# contained synthetic HA seeds that were placed in the billet. SB-1, SB-2, and SB-3 were “dogbone” forgings about 12 inches in diameter and 4 inches high, while SB-4 was a “backflow” forging about 12 inches in diameter and 7 inches high at its largest dimension. The dogbone and backflow forgings were inspected from both faces, and each side required two scans corresponding to different regions of thickness.

Forgings B1BW3B and B3W2E were prepared using Contaminated Billet Study (CBS) material obtained from the Engine Titanium Consortium and had natural HA indications which were detected and rejected by multizone billet inspection at a production titanium supplier (RMI). Forgings SB-5, SB-6, B1BW3B, and B3W2E were semi-finished shapes designed as spin disks, about 12 inches in diameter and 5.5 inches high. These forgings were inspected from two surfaces, the bore face and the bore.

Ultrasonic inspection took place at the General Electric (GE) Quality Technology Center in Evendale, Ohio. Laboratory equipment and instrumentation meeting all standard production inspection requirements were used for all inspections. GE conducted three different calibrated inspections on the forgings: Conventional #2 flat-bottom hole (FBH), Conventional #1 FBH, and Multizone #1 FBH.

#### 3.2.2.2 Results.

All synthetic HA seeds were detected in the dogbone and backflow forgings by the Multizone #1 FBH inspection, except for one seed located near the edge of a machined surface. Both conventional inspections detected most of the seeds in these forgings with reasonably high amplitude and signal-to-noise ratio. However, high levels of background noise would have made Conventional #1 FBH impractical as a production inspection technique for the dogbone forgings. The background noise levels in the Conventional #1 FBH scans of the backflow forging were significantly lower than for the dogbone forging, perhaps due to the metallurgical condition resulting from the more severe forging process. The inspection results from the semi-finished forgings also supported the general conclusion that the Multizone #1 FBH inspection can more effectively detect HA anomalies than either Conventional #1 or Conventional #2 inspections.

This advantage in multizone detectability becomes more evident as the reflectivity of the HA anomalies diminishes due to smaller size or lower N content. The effects of HA composition and diffusion zones on ultrasonic detectability were inconclusive.

All of these ultrasonic inspection results suggested that both synthetic and natural HA inclusions are easier to detect in the billet than in the forgings. The reported inspection data from dogbone, backflow, pancake, and semi-finished forgings are summarized in figure 3.9. Here all the Multizone #1 data from the forgings have been numerically converted to the same calibration (gain) level as the Multizone #2 data from the billet inspections conducted previously. The 45-degree line in this figure 32 represents equivalent response from the billet and forging inspections. Data falling above the 45-degree line indicate a larger response from the billet inspection, while data below the line indicate the corresponding forging provided a larger ultrasonic response.

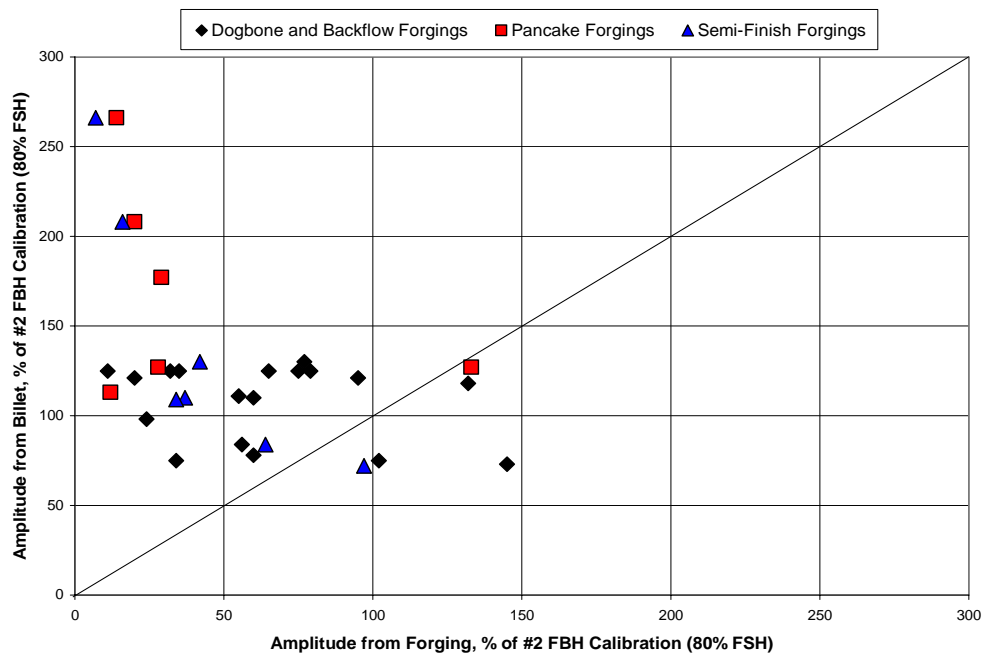


FIGURE 3-9. HARD ALPHA ULTRASONIC RESPONSE IN BILLETS VS SUBSEQUENT FORGINGS

This detection advantage in billets can be ameliorated somewhat if the forging can be inspected at a higher calibration level (gain level) than the billet. This would appear to be possible in most cases if a Multizone inspection is used on the forging. However, the increase in background noise level associated with increasing conventional inspection sensitivity from a #2 FBH to a #1 FBH will undoubtedly result in some forgings (or parts of forgings) being uninspectable at the high sensitivity conventional #1 FBH level. These data tend to corroborate the JETQC production defect information, which indicates more HA anomalies have been ultrasonically detected in billets than in the subsequent forgings.

### 3.3 PROCESSING CONDITIONS NEEDED TO CRACK HARD ALPHA ANOMALIES.

The DEFORM microcode (see Section 3.1) was also used to determine the conditions required to crack HA anomalies. This study was designed to provide insight into the likelihood of existing HA remaining uncracked under typical ingot conversion and component forging conditions, to provide insight into typical orientations of HA in forgings, and potentially to direct the future development of inspection procedures to enhance detectability of HA anomalies.

The study comprised four major activities. The first activity was to determine HA cracking strain and damage (extent of cracking) as a function of N content and deformation parameters. The second activity was to link these results with DEFORM in order to predict damage (extent of cracking) in representative forging shapes, and to validate the predictions by comparisons with observed cracking in the seeded billet studies. The third activity was to use this capability to determine the extent of HA cracking under typical production conditions, including representative ingot to billet conversion and three forging shapes. The fourth activity was to predict the forging flow lines along which melt-related anomalies tend to orient, using the same generic forging shapes. Each of these four activities is described briefly in turn. Further details are provided in Appendix F.

#### 3.3.1 Strain to Crack Hard Alpha.

The objective of the first activity was to determine the relationship between HA nitrogen content and strain-to-cracking in the HA. The strain to HA cracking was determined as a function of five variables: HA nitrogen content, diffusion zone (DZ) nitrogen content, deformation temperature, deformation strain rate, and damage. Hard alpha damage was obtained as a function of the first four of these variables plus macro strain. The results were graphed in contours of two of the five variables, for fixed values of the other three variables. Representative graphs are shown in figures 3-10 and 3-11, and more graphs are available in Appendix F.

The constitutive property data generated experimentally in TRMD-I indicated that HA deforms plastically when the N content is less than 4 weight %, but fractures when the N content is 4 weight % or greater. Guided by these experimental observations, constitutive equations were developed [3, 4] to describe the fracture behavior of HA with N content >4%, and the plastic flow behavior of HA with N content <4%, which is denoted as a DZ in this study. These equations were used here to obtain the damage and strain to crack HA. The damage formulation is applied only to HA with >4% N. Calculations were done only up to 8% HA N content, since there is little difference for higher N contents.

Note that the microcode does not explicitly predict HA cracking, but instead uses a damage variable to simulate the effects of HA cracking (0 = no cracking; 1 = fully cracked). Therefore, the cracking strain and the extent of cracking were based on the accumulated HA damage.

The flow stress of intact and damaged HA (at 8% HA N<sub>2</sub> and 3% DZ N<sub>2</sub>) and Ti-64 were compared at macro strains ranging from 0.05 to 2.00 over a range of strain rate and temperature. This was done to show how the relative strengths of HA and Ti-64 change depending on the deformation region (strain, strain rate, temperature). Results were generated as contour plots of flow stress in temperature-strain rate space for two contrasting values of macro strain.

With increasing macro strain, HA flow stress was observed to decrease due to increased damage and cracking. Damage and cracking were found to initiate at high strain rate and/or low temperature and spread to lower strain rates and higher temperatures with increasing macro strain.

Since HA flow stress depends on damage, strain, strain rate and temperature in a complex way, the strain-to-cracking and damage do not vary monotonically with the deformation parameters. However, the strain to HA cracking was generally found to *increase*, and damage was generally found to *decrease*, with decreasing HA nitrogen content, decreasing diffusion zone nitrogen content, increasing temperature, and decreasing strain rate.

### 3.3.2 Cracking Strain vs. Forging Strain.

The objective of the second activity was to evaluate the strain-to-cracking for HA relative to the strain produced during ingot conversion and during component forging. Contours of strain during the forging of three generic non-proprietary shapes were obtained for one material (Ti-6Al-4V).

A user subroutine was written to process the damage and strain-to-cracking data in DEFORM. The subroutine creates contour plots of the HA damage based on the local forging temperature, strain and strain rate for given HA and DZ nitrogen contents. The damage values indicate the extent of cracking for the given HA and DZ nitrogen contents. High damage values (approaching 1) indicate severe cracking whereas low damage values (close to zero) indicate only the onset of cracking. Representative graphs are shown in figure 3-12.

The model was validated using the data from the seeded dog-bone and back-flow forgings from TRMD-I. A total of 44 seeds were fabricated in TRMD-I, some with and some without diffusion zones, some individual and some clustered. These seeds were inserted into billets SB1–SB4 for subsequent forging, and 28 of the 44 seeds were cut up after forging for detailed investigation of cracking. Observed extent of cracking correlated approximately with predicted HA damage.

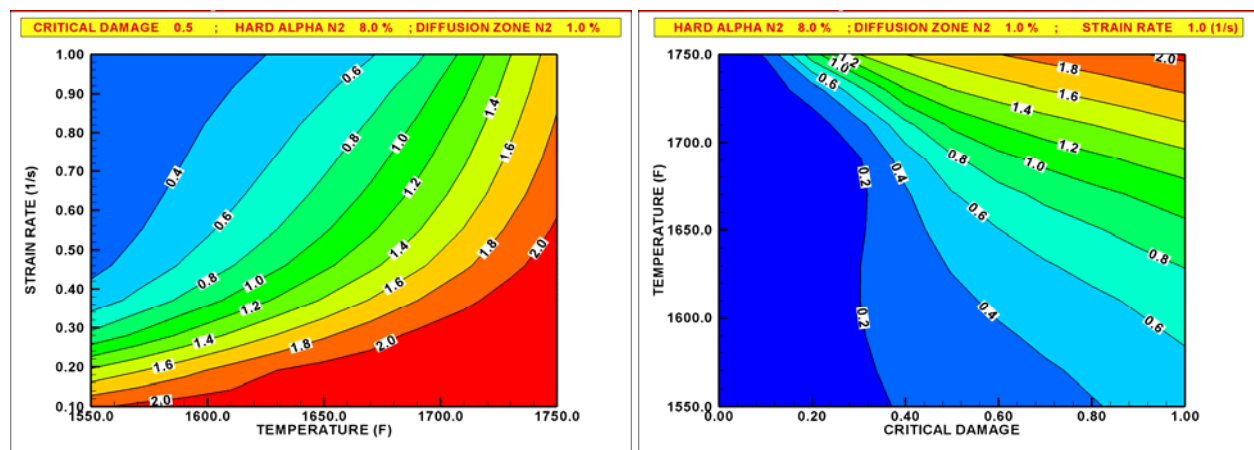


FIGURE 3-10. CONTOURS OF STRAIN-TO-CRACKING AS A FUNCTION OF (LEFT) STRAIN RATE AND TEMPERATURE (RIGHT) TEMPERATURE AND DAMAGE

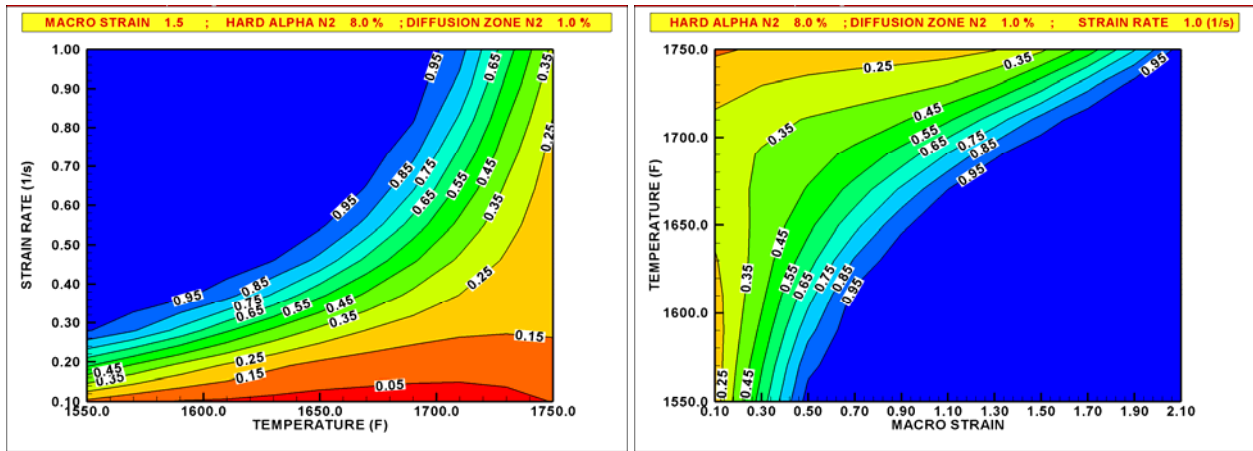


FIGURE 3-11. CONTOURS OF HA DAMAGE AS A FUNCTION OF (LEFT) STRAIN RATE AND TEMPERATURE (RIGHT) TEMPERATURE AND MACRO STRAIN

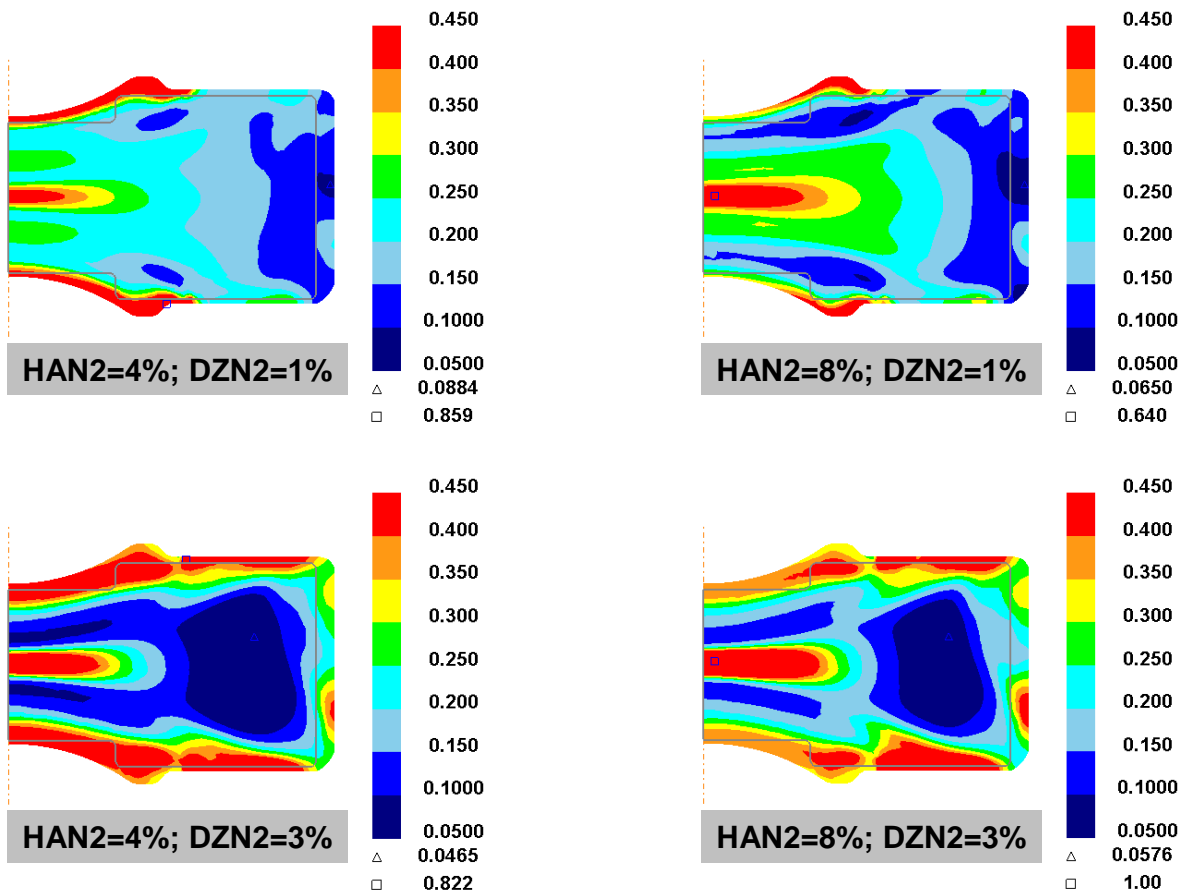


FIGURE 3-12. REPRESENTATIVE DAMAGE CONTOURS IN SB1 – SB3

### 3.3.3 Cracking During Billet Conversion and Component Forging.

The objective of the third activity was to determine HA nitrogen content that would not crack during typical production ingot conversion and component forging of Ti-6Al-4V, using generic shapes. A combination of the strain-to-cracking data and the forging macro-strain data was used to make this determination.

Damage was computed for the ingot-to-billet conversion process assuming a 36" initial diameter and uniform strain set equal to  $\ln(\text{square of initial to final diameter ratio})$ . The damage results were tabulated as a function of diameter reduction, HA N2, DZ N2, strain rate, and temperature. The study showed that ingot-to-billet conversion will, under commonly used processing conditions, crack all HA with nitrogen contents greater than 4%, which was the lowest HA nitrogen content evaluated. The extent of cracking will be less if the conversion is carried out at high temperatures (~1750F) or low strain rates (~ 0.1/sec). In general, however, typical conversion temperatures and strain rates were observed to result in damage ~1 (i.e., fully cracked HA).

Three generic shapes were used to illustrate the strain-to-cracking capability for component forging. The first shape used was the seeded billet forging (SB1 – SB4) from TRMD Phase I. The other two shapes were Rolls-Royce forgings that had been modeled in TRMD-I (AE 3007 fan disk and AE 2100/3007 Stage 14 compressor disk). Damage, effective strain, effective strain rate, and temperature contour plots were generated. The plots represent different time instants during forging and illustrate the evolution of damage as deformation progresses during forging. Temperatures greater than 1700°F and strain rates less than 0.5/sec were found to cause low rates of HA damage accumulation. Note that these calculations considered the damage only from the forging process, and damage from the conversion process should be added to assess the total extent of HA cracking.

For nitrogen content less than 4%, the anomaly is treated as a diffusion zone. The DZ results from partially dissolved HA cores during melting or conversion steps. Based on data from the TRMD-I flow stress experiments, the DZ-only anomaly is unlikely to crack after billet conversion and forging; it would only deform along with the base material, but to a lesser extent depending on its nitrogen content. In reality, there is no sharp transition between a DZ and a HA at 4% nitrogen. The transition from ductile to brittle behavior occurs over a range of N contents depending on the deformation conditions (strain, strain rate, and temperature) and the beta to (beta + alpha) transition temperature. More work is needed to characterize the transition zone.

### 3.3.4 Anomaly Orientation.

The objective of the fourth activity was to determine the orientations of melt-related anomalies during the conversion from ingot to billet and during forming from billet to component forging. In particular, the important determination was whether melt-related anomalies would likely end up oriented normal to forging surfaces. Forging flow lines along which melt related anomalies tend to get oriented, along with material deformation patterns, were predicted for the same three generic shapes defined in the previous activity (section 3.3.3).

In some regions of these forgings, the flow lines are normal to forging surfaces. Melt-related anomalies which tend to orient along the flow lines might not be detectable if scanned from the face to which the flow lines are normal. When flow lines are normal to a face, a scan from another face or a shear scan should be used.

### 3.4 MONITOR DEVELOPMENT OF SFTC CODE FOR BULK RESIDUAL STRESS.

Bulk residual stresses resulting from the forging and heat treatment of titanium disks may contribute to fatigue initiation and crack growth of material anomalies such as hard alpha inclusions. Tensile residual stresses may accelerate fatigue crack initiation and growth and subsequently reduce the fatigue life, while compressive residual stresses could retard the crack initiation and growth thus providing longer fatigue life capability. In addition, development of high residual stresses during quenching from heat treatment can produce quench cracks in the forgings. Scientific Forming Technologies Corporation has developed the DEFORM code to predict residual stresses resulting from the forging and heat treatment processes. The code development was reviewed to assess its performance relative to the needs of the TRMD program and its compatibility with the forging and heat treat processes used to manufacture titanium and superalloy disks. The actual code verification studies were performed by Pratt & Whitney under alternate programs, and primarily on superalloy disks, but have been summarized in the TRMD Phase II program as part of an effort to share lessons learned with the industry. Experience gained with superalloy disks is directly transferable to titanium disk materials.

In the last decade, use of finite element analyses for predicting residual stress states induced by processing has significantly increased. This has been driven by three main factors: the drive to reduce the cost of aerospace components, the development of user-friendly analysis routines and robust material models, and improved confidence in the predictions. Confidence in predictions has been gained through a broad range of calibration at various steps in the heat treat process with respect to the surface stress state (figures 3-13 and 3-14), internal stress state (figures 3-15 and 3-16), influence of heat treat rates (figure 3-17), and influence of heat treat shapes (figure 3-18).

A closer review shows very good agreement between predicted and measured surface residual stresses in both the as quenched, high residual stress state (figure 3-13) and stress relieved, reduced level of residual stress (figure 3-14) state. The same holds true for internal stress states measured in the as-quenched (figure 3-15) and machined condition (figure 3-16). Review of figures 3-17 and 3-18 shows that residual stress state can be strongly influenced by both component geometry (heat transfer coefficients/thermal behavior) and processing parameters (applied conditions). These are representative examples of several of the validation exercises conducted to develop confidence in the predictive capabilities of the tool and methodologies, provided an adequate knowledge of heat transfer coefficients and an appropriate material is available. It should be noted that this type of stress modeling has been successfully used in conjunction with failure criteria to define the process parameters and part configurations required to prevent quench cracking.

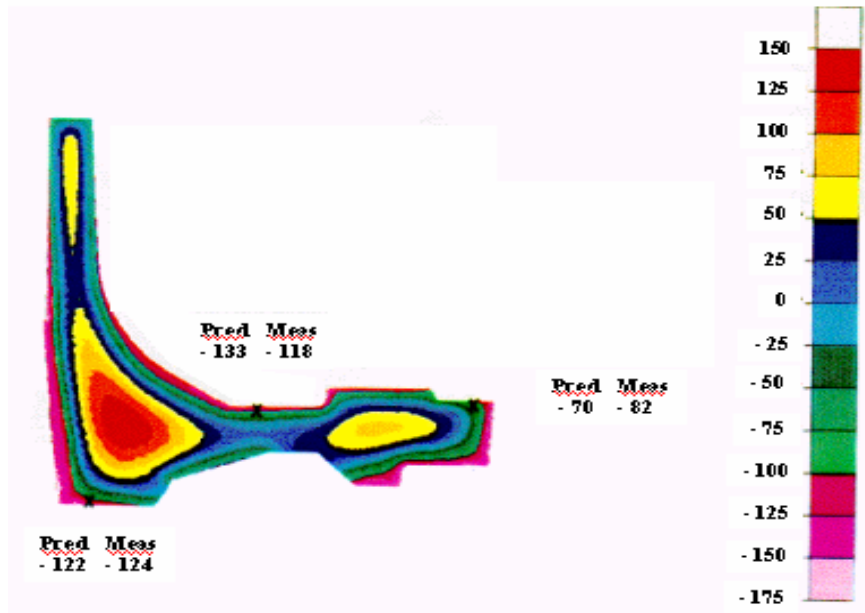


FIGURE 3-13. SURFACE STRESSES PREDICTED ACCURATELY FOR AS-QUENCHED CONDITION

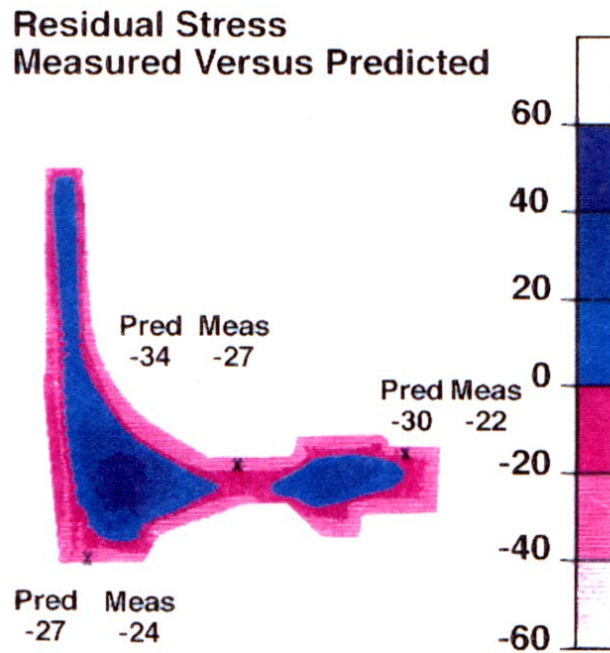


FIGURE 3-14. SURFACE STRESSES PREDICTED ACCURATELY FOR STRESS RELIEVED CONDITION

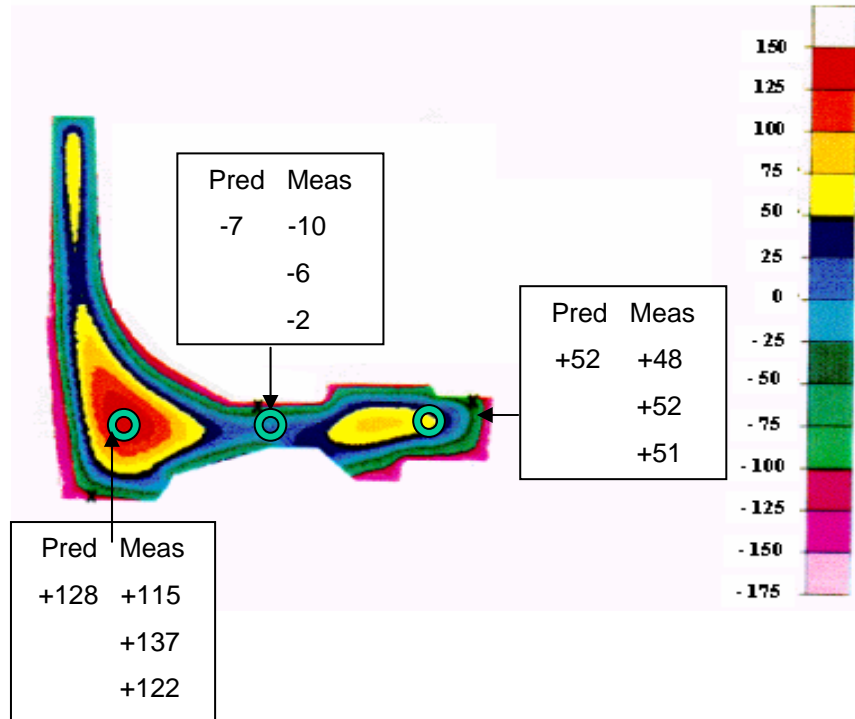


FIGURE 3-15. SUB-SURFACE STRESSES PREDICTED ACCURATELY FOR AS-QUENCHED CONDITION

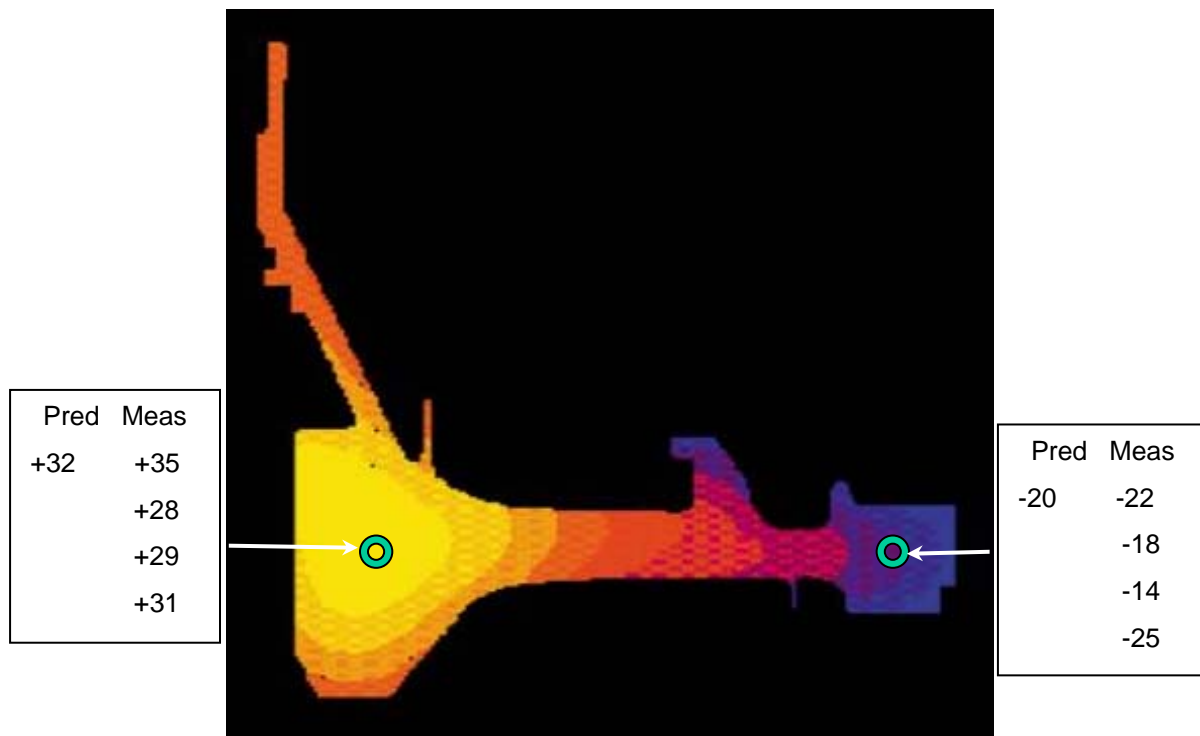


FIGURE 3-16. INTERNAL STRESSES PREDICTED ACCURATELY FOR QUENCHED/ROUGH MACHINED CONDITION

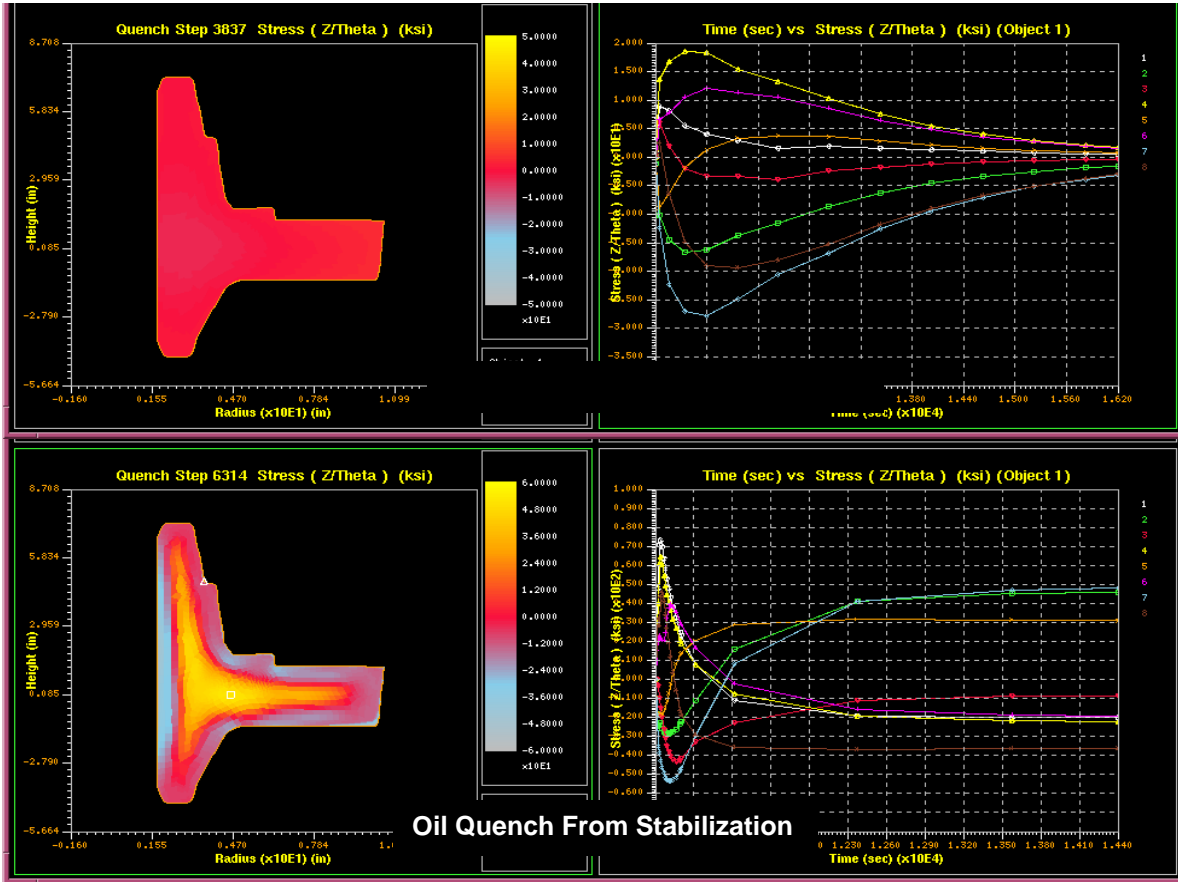


FIGURE 3-17. PREDICTION OF INFLUENCE OF COOLDOWN RATES

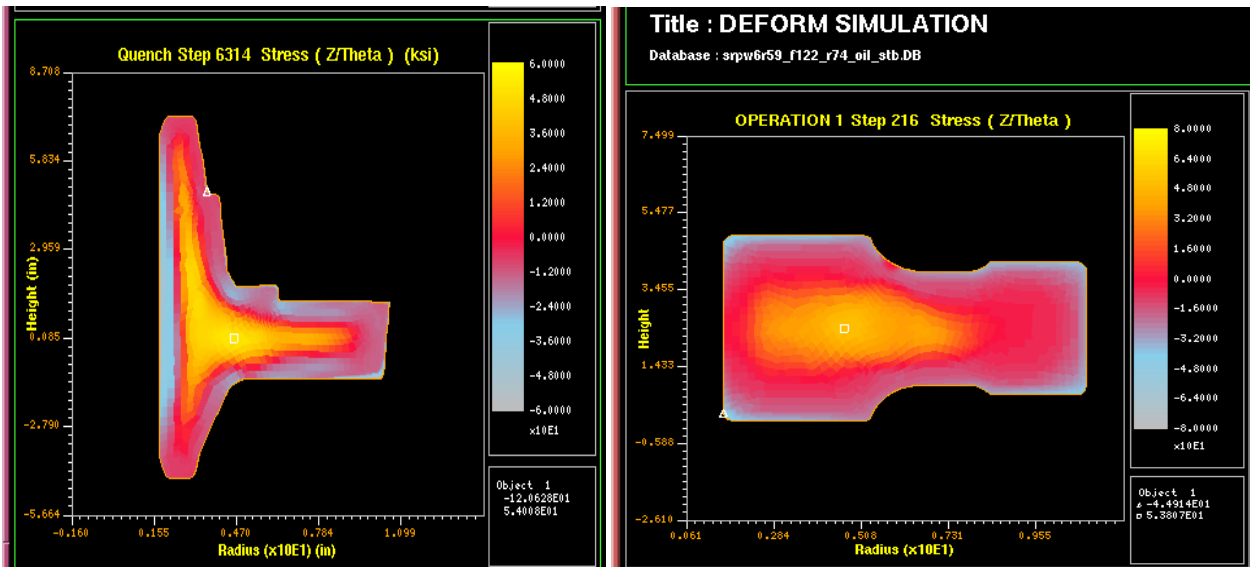


FIGURE 3-18. PREDICTION OF INFLUENCE OF GEOMETRY EFFECTS ON LOCAL COOLDOWN

The primary measurement technique in these studies was either through the center hole drill (monitoring strain change while drilling a hole through the center of a rosette strain gage) or plug removal (monitor strain change of a strain gage placed on the surface when the plug is electro-discharge machined from the part). Internal stresses were measured by inserting strain gages into the holes present in the disks when the plugs were removed, electro-discharge machining a cylinder out of the part, and monitoring strain change. The measured stresses were then compared with analytical predictions for the locations of interest. General agreement across a range of superalloy materials indicates that generalization of analytical residual stress prediction for aerospace rotor materials is enabled by the development of appropriate material constitutive models. (It should be noted that the analytical predictions of internal residual stresses required an adjustment using an element removal and redistribution technique.)

One item that to take into consideration is that some materials (such as Waspaloy) can exhibit a broad range of microstructural variation dependent upon the specified processing and, as a result, will exhibit a range of residual stress distributions dependent upon the microstructure of the part and process of interest. One area for future research is the development of the capability to modify constitutive material behavior based on microstructural inputs.

While DEFORM's demonstrated capabilities in the area of forging and heat-treat induced residual stress simulation are satisfactory, there are additional opportunities for enhancement. The first is improving the ability to map residual stress states into alternate finite element analysis codes such as ANSYS for additional analysis. This will enable more robust structural analysis of the influence of disk residual stresses on structural behavior in areas such as creep, burst, and fatigue life prediction. In addition, the need for coupling of material behavior and processing parameters should be considered so that material effects could be more reliably simulated. Outside the scope of the work conducted and the primary focus for DEFORM development is the process for incorporation of surface effects such as machining or peening induced residual stresses. These play a key role in disk fatigue behavior, and improved methods for the prediction of machining (tool/workpiece interactions) and peening (plastic deformation/bleed off) effects as well as their superposition onto forging/heat treat processing and integration into subsequent structural analysis should be addressed.

## 4. CRACK NUCLEATION AND GROWTH DATA AND MODELING.

### 4.1 MECHANICAL PROPERTIES OF TITANIUM WITH ELEVATED OXYGEN.

A Ti-6242 compressor disk failure from an uncracked, non-voided, oxygen-rich stabilized hard alpha raised questions about the sensitivity of other titanium alloys such as Ti-64 and Ti-17 to similar anomalies. Internal GE Aircraft Engines studies demonstrated that at room temperature, elevated oxygen caused Ti-6242 to lose ductility, while dwell LCF tests on base oxygen material containing high oxygen seeds showed a significant reduction in dwell fatigue life and formation of internal, flat facets at the high oxygen seed crack initiation sites. The fracture morphology of these bars was similar to that observed in the compressor disk failure. Similar studies on Ti-64 showed no degradation in ductility at low temperature. Based on the Ti-6242 and Ti-64 studies, it was determined that beta processed Ti-17 should be assessed to evaluate whether oxygen impacted low temperature ductility and dwell fatigue properties.

Ti-17 ingots were double VAR melted, converted to 4" diameter bar, and then extruded to 2" diameter at 1665°F. One ingot extrusion contained uniformly elevated oxygen (0.5%), one contained high oxygen (0.5%) seeds, and a third extrusion was base material with normal oxygen levels. Each extrusion was solution heat treated at 1475°F for 4 hours, water quenched, and aged at 1190°F for 8 hours. Tensile and fatigue specimens were machined from the base and high oxygen extrusions, and fatigue specimens were machined from the seeded extrusion.

Tensile testing of the base and high oxygen alloys was conducted at room temperature, 250°F and 500°F. LCF testing was conducted on both alloys at room temperature and 250°F. LCF tests were conducted at 30 cycles per minute (cpm), and some tests included a 2-minute dwell period. The dwell cycle tests were conducted at different stresses in order to determine the stress to give a 2000 cycle dwell life. Triplicate 30 cpm LCF tests were then conducted at this stress. After the LCF testing on the base and high oxygen specimens was completed, seeded LCF specimens were tested in 30 cpm and 2-minute dwell.

Tensile results are shown in figure 4-1 in terms of the changes in properties with oxygen additions. The high oxygen material had increased tensile strength of approximately 25 ksi at room temperature and approximately 15 ksi at 500°F. Room temperature plastic elongation for the high oxygen material was reduced by one half to 5%, but at higher temperatures, plastic elongation in the higher oxygen material was equivalent to, or higher than, the baseline material. The impact of oxygen on both strength and ductility for Ti-17 was intermediate between the effects on Ti-6242 and Ti-64.

The effect of oxygen additions on dwell fatigue behavior is summarized in figure 4-2. At room temperature, the stress for 2000 dwell cycles was 14 ksi higher for high oxygen Ti-17 material, which was also intermediate between the cold dwell effects on Ti-6242 and Ti-64. At 250°F, there was almost no difference in stress for 2000 dwell cycles between the base and high oxygen Ti-17. The 30 cpm LCF lives were longer for oxygen-containing material, and were higher at room temperature. The room temperature seeded dwell debit for Ti-17 was ~10× versus ~32× for Ti-6242, and an estimated no impact for Ti-64. Crack initiation sites for seeded Ti-17 bars were relatively rough, compared with flat, faceted crack initiations in seeded Ti-6242 bars.

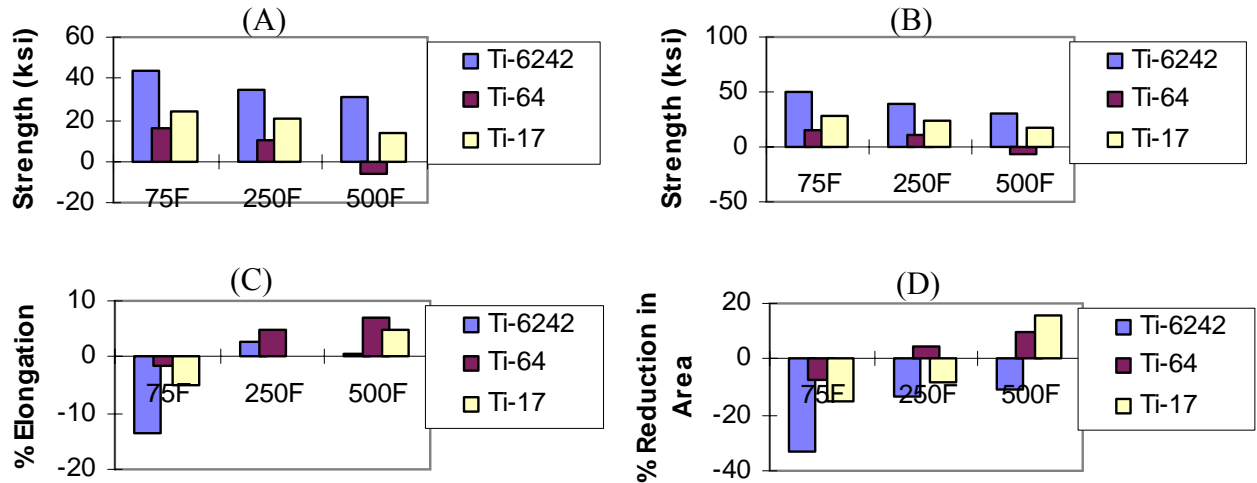


FIGURE 4-1. EFFECT OF OXYGEN ADDITIONS ON TENSILE PROPERTIES  
 (A) ULTIMATE TENSILE STRENGTH  
 (B) 0.2% OFFSET YIELD STRENGTH  
 (C) PERCENT ELONGATION  
 (D) PERCENT REDUCTION IN AREA

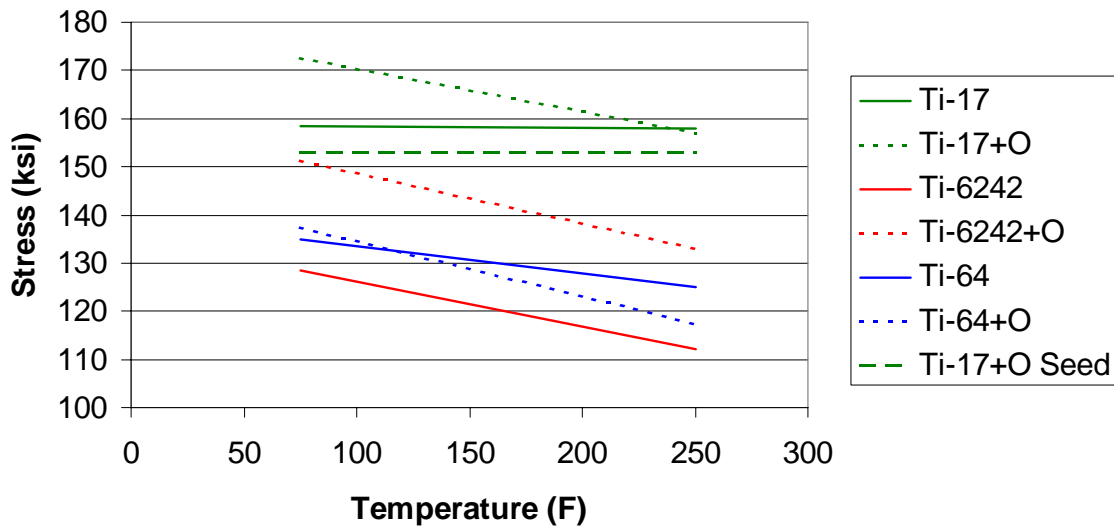


FIGURE 4-2. EFFECT OF OXYGEN ADDITIONS ON DWELL FATIGUE PROPERTIES:  
 STRESS TO GIVE A 2000 CYCLE DWELL FATIGUE LIFE

Based on these tensile and fatigue data, it is believed that Ti-17 is less sensitive to high oxygen anomalies than Ti-6242. There are several reasons to account for this reduced sensitivity. Increased sensitivity to dwell fatigue is generally associated with higher primary alpha content, higher alpha stabilizer and lower beta stabilizer content, and colony structure in the anomaly and in the surrounding material. In comparison to Ti-6242, Ti-17 generally exhibits lower primary

alpha, lower alpha stabilizer, and higher beta stabilizer content. This may also help to explain the absence of a faceted initiation in the seeded Ti-17 bars. Since a high oxygen anomaly in Ti-17 is processed closer to its beta transus, there is a reduced probability of colonies in the resulting microstructure, and the surrounding material will have been beta processed and subsequently transformed to a basketweave structure.

Based on these tensile and fatigue data, it is also believed that Ti-17 is more sensitive to oxygen anomalies than Ti-64. There are at least two reasons to account for this increased sensitivity. First, the absolute ductility of high oxygen Ti-17 at room temperature is significantly lower than high oxygen Ti-64. During a load-controlled dwell fatigue test in Ti-17 containing a high oxygen seed, the load will be shed from the weaker base material onto the stronger high oxygen seed material. Since the high oxygen seed has a relatively low strain capability, the seed will crack relatively easily, leading to a low fatigue life. In contrast, a Ti-64 high oxygen seed in Ti-64 has a much greater strain capability than a Ti-17 high oxygen seed in Ti-17, resulting in a smaller reduction in dwell fatigue life. Furthermore, in the case of Ti-17, there is a larger strength difference between high oxygen and base material than for Ti-64. The result is that more load will be shed onto the high oxygen seed in Ti-17, and in conjunction with the lower ductility in Ti-17 high oxygen material, this will lead to a lower dwell fatigue life.

There is also a significant difference between the processing of Ti-17 and Ti-6242 or Ti-64 that reduces the probability that a high oxygen anomaly will be present in Ti-17. Ti-17 ingots are homogenized at high temperatures for long periods of time to reduce the level of chromium segregation. Studies have shown that this homogenization treatment results in a large reduction in oxygen content of any high oxygen anomaly in Ti-17. This type of homogenization treatment is typically not applied to Ti-64 or Ti-6242.

Further details of this study are documented in Appendix G.

#### 4.2 FATIGUE TESTING OF FORGED COUPONS WITH HARD ALPHA ANOMALIES.

Hard alpha anomalies are often extensively voided and cracked in the final forged shape. Current life prediction methodologies assume that an initial fatigue crack size equal to the size of the HA region (high nitrogen core plus surrounding diffusion zone) is present at the beginning of life. This assumption could be overly conservative, however, for smaller HA anomalies and zones with lower nitrogen content, which are less likely to be extensively cracked and voided after the forging process. Therefore, it is useful to assess the cracking tendencies of the HA anomalies under fatigue loading in order to evaluate the possibility that some nonzero crack nucleation life could be included in the fatigue life prediction methodology.

An experimental program was conducted in TRMD Phase I [5, 9] to characterize the damage evolution occurring at HA anomalies. Mechanical tests were conducted on Ti-6Al-4V specimens containing either synthetic or naturally occurring hard alpha material. Comparisons of observed cracking with predictions based on fatigue crack growth (FCG) analysis suggested that a significant number of fatigue cycles could be required to form a dominant, growing fatigue crack in the matrix, for both synthetic and natural HA anomalies. However, the small number of tests performed in TRMD-I represents a limited parameter range, and the tests may not be fully representative of hardware under service conditions. For example, actual hardware would have

experienced a complete forging operation after anomaly formation, and it is possible that this forging operation would have either nucleated more severe initial cracks in the hard alpha anomaly or grown cracks into the matrix.

Additional testing was performed in TRMD Phase II to continue these investigations. The coupon specimens in TRMD-II were extracted from forgings that had been seeded with synthetic HA anomalies prior to forging for the purpose of validating the DEFORM microcode (see section 3.1). A selection of different anomaly compositions was tested, including high nitrogen core plus diffusion zone, high nitrogen core only, and low nitrogen DZ only (also called “was-beta”). The Flight\_Life fracture mechanics computer code was used to predict the fatigue crack growth lifetime of each test, and the analytical and experimental results were compared. A more complete description of this testing and analysis is provided in Appendix H.

#### 4.2.1 Material and Procedures.

The seeded forgings from which the specimens were extracted had been produced during TRMD-I. The artificial HA seeds for the forging mults were manufactured by GE Corporate Research and Development Center using a proprietary process and placed into the forging mults. The mults were then forged into one of two different shapes (“dogbone” and “backflow”) using hot-die techniques. The synthetic cores had a nominal nitrogen content of 12%, and the diffusion zones were nominally 2% nitrogen.

Maps of the anomalies in the forgings were provided from ultrasonic inspections performed by GE Aircraft Engines. Five anomalies of different character were selected for testing. Specimen blanks and then specimens were carefully machined from the forgings so that the anomaly of interest would be located in the center of the specimen gage section. Simple flat “dogbone” test coupons with a rectangular gage section typically 0.5” thick and 1.0” wide were used. In addition to these five synthetic anomalies, one additional specimen of similar size and shape remaining from TRMD-I was tested. This specimen contained a small, embedded 6% nitrogen core + DZ anomaly. Fatigue testing was performed in a servohydraulic test machine outfitted with hydraulic grips at a load ratio of  $R = 0.1$ . Each test was performed at a single constant load amplitude, but different tests were conducted at different load amplitudes. Cyclic frequencies were in the range of 1-10 Hz. Acoustic emission was monitored during fatigue cycling.

#### 4.2.2 Results and Analysis.

The experimental record indicates the total number of fatigue cycles required to cause specimen separation. Some of these cycles were required to nucleate a fatigue crack, and the remaining portion of the cycles was required to propagate the fatigue crack to failure. However, the experimental record provides no explicit information about the numbers of cycles associated with nucleation versus propagation. As noted earlier, the conventional analysis assumption is that the nucleation life is zero, and that the total fatigue lifetime is equal to the FCG lifetime.

In order to evaluate the accuracy of this assumption for the six coupon tests, the FCG life for each specimen was calculated using the Flight\_Life FCG analysis module in the DARWIN computer code. FCG properties were based on the Ti-6Al-4V vacuum FCG testing performed in

TRMD-I. The initial crack size was selected as the largest ellipse that could be inscribed within the irregularly-shaped anomaly on the post-test fractograph (a typical fracture surface for a cluster specimen is shown in figure 4-3). The dimensions were assigned without differentiating between core and DZ.

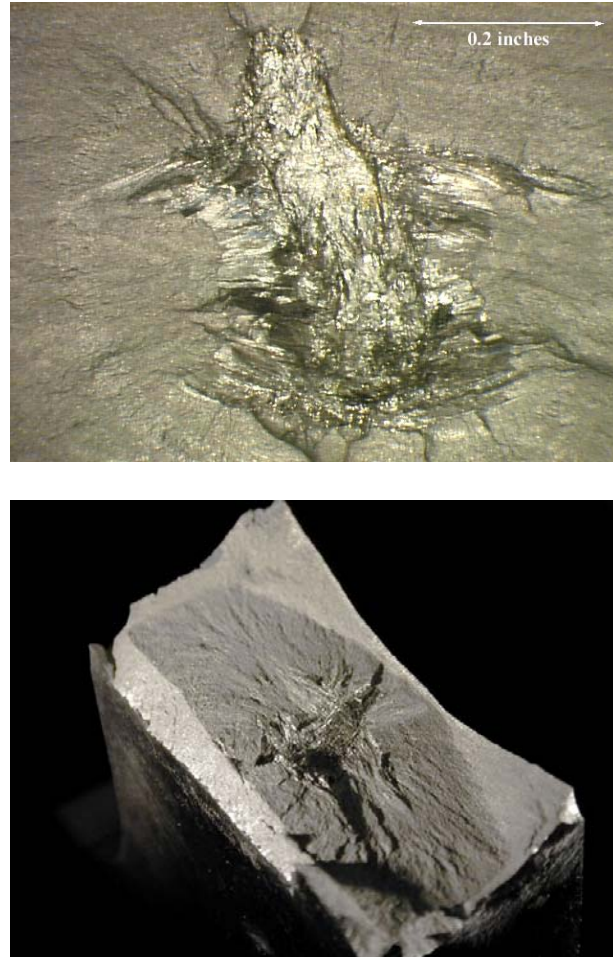


FIGURE 4-3. FRACTURE SURFACES OF SPECIMEN SB3-25C  
(CLUSTER WITH DIFFUSION ZONE)

The “actual” total experimental fatigue life is compared graphically with the “predicted” fatigue crack growth life for the six tests in figure 4-4. The actual total fatigue life was significantly larger than the calculated FCG life for all six tests. The actual total life was nearly always at least twice as long as the calculated FCG life, and the average ratio of actual-to-predicted life (A/P) was about 3.5. The difference between the two numbers was greatest for the was-Beta specimen in which the anomaly was completely low nitrogen “diffusion zone” material without any high nitrogen core; in this case, the A/P ratio was 6.9.

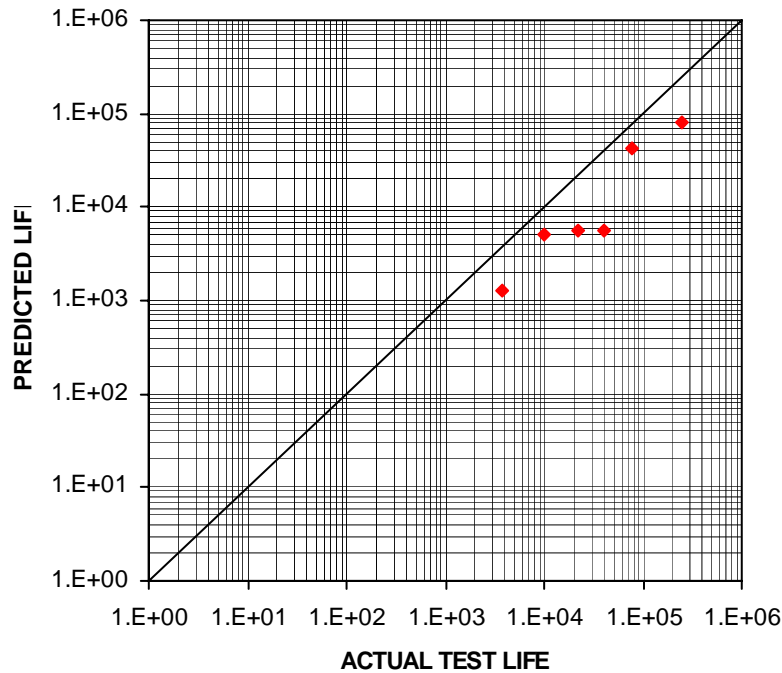


FIGURE 4-4. COMPARISON OF PREDICTED FCG LIFETIME AND ACTUAL TOTAL FATIGUE TEST LIFETIME FOR FORGED COUPONS WITH HARD ALPHA ANOMALIES

There are several possible explanations for the difference between observed total life and calculated FCG life. First of all, it is possible that some significant number of cycles was required for the crack to form (or “nucleate”) and begin growing. Second, it is possible that the formation and interaction of multiple cracks on multiple planes caused some retardation of crack growth. Third, it is possible that some residual stresses may have remained around the HA anomaly that reduced the crack driving force and therefore reduced the FCG rate (see section 4.3), although the applied stresses in these tests may have been great enough to reduce the potential residual stress effect. Fourth, it is possible that some of the differences can be attributed to the difference between high nitrogen core material and low nitrogen DZ material, since the initial crack sizes treated both anomaly compositions as being the same. This line of thinking is generally supported by the long life observed for the DZ-only anomaly.

#### 4.3 RESIDUAL STRESSES ASSOCIATED WITH HARD ALPHA.

Coupon tests on specimens and spin pit testing on forgings containing seeded HA defects were conducted during TRMD-I [7] and TRMD-II (see sections 4.2 and 4.4). The results of the testing indicated that the fracture and fatigue strengths of the embedded HA were higher than anticipated. The presence of residual stresses caused by differential thermal expansion was postulated as a potential explanation for the observed behavior. A small study was therefore conducted in TRMD-II to estimate the magnitude of these residual stresses and to determine their potential impact on fracture and fatigue strength: how do the residual stresses influence the applied stress required to initiate cracking during monotonic loading, and how do the residual

stresses influence the applied stress required to sustain fatigue crack growth in the vicinity of the HA anomaly? A full report of this investigation is provided in Appendix I. For convenience, the experimental and analytical procedures and the key results are summarized below.

#### 4.3.1 Review of Experimental Results from TRMD-I.

Artificial hard alpha anomalies with a cylindrical shape, a core nitrogen content of 5.5% (denoted HA-6N), and a surrounding diffusion zone were manufactured and implanted into Ti-6Al-4V material blocks by GE Corporate Research and Development (GE-CR&D). The blocks were subsequently machined into dog-bone specimens with a gage cross-section 1 inch x 0.5 inch. The HA defects were of two different sizes and were either surface-connected or fully embedded. Static and fatigue tests were conducted with acoustic emission (AE) and potential drop (PD) monitoring, and the surface defects were closely monitored visually. Further details of the test procedures and results are available elsewhere [5, 7, 9].

Crack initiation in surface-connected HA cores under monotonic loading was observed in all cases at stresses less than 20 ksi, and in many cases less than 10 ksi. In the embedded specimens, significant cracking of the subsurface cores first occurred at applied tensile stresses on the order of 80 to 110 ksi, according to the PD and AE results.

Fatigue tests were performed at  $R = S_{\min}/S_{\max} = 0.1$  at a variety of stress levels. Cracking of the defect and growth in the matrix of the surface HA specimens was observed at maximum stress levels of 40 and 50 ksi. Subsurface specimens exhibited defect cracking but no crack growth into the matrix at 50 ksi. Significant crack growth into the matrix was observed in both of the embedded HA specimens tested at 75 ksi. A fatigue test specimen with a natural HA anomaly from the ETC contaminated billet study sustained over 90,000 cycles at maximum stress levels from 50 to 75 ksi, finally failing after 13,300 cycles at 100 ksi. The embedded HA specimens were all more resistant to fatigue than the surface defect specimens, and life predictions using Flight\_Life consistently underpredicted the experimentally observed lives.

#### 4.3.2 Measurement of Thermal Expansion Coefficient.

GE CR&D fabricated and tested specimens to determine the coefficient of thermal expansion (CTE) of synthetic hard alpha manufactured from pure titanium or Ti-6Al-4V. Specimens with five nitrogen contents (nominally 2%, 4%, 6%, 9%, and 12%) were tested along with two baseline Ti-6-4 specimens. Measurements of the percent expansion were made using a push-rod dilatometer between room temperature and the post-HIP (hot isostatically pressed) temperature of 1650°F (900°C). The CTE was determined from the slope of the percent expansion versus temperature plots. The CTE values ranged from 4E-6 to 6E-6 /°F, with generally lower values for higher N contents.

#### 4.3.3 Analysis of Residual Stresses In and Around HA Defects.

Residual stresses in the HA defect and surrounding matrix can arise from differences in CTE, elastic modulus, and Poisson's ratio between the HA and the Ti-6Al-4V matrix. At the post HIP temperature of 1650°F (900°C), the material is assumed to be residual stress free. As the material cools to room temperature, the differences between the HA and the matrix introduce residual stresses. The residual stress profile was calculated based on a literature solution for thermal

expansion differences between cylindrical or spherical inclusions and the surrounding matrix. In all analyses, the embedded HA was found to be subjected to uniform triaxial compression at room temperature, with estimated stress values ranging from 18-55 ksi depending on nitrogen level. The maximum tensile stress in the matrix occurred at the particle-matrix interface, and the magnitude of the stress decreased dramatically as distance from the particle increased. The effect of the particle was practically negligible at a distance of one particle radius away from the interface.

#### 4.3.4 Fracture Strength Modeling.

A fracture model for bulk HA developed by Chan in TRMD-I [3, 4] was combined with the calculated residual stress fields to determine the nominal stress required to cause cracking of the HA core. The local pressure (based on the principal stresses) varies as a function of the nominal tensile stress, as the stress state becomes less triaxial under external loading. This loading path can be compared with the Chan fracture criterion to determine the nominal tensile stress when particle cracking occurs. The stress state, and hence the local pressure, is significantly different for surface vs. sub-surface defects.

This model predicted cracking at about 50 ksi for the surface case and 160 ksi for the subsurface case, compared with the experimentally measured values of 10-20 ksi for surface defects and 80-115 ksi for embedded HA. Therefore, the model correctly explains the substantial difference between surface and subsurface results, although the specific values are predicted incorrectly due to geometrical idealizations in the simple residual stress model. The analysis implies that the triaxial residual stresses caused by the thermal expansion differences delay the onset of fracture in the subsurface HA particles during the static load tests.

#### 4.3.5 Fatigue Modeling.

Fatigue modeling focused on the effect of CTE differences on the stress intensity factor,  $K$ , for cracks spanning the HA defect and attempting to grow into the matrix. The residual stress effects were estimated by superposition of  $K$  values for remote loading and local residual stresses, where the  $K$  due to residual stress was estimating using a weight function approach.

The compressive residual stresses in the HA particle were found to result in a negative stress intensity factor when the crack is within the particle. When the crack completely spans the particle and even when it has grown into the matrix, the compressive residual stresses in the HA particle attempt to keep the crack closed and substantially reduce the total  $K$ . This reduction in  $K$  can impact the onset of fatigue crack growth as well as influence the total fatigue life. However, the total  $K$  quickly converges to the applied  $K$  value as the crack grows into the matrix.

Comparisons of the calculated  $K$  with the crack growth threshold properties as expressed by  $\Delta K_{th}$  successfully predicted no growth in 50 ksi fatigue tests, while successfully predicting growth in 75 ksi fatigue tests. Similar analyses neglecting residual stresses would have predicted growth at 50 ksi. A broader parameter study found that the effect of the residual stresses was greatest for high nitrogen contents and lower applied stresses (especially below 40 to 60 ksi), and lowest for low nitrogen contents and high applied stresses (generally negligible above 100 ksi).

Fatigue life predictions were performed by integrating a simple crack growth equation for Ti-6Al-4V in vacuum from an initial size equal to the defect size to a nominal final size, choosing a crack closure model to address the changes in effective stress ratio as the crack grows. Including the residual stresses in the fatigue crack growth model caused an increase in the predicted life ranging from 1.3 to 4, depending on the specific nitrogen level and applied stress level. Note that designs and life predictions made using the traditional analysis methods neglecting these residual stresses will be conservative.

#### 4.4 SPIN PIT TESTS OF TITANIUM ROTORS CONTAINING HA ANOMALIES.

Spin pit tests of Ti-6Al-4V disks containing natural and seeded hard alpha inclusions were performed to validate the Flight\_Life fracture mechanics code in DARWIN and the assumptions used to develop the hard alpha anomaly distributions in the FAA Advisory Circular AC 33.14. The spin pit tests were conducted with three disks forged during TRMD-Phase I [7]. Disks B1BW3B and B3W2E contained natural anomalies from the Engine Titanium Consortium contaminated billet study. Disk SB6 contained an artificial seed introduced into the billet during TRMD-Phase I. Appendix J summarizes the accomplishments under this spin test program. Highlights of this investigation are provided below.

##### 4.4.1 Pre-Test Analysis.

DEFORM analyses were performed during TRMD-I to select the candidate forging, to identify the seed placement location for the seeded mults, and to identify which of the mults containing naturally occurring anomalies were acceptable for spin testing. The inclusions were backtracked through the forging process from the desired location in the forged disk to identify where the inclusions needed to be in the mults. To maximize the crack growth from these inclusions, it was desired to have the seeds as close to the corner of the disk bore as possible without intersecting the surface, since this location had the highest predicted stress during the spin testing.

A simple disk forging sonic inspection shape was selected as the configuration for spin testing. Prior to spin testing, ANSYS 2D axisymmetric stress analyses were performed to predict the stresses at the inclusions for multiple candidate forgings. The ANSYS stress analysis results were subsequently input into a stand-alone version of Flight\_Life to predict the crack growth life from the inclusions and select the desired test speeds. It was desired to select a speed that would result in approximately 15,000 cycles of crack growth life assuming a 0.2” inch crack (the size of the diffusion zone of the seed placed in disk SB6). The actual size of the natural anomalies in disks B1BW3B and B3W2E was unknown at the start of testing, but it was assumed that they were approximately the same size as the SB6 seed. In the pre-test analysis, it was assumed that there was no incubation and crack growth would initiate at the start of testing.

##### 4.4.2 Test Setup and Test Plan.

The rig hardware was designed and the spin testing was performed at Test Devices in Hudson, MA. The spindle and arbor interference fit assembly minimized cost to the program utilizing standard rig hardware already familiar to Test Devices. Since the objective of this testing was to assess the crack growth from internal HA inclusions, and surface initiated cracks

were not desired, the surfaces of the disks were shot peened to 6A intensity to reduce any concerns regarding premature surface initiated failure.

Strain gages were installed on disk SB-6 to validate the analytical stress predictions. Strain measurements were recorded during an initial three cycles of testing prior to the LCF cyclic testing. In all cases, the model agreed well with the test measurements.

The initial disk spin test plan called for spinning in 5,000 cycle increments with removals from the rig for interim fluorescent penetrant inspection (FPI) and sonic inspections. The sonic inspections were intended to further assist with monitoring the growth of the inclusions. After the completion of the second set of 5,000 spin cycles (10,000 total), the disks would again receive FPI and sonic inspections. If the sonic inspections indicated that the defects were not growing, adjustments to the test speeds would be made prior to continuing testing. During the testing, the disks' vibration amplitude and phase were monitored in an attempt to identify the onset of crack growth and to halt the testing before the cracks grew to rupture and risk damaging the fracture surface.

#### 4.4.3 Test Results.

All three disks completed their initially planned 10,000 cycles of testing without a rupture and without strong conclusive evidence of crack propagation. Since disk SB-6, which was tested first, did not indicate any growth, the speed of the other two disks was increased for their initial 10,000 cycles of testing.

In addition to the normal incidence ultrasonic (UT) inspections initially planned, angled UT scans were performed at each inspection interval starting at 5,000 cycles. The response signal of the angled scans separates as a crack extends out from the core. Signal separation was observed with disks SB6 and B3W2E at 5,000 and 10,000 cycles, but disk B1BW3B did not indicate any signal separation at 5,000 or 10,000 cycles. FPI inspections of all three disks did not indicate any surface-connected cracks.

While the angled scans did indicate some possible crack growth after 10,000 cycles, the normal incidence inspections were inconclusive at the time, and the Test Devices crack monitoring system had not indicated any crack growth. Specimen testing during TRMD-I had indicated that stresses of 75-100 ksi were required to initiate crack growth from embedded HA inclusions. During the first 10,000 cycles of testing, predicted stresses at the inclusions ranged from 40 to 55 ksi. The speeds were increased to generate stresses of 75 ksi at the locations of the inclusions, and the disks were spun for an additional 7,500 cycles.

All three disks containing embedded HA inclusions successfully grew cracks from the inclusions. Disks SB6 and B3W2E both burst prior to completion of the planned 7,500 additional test cycles at increased speeds but tested beyond the initial life predictions. The crack monitoring system did not indicate any crack growth in either of these tests prior to a vibration amplitude spike during the final cycle when the disks burst.

Disk B1BW3B completed, without a burst, 17,500 total cycles of spin testing (10,000 cycles at 18,000 max rpm and 7,500 cycles at 24,100 max rpm). Inspections at Pratt & Whitney gave mixed results, but were generally consistent with significant crack growth. Multizone and shear scan inspections at GEAE also indicated crack growth. Testing of disk B1BW3B was therefore discontinued, and the disk was cut open for fractography rather than risk damaging the fracture surface with continued testing.

#### 4.4.3.1 Post-Test Fractographic Inspections.

Disks SB6 and B3W2E were shipped to Pratt & Whitney for fractography after bursting in the spin rig. The goals of the fractography were to evaluate the crack growth from the embedded HA inclusions to identify the origin location of the fracture, map the size and shape of the inclusions, and determine the number of striations on the fracture surface. The fractography was performed by visual inspection with the assistance of a Scanning Electron Microscope (SEM). Prior to completing the fractography on the spin disks, two coupon specimens previously fatigue tested in TRMD-I were assessed to provide a baseline reference. Representative fractography of disk SB6 is shown in figure 4-5. The fatigue fracture initiated from the embedded HA seed. Higher magnification scanning electron microscope (SEM) fractography was completed in seven directions surrounding the inclusion. Fracture features were similar to those observed in the seeded coupon specimens except that no striations were observed in disks SB6 and B3W2E. Some limited striations were identified at a single location on disk B1BW3B.

#### 4.4.3.2 Flight Life Comparisons to Test Data.

Results from the fractographic assessments of the three spin disks were used to evaluate the crack growth predictions from Flight\_Life. Pre-test crack growth predictions were updated to include the measured HA core sizes and locations. No incubation was assumed in the analyses. The analyses assumed the initial crack was circular with a diameter equal to the diameter of the core (for SB6) or the maximum length of the core in the plane of the crack (for B3W2E and B1BW3B). The crack growth predictions for SB6 and B3W2E, which had both run to rupture, matched the test results within a few hundred cycles. The predictions for disk B1BW3B exceeded the actual test results by approximately 1000 cycles, still remarkable agreement. Contrary to the assumptions used by RISC to set up the initial HA anomaly size distributions, for both the seeded HA as well as the natural HA, the test experience indicated a closer correlation of initial crack size to the core size than to the total core plus diffusion zone size.

#### 4.4.3.3 Vacuum Fatigue Crack Growth Specimen Testing of Spin Disk Material.

To verify that the crack growth properties for the TRMD spin test disks were comparable to the assumptions in the analysis, vacuum fatigue crack growth tests were conducted on specimens machined from the spin disks. The plane of crack growth in the specimens was aligned with the crack growth plane (the axial/radial plane) in the spin disks. The tests were run at room temperature at a stress ratio of  $R = 0.1$  for each of the disks. A total of seven tests on three specimens from two disks were completed. The test results were very repeatable and agreed well with data generated at GE during TRMD-I [7].

Core            ————  
Diffusion zone    - - - -

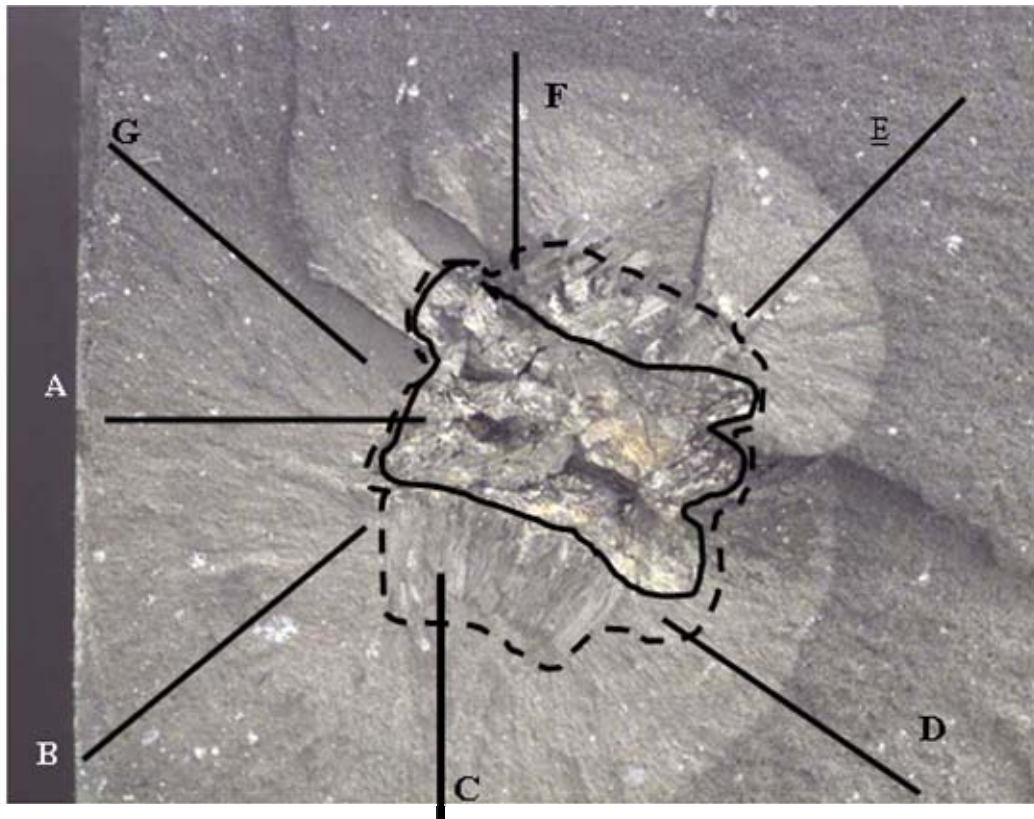
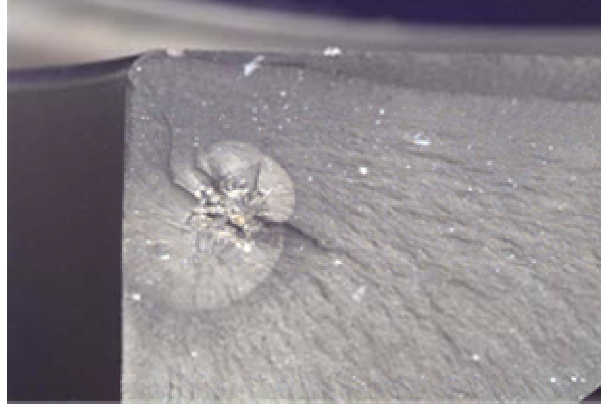


FIGURE 4-5. DISK SB6 FRACTURE SURFACE AT INCLUSION WITH SCANNING DIRECTIONS IDENTIFIED

#### 4.5 VACUUM FATIGUE CRACK GROWTH TESTING.

Many types of inherent anomalies in both nickel and titanium alloys occur at subsurface locations. Since any fatigue cracks that nucleate at these anomalies are not exposed to the atmosphere, they grow in a vacuum-like environment. Numerous researchers have noted a difference between fatigue crack growth rates in vacuum and in air. However, the data available in the literature are limited for both titanium and nickel alloys. Moreover, the available data are not sufficient to support a complete lifing system for fatigue crack growth in turbine engines, and

therefore it is difficult to accurately evaluate the risk associated with crack nucleation at sub-surface material anomalies. It is for these reasons that extensive characterization of titanium alloys was conducted in TRMD Phase I. TRMD Phase II extended this vacuum fatigue crack growth testing to nickel alloys that also included a powder metallurgy (PM) nickel alloy. A complete documentation of the test procedures and results is provided in Appendix K.

#### 4.5.1 Materials and Test Procedures.

Vacuum fatigue crack growth tests were performed during TRMD-II on four different rotor grade materials: Ti-6242, Waspaloy, IN-718 and PM U720. The Ti-6242 and Waspaloy were supplied by Pratt & Whitney (P&W), the IN-718 was supplied by GE Aircraft Engines (GEAE), and the PM U720 was supplied by NASA Glenn Research Center. Details of the material pedigrees are provided in Appendix K.

Tests were conducted for a matrix of temperatures and stress ratios at Honeywell and GEAE (GEAE performed only a portion of the IN-718 test matrix) following standard test procedures used at those companies to generate production data. Test conditions are summarized in table 4.1.

TABLE 4-1. SUMMARY OF VACUUM FCG TEST CONDITIONS

Material	Test Lab	Stress Ratios	Temperatures (°F)
Ti-6242	Honeywell	0.05	600
Waspaloy	Honeywell	-0.5, 0.05, 0.5	500, 800, 1200
IN-718	GE, Honeywell	0, 0.5, 0.7	75, 600, 1000, 1200
PM U720	Honeywell	0.05, 0.5	800

Although the tests were conducted at different sites, similar test procedures were followed. Region II (Paris regime) tests were conducted with small surface crack tension, SC(T), specimens, also known as Kb bar specimens. Tests in the near-threshold regime were conducted at Honeywell on the same SC(T) geometry and at GE on a single edge notch button head (SENBH) specimen. Details of specimen geometries are provided in Appendix K.

Crack lengths were monitored using the direct current electric potential drop method, with crack sizes post-test corrected from visual measurements of marked initial and final crack dimensions on the fracture surfaces. Stress intensity factors were calculated from established solutions in the literature. Tests were conducted under either constant load or constant  $\Delta K$ -gradient (increasing or decreasing) at constant R. Vacuum levels were better than  $10^{-7}$  Torr for all tests. Test frequency was 0.33 Hz (20 cpm) for all tests.

#### 4.5.2 Results.

A complete set of graphical and tabular results is provided in Appendix K. For convenience, selected results are provided below.

#### 4.5.2.1 TI-6242.

Two tests were conducted with the coarse-grained Ti-6242 supplied by P&W. Results are presented in figure 4-6 in comparison with the TRMD-I results for Honeywell's fine grained Ti-6242.

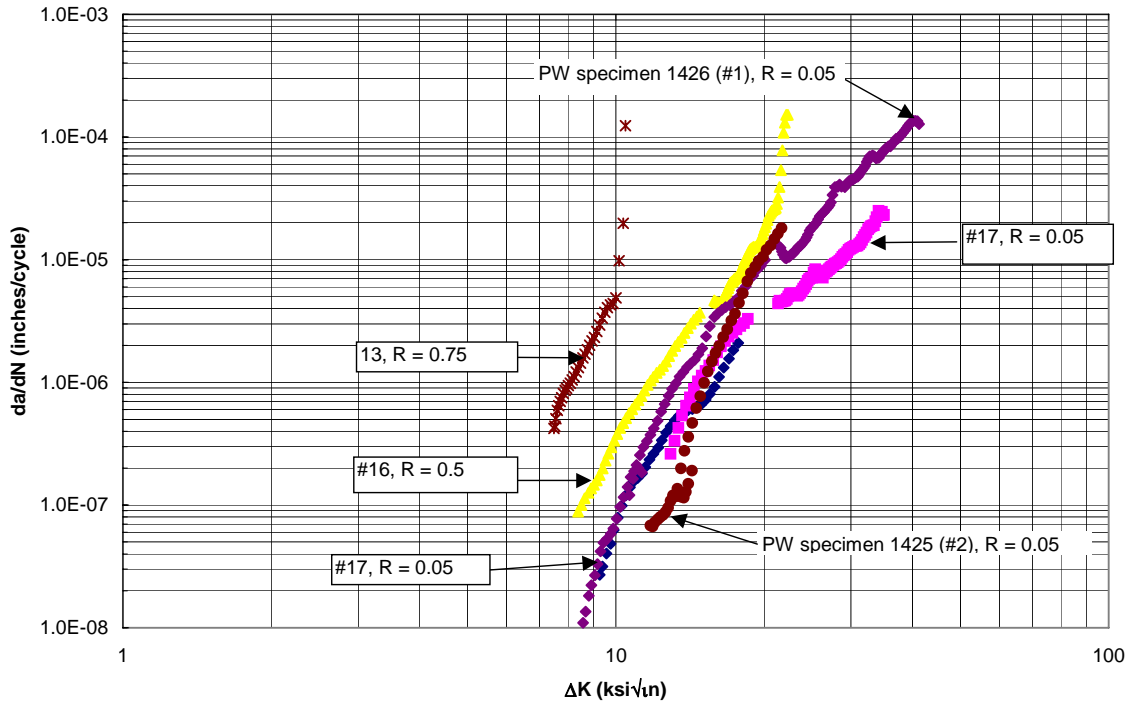


FIGURE 4-6. VACUUM FCG RESULTS FOR P&W AND HONEYWELL TI-6242 MATERIALS AT 600°F

#### 4.5.2.2 WASPALOY.

A total of 18 vacuum fatigue crack growth tests and one air fatigue crack growth test were conducted on Waspaloy. The effects of temperature and stress ratio on crack growth rate are summarized in a series of graphs in Appendix K. Representative results for  $R = 0.05$  at three different temperatures are shown in figure 4-7. Figure 4-8 directly shows the effect of environment—air vs. vacuum—at 500°F and  $R = 0.05$ .

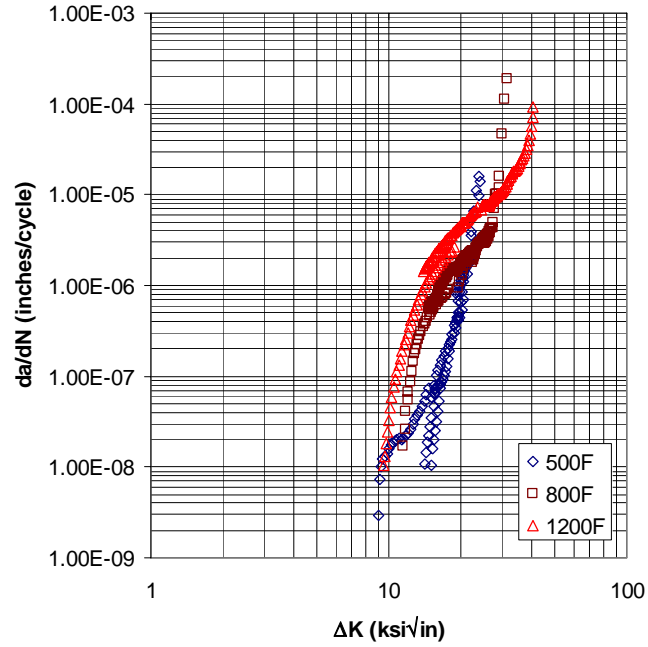


FIGURE 4-7. VACUUM FCG RESULTS FOR WASPALOY AT  $R = 0.05$  AND THREE DIFFERENT TEMPERATURES

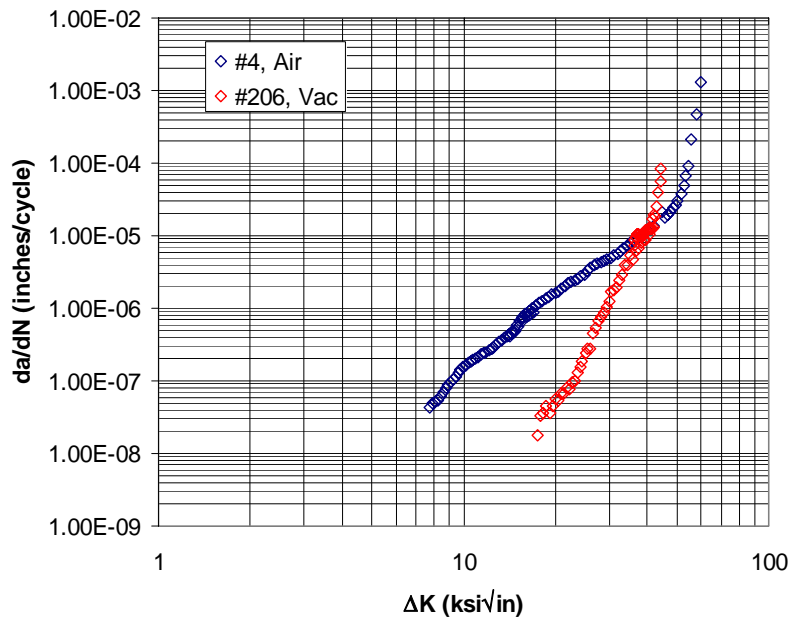


FIGURE 4-8. EFFECT OF ENVIRONMENT (AIR VERSUS VACUUM) ON FATIGUE CRACK GROWTH RATES IN WASPALOY AT 500°F,  $R = 0.05$

### 4.5.2.3 IN-718.

A total of 13 successful vacuum fatigue crack growth tests were completed on IN-718. Testing was performed at GE and Honeywell. Representative results at  $R = 0$  for four temperatures are shown in figure 4-9.

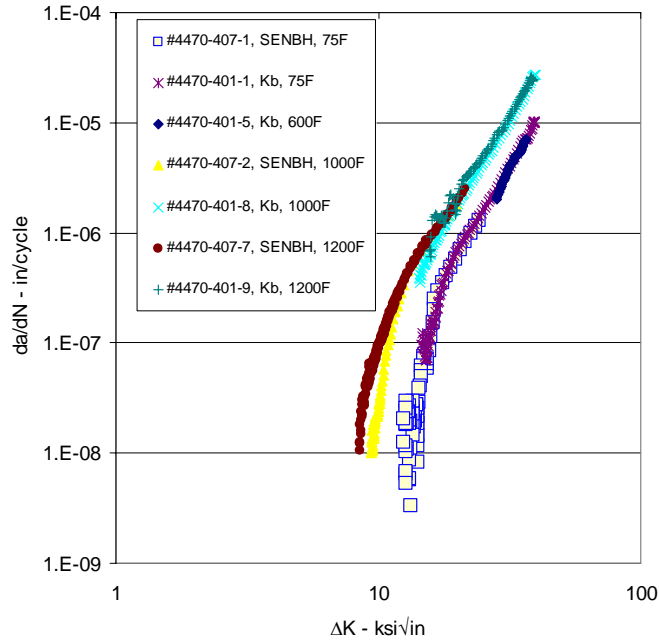


FIGURE 4-9. VACUUM FCG RESULTS FOR IN-718 AT  $R = 0$  AND FOUR DIFFERENT TEMPERATURES

### 4.5.2.4 PM U720.

A total of five vacuum fatigue crack growth tests were completed on PM U720. The PM U720 material pedigree and test data are export controlled. Hence, this information is not included in this report. However, the data are available from SwRI after adequate demonstration of export authorization.

## 4.6 NICKEL ANOMALY FATIGUE TESTING.

The TRMD team has been working with nickel melters to obtain Waspaloy or Inco718 material with sonic indications to support a fatigue test program. The intent of the test program is to investigate the fatigue initiation and propagation of cracks from embedded anomalies in conventional nickel alloys. Existing quality control specifications were complied with to allow for required material cut-ups to disposition suspect indications. These requirements, which are necessary for flight safety, limited the availability of suspect material that could be obtained.

In two batches of material, after the required number of cut-ups was completed, additional material remained with sonic or surface indications that could be forged and machined into fatigue specimens. The first batch of double melt Inco718 material included eight billet sections (mults) with nine indications from three different heats (table 4-2). Prior to obtaining the

material, DEFORM analyses were performed, which confirmed that these indications were at acceptable depths for machining of fatigue specimens from pancakes to be forged from the mults. The mults were then delivered to Pratt & Whitney for additional ultrasonic inspections, forging into pancakes, and machining of test specimens.

TABLE 4-2. PRODUCTION UT INSPECTION RESULTS FOR NI BILLET INDICATIONS

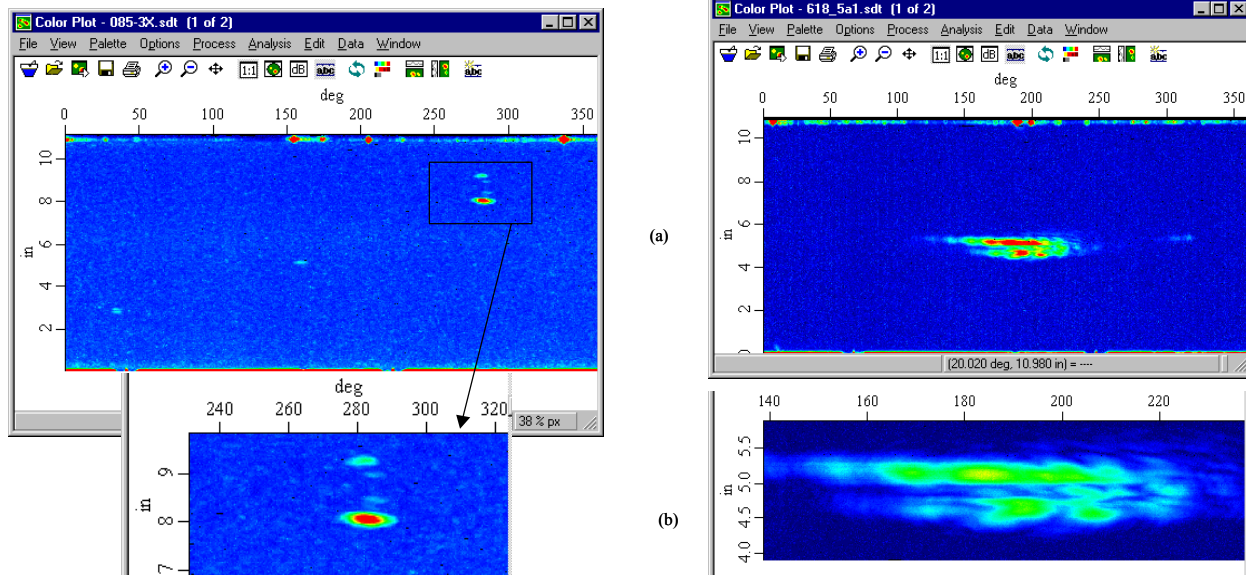
Indication	Heat	Billet Diameter (in)	Maximum UT Response	Radial Depth (in)	Length (in)	Axial Location (in)
1A	804085	8.0	110% of #2 FBH	3.5	0.520	4.5 to 5
2X	804085	8.0	110% of #2 FBH	2.65	0.320	7.6 to 7.9
2X	804085	8.0	100% of #2 FBH	2.65	0.320	8.1 to 8.4
3A	804085	8.0	110% of #2 FBH	3.9	0.500	3.5 to 4.0
3X	804085	8.0	160% of #2 FBH	2.7	0.700	2 to 2.7
5A	804618	8.07	112% of #2 FBH	3.7	0.275	5
5A	804618	8.07	75% of #2 FBH	3.8	0.230	5
5A	804539	7.874	75% of #2 FBH	2.2	0.205	5
5X	804539	7.874	75% of #2 FBH	1.6	0.216	5

The second batch of Inco718 material was identified near the end of the program and consists of billets with approximately two or three freckles per cross section. The freckles were identified through surface inspections of the ends of the billets, and it is suspected that the freckles may run the full length of the mults. This material was procured under TRMD Phase II and will be forged into pancakes in a subsequent program with the FAA.

Both the sonic indications and the freckles will be tested in this subsequent program. No triple melt Inco718 or Waspaloy was obtained during TRMD Phase II for fatigue testing of anomalies.

#### 4.6.1 Additional UT Inspection of Inco718 Mults.

After receipt of the Inco718 mults with production sonic indications, an additional set of laboratory UT inspections was completed at Pratt & Whitney. These additional inspections would be used as a baseline for comparison in a common environment with subsequent UT inspections of pancakes forged from these mults. C-scan images were recorded for each of the mult inspections at Pratt & Whitney. Figure 4-10 includes representative c-scan images of two of the mults. Along with the maximum responding indications reported from the production inspections, additional smaller indications on some of the mults were identified from the c-scan images. Mult 804085-3X contained five additional indications along with the one high responding indication as identified in figure 4-10. A full discussion of the Pratt & Whitney UT inspections of the mults is included in Appendix L.



804085-3X

804618-5A1

FIGURE 4-10. C-SCAN IMAGES FOR MULTS 804085-3X AND 804618-5A1

#### 4.6.2 UT Inspection of Inco718 Forgings.

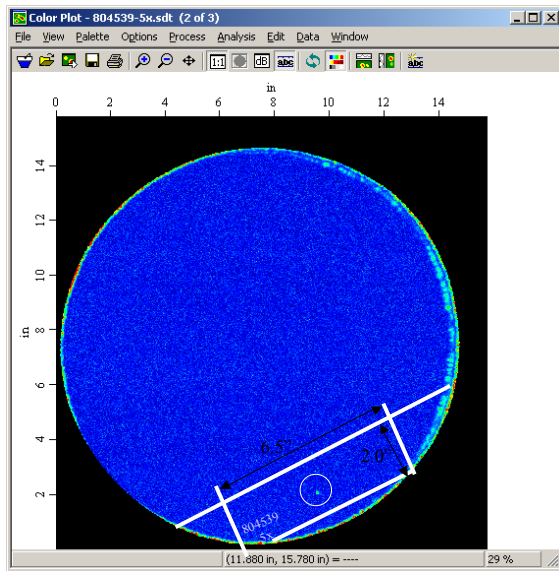
After the mults were forged to the pancake shape of 16” diameter and 2.9” thick, UT inspections were performed to determine the positions of the indications. Indications were seen in only three of the eight pancakes. Several attempts were made to use zoned scanning and angle scanning to try to identify the positions of the previous indications in the other five pancakes. DEFORM analyses were used to help focus the locations in the pancakes to search for the indications. It appears that the indications in those five mults may have been either voids that closed during the forging operation, or, the ultrasonic indications in the mults were caused by large grains that were refined during recrystallization at the pancake forging step. Table 4-3 contains a summary of the maximum UT responses for the production and laboratory billet inspections and forging inspections. It is interesting to note that the indications found in the pancakes are not always the highest responding indications in the mults. Indication 804085-3X, shown in figure 4-10, was one of the strongest indications in the mults, yet was not identified in the pancake. A more comprehensive discussion of the forging inspections is included in Appendix L.

For the three pancakes with identified indications, blanks with dimensions of approximately 2” x 3” (thickness) x 6” with the indications centered were cut from the pancakes to make round LCF samples with a 0.5” diameter gage section. Figure 4-11 contains representative c-scan images of two of the pancakes with identified indications in the forging and includes illustrations of the orientation of the blanks machined from the pancakes. The blanks were re-scanned and the positions of the indications verified for production of the LCF samples. As the finished specimens are machined, attempts will be made to center the indications within the gage section and, where possible, to keep the anomalies sub-surface.

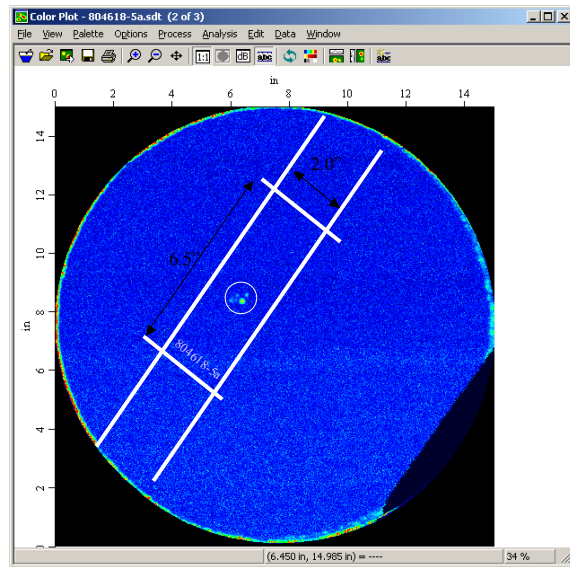
TABLE 4-3. MAXIMUM UT RESPONSE FOR BILLET AND PANCAKE INDICATIONS

Indication	Heat	Maximum Production UT Response in Mults	Maximum Laboratory UT Response in Mults	Maximum Laboratory UT Response in Pancakes
1A	804085	110% of #2 FBH	60% of #2 FBH	Not Found
2X	804085	110% of #2 FBH	130% of #2 FBH	Not Found
3A	804085	110% of #2 FBH	90% of #2 FBH	Not Found
3X	804085	160% of #2 FBH	190% of #2 FBH	Not Found
5A	804618	112% of #2 FBH	200% of #2 FBH	125% of #1 FBH*
5A	804618	75% of #2 FBH	40% of #2 FBH	Not Found
5A	804539	75% of #2 FBH	60% of #2 FBH	50% of #1 FBH*
5X	804539	75% of #2 FBH	55% of #2 FBH	100% of #1 FBH*

\* C-scan images from pancake UT inspections show larger indications than maximum UT response amplitude



804539-5X



804618-5A

FIGURE 4-11. C-SCAN IMAGES FOR MULTS 804539-5X AND 804618-5A

#### 4.7 THERMO-MECHANICAL FATIGUE CRACK GROWTH TESTING.

Aircraft turbine engines operate in a complex thermal environment, and frequently the stress and thermal cycles are not totally in phase. The so-called “stress rainflow” method is often used to define cycles for fatigue crack growth analysis. In this method, the major cycle is defined in terms of the maximum stress in the cycle and the temperature at the maximum stress time point. There is often a time point later in the mission with a higher temperature but a lower stress, and this characteristic of the history may be ignored by the stress rainflow method. It is possible, however, that this higher temperature may have some impact on the FCG rate.

In order to investigate this issue further, the TRMD program team conducted an exploratory study of thermo-mechanical fatigue (TMF) crack growth. The common high-temperature, nickel-based superalloy Inconel 718 was chosen for investigation. A simple matrix of isothermal and TMF experiments was designed for the specific purpose of determining if the out-of-phase thermal history had a significant influence on FCG rates, and if the stress rainflow method was an adequate means of characterizing the damage in TMF cycles. All crack growth tests and analysis were performed at GE Aircraft Engines. Further details are provided in Appendix M.

Crack growth specimens were obtained from two compressor rotor spool production forgings. The grain size was estimated to be ASTM GS 10. Crack growth testing was performed using a Kb bar specimen geometry, with crack length measurement by the direct current electrical potential drop technique.

Four different TMF cycle types were employed. TMF cycles were designed to balance (a) being representative of engine cycles, (b) having significantly different lives than comparable isothermal cycles, (c) slow thermal cycling to avoid excessively high transient thermal stresses, and (d) test times within program costs. The typical duration of a single TMF cycle (all types) was approximately 210 seconds.

The first cycle in all four TMF types was conducted with a maximum stress of 120 ksi and a temperature of 450°F. In Type I, a second isothermal cycle was conducted at 1100°F with a maximum stress of 60, 80, 100, or 120 ksi. In Type II, the second cycle was a thermal cycle from 450°F to 1100°F and back to 450°F, all at zero stress. In Type III, the second cycle was isothermal at 1100°F and involving cycling to a compressive stress of -60 ksi. In Type IV, the first cycle is unloaded only to 60 ksi, the specimen is held at 60 ksi while heated to 1100°F, and then the specimen is unloaded to zero stress at 1100°F. Isothermal tests were performed at 450°F, 800°F, and 1100°F. Two experiments were planned for each of the ten test conditions, and 19 of the planned 20 experiments were performed successfully.

The six isothermal FCG tests indicated that FCG rate increases with increasing temperature. The 800°F crack growth rates were slightly higher than the 450°F results. The 1100°F crack growth rates were much higher than those at 450°F; at low to intermediate  $\Delta K$ , the 1100°F crack growth was approximately 10 times faster than the 450°F results.

The lifetimes of all TMF tests were predicted by the conventional stress rainflow method, and these predictions are compared with the actual test lives in figure 4-12. Also shown on this figure are predictions and test results for additional TMF tests on René 95 and René 88DT conducted independently by GE Aircraft Engines (not under TRMD-II). The figure shows that the stress rainflow predictions exhibited a non-conservative bias in the predictions. In other words, TMF cycles produced faster crack growth rates, on average, than were predicted by the stress rainflow method. The bias was less severe for IN-718 than for the René alloys.

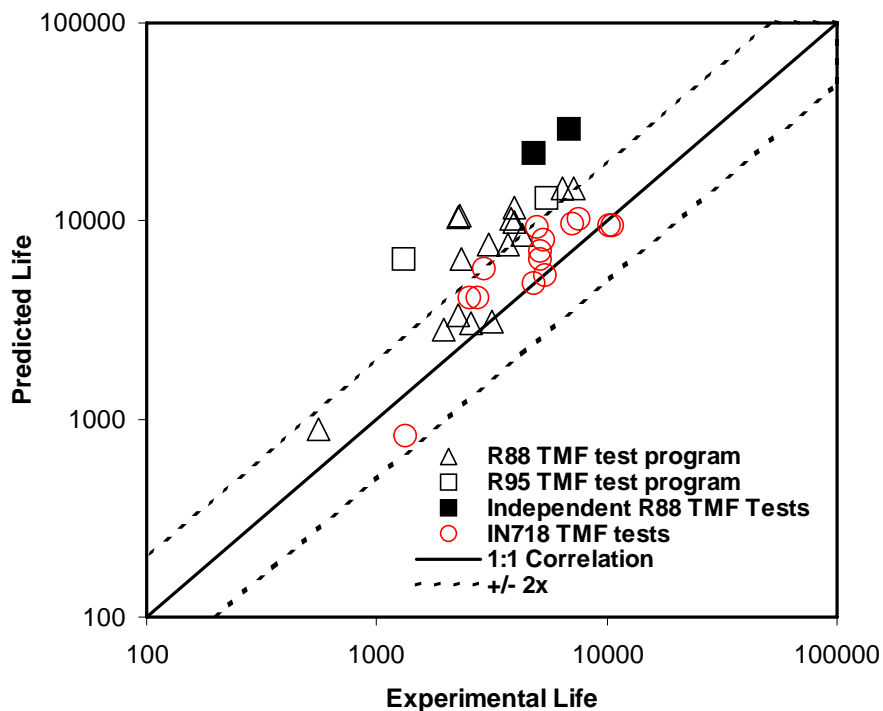


FIGURE 4-12. COMPARISON OF EXPERIMENTAL LIFETIMES WITH PREDICTIONS BASED ON THE CONVENTIONAL STRESS RAINFLOW METHOD FOR IN-718, RENÉ 95, AND RENÉ 88DT SUBJECTED TO TMF HISTORIES

#### 4.8 ENHANCEMENT OF FLIGHT LIFE MODULE.

The Flight\_Life module that performs fracture mechanics analysis in DARWIN was initially developed during TRMD Phase I and was included in all previous versions of DARWIN developed under TRMD-I. The core analysis capabilities of Flight Life—crack growth equations, mean stress models, temperature models, crack growth integration schemes, etc.—remained unchanged in TRMD Phase II. However, the available stress intensity factor (SIF) solutions in Flight\_Life were significantly enhanced and expanded in TRMD-II, and some other new features were introduced.

##### 4.8.1 Stress Intensity Factor Solutions.

Table 4-4 summarizes all of the SIF solutions that were either introduced or enhanced during TRMD-II, along with a notation of the DARWIN version in which the new or improved solution first appeared. These new capabilities comprise enhancements in the available geometries, in the handling of arbitrary stress gradients, and in computational speed.

TABLE 4-4. SUMMARY OF NEW OR ENHANCED SIF SOLUTIONS DEVELOPED DURING TRMD-II

Solution	Description	Type	First DARWIN Version	Comments
SC02	Surface crack in plate	UWF/Poly	4.0	Wider $a/c$ and $a/t$ limits; replaced by SC17
SC15	Central surface crack at hole (wide plate)	UWF	4.0	Superseded by SC18
SC17	Surface crack in plate	UWF/Poly	5.0, 5.1	Better accuracy, wider $a/c$ in 5.1
SC18	Surface crack at offset hole (finite plate)	UWF	5.0, 5.1	Supersedes SC15 (better accuracy in 5.1)
CC01	Corner crack in plate	Bilinear	3.4	Only improved speed
CC05	Corner crack at hole (wide plate)	UWF	4.0	Superseded by CC08
CC08	Corner crack at offset hole (finite plate)	UWF	5.0, 5.1	Supersedes CC05 (better accuracy in 5.1)
CC09	Corner crack in plate	BWF/Poly	5.2	First bivariant solution
CC10	Corner crack at offset hole (finite plate)	BWF	6.0	Second bivariant solution
EC02/03	Embedded crack in plate	UWF/Poly	4.0	Added WF form and increased $a/c$ limits
TC11	Through crack at hole (wide plate)	UWF	4.0	Superseded by TC12
TC12	Through crack at offset hole (finite plate)	UWF	5.0	Extends and supersedes TC11
Notes: UWF = univariant weight function, Poly = polynomial, BWF = bivariant weight function				

#### 4.8.1.1 Available Geometries.

All SIF solutions in TRMD-I were for cracks in simple rectangular cross-sections. In order to address the problem of surface damage at bolt holes, new SIF solutions for cracks in the bore of a round hole were required. A first set of crack-at-hole solutions for corner, surface, and through cracks at centered holes in wide plates (sufficiently wide to neglect any finite width effects) were introduced in DARWIN 4.0. A second set of solutions for corner, surface, and through cracks at off-center holes in finite width plates were introduced in DARWIN 5.0, including the effects of a surface crack that is off-centered through the plate thickness. The finite geometry correction scheme was further improved and modified solutions introduced in DARWIN 5.1. These implementations included all of the appropriate geometry transitions (surface to corner, corner to through). All of these new crack-at-hole solutions were based on a univariant weight function method, with most reference solutions generated using advanced three-dimensional boundary element software for fracture mechanics analysis, FADD3D [10]. Further details of the mathematical weight function formulation for these crack-at-hole solutions are provided in Appendix N.

The crack aspect ratio limits for embedded and surface cracks were increased several times, as noted in the discussions below.

#### 4.8.1.2 Arbitrary Stress Gradients.

All of the SIF solutions in TRMD-I were based on sixth-order polynomial representations of a stress gradient varying in one dimension only (so-called univariant), except for the CC01 corner-crack-in-a-plate solution (obtained from the NASGRO<sup>®</sup> fracture mechanics computer software [11]) with linear stress gradients along adjacent edges. However, some stress gradients encountered in practice are not satisfactorily represented by a polynomial expression. Therefore, new weight function formulations for the surface crack and embedded crack in a rectangular cross-section were derived and implemented in Flight\_Life. These formulations directly integrate the so-called weight functions with the actual finite element stress values along the crack line in order to calculate the SIF.

The new weight function formulation for the elliptical embedded crack in a plate in DARWIN 4.0 was based on the same solution set as the original polynomial solutions, except that the aspect ratio limit of  $a/c = 2$  was removed (currently any aspect ratio is permitted, and in the extremes, the SIF value properly approaches the corresponding through crack solution). The  $a/c = 2$  limit first introduced in DARWIN 3.3 was itself an increase from the original  $a/c = 1$  limit under TRMD-I.

The first implementation of a weight function solution for the semi-elliptical surface crack in a plate (SC02) was based on the reference solutions for the existing NASGRO SC02 solution, which gave slightly different results than the original Flight\_Life SC02 polynomial solutions. The NASGRO reference solutions were also supplemented to increase the aspect ratio limit from  $a/c = 1.0$  to 2.0 (here  $a$  is the maximum crack depth, and  $2c$  is the total surface length), and the Flight\_Life polynomial solutions were revised for consistency. Due to some lingering concerns about the accuracy and speed of this NASGRO solution, a completely new weight function solution was later derived for Flight\_Life based on a completely new set of reference solutions

generated using FADD3D. This new solution was introduced in DARWIN 5.0 as SC17, also including a new polynomial solution that was consistent with the new weight function solution for common stress fields. The aspect ratio limit of SC17 was increased from  $a/c = 2.0$  to 4.0 in DARWIN 5.1.

These univariant formulations (either weight function or polynomial) do not model variations in the crack plane stresses in any direction except for the specified gradient orientation. However, in some applications, the stresses may vary significantly in all directions on the crack plane. The development of efficient SIF solutions that can accurately accommodate this entirely arbitrary stress variation (so-called bivariant solutions) is an extremely challenging task. Previous attempts to solve this problem have all exhibited substantial accuracy and/or speed limitations.

A completely new formulation for bivariant weight function SIF solutions with superior speed and accuracy was derived under TRMD-II, and new reference solutions to support this formulation were generated using FADD3D for the quarter-elliptical corner crack in a plate (CC09) and the corner crack at a hole (CC10). Further details of the background, the mathematical formulation, and the resulting solutions are provided in Appendix N. This work represents a substantial advance in the state-of-the-art for engineering fracture mechanics analysis.

#### 4.8.1.3 Computational Speed.

Fracture mechanics life analysis can be computationally time-consuming, and the repetitive calculations required for probabilistic analysis can substantially increase the total computational burden. Improvements in SIF accuracy almost inevitably result in further computation expense. Weight function solutions, because they involve numerical integration of the crack plane stresses, are often much slower than polynomial solutions, which have been pre-integrated. A large matrix of reference solutions introduces data storage challenges, which can further compromise speed. As geometries become more complex and the number of degrees of freedom increases (e.g, plates with holes, finite width plates, offset holes, offset cracks), the storage requirements and the associated time penalties can mushroom. Bivariant solutions require two-dimensional numerical integration, which can dramatically increase the required computational time. In the extreme, all of this geometrical and analytical sophistication can be crippling.

Therefore, significant effort was expended during TRMD-II to improve the computational efficiency of existing and new SIF solutions. For example, the original NASGRO CC01 solution was modified for DARWIN 3.4 to increase its speed by about 8x without changing the results. The original NASGRO SC02 solution was also modified to increase its speed substantially, and the new SC17 solution for the same geometry exhibited a further increase in speed (compared to the improved SC02) of about 5x. A new storage and pre-processing scheme for large matrices of weight function reference solutions was introduced in DARWIN 5.1, and these numerical databases were converted to binary format in DARWIN 5.2 for additional increases in speed.

The dramatic increase in computational burden introduced by bivariant weight function solutions was addressed by developing a new dynamic tabular interpolation scheme. In this scheme, rather

than calculate new values of the SIF using the full numerical integration on each cycle in which the crack grows to a new size and shape, a small matrix of SIF solutions for  $a/c$  and  $a/t$  values in the vicinity of the initial conditions is generated at the beginning of the calculation. The specific SIF value needed on each cycle during the life calculation is extracted from this table using a rapid and highly accurate interpolation method, and the table is updated on an as-needed basis as the crack grows beyond the geometry limits of the initial table. The total computational burden can be dramatically decreased by this scheme—by several orders of magnitude for some problems. Further details are provided in Appendix N.

#### 4.8.2 Other Flight Life Enhancements.

The Walker interpolation method for stress ratio effects in DARWIN was only available for tabular data formats during TRMD-I. In DARWIN 3.3, this method was extended to all four existing crack growth equations in Flight\_Life. The Walker interpolation formulation was more recently modified for improved robustness under a few specific conditions (e.g., interpolation between positive and negative stress ratios when user-supplied data are not available at  $R = 0$ , and interpolation at stress ratios immediately adjacent to stress ratios at which data were supplied by the user). The new formulation is scheduled for release in a future DARWIN version.

An improved shakedown module was implemented in DARWIN 3.3. The old shakedown module redistributed stresses based on a force balance only, while the new module redistributes stresses based on equilibrium of both forces and moments. Further information about the new method is provided in the DARWIN on-line help system.

As cracks become large and approach instability conditions, the conventional linear elastic stress intensity factor can sometimes slightly underestimate the driving force for fracture, especially when maximum stresses are large, remaining ligaments are small, and the small-scale yielding assumptions of linear fracture mechanics are compromised. A simple correction to the SIF that compensates for this condition is to augment the crack size by one-half of the estimated size of the crack-tip cyclic plastic zone, based on conventional (monotonic) tensile properties, and then to recalculate the SIF with this effective crack length. This logic was first added to DARWIN 3.4. The effective crack size is used only for evaluation of crack transitioning (a local instability) or final (global) crack instability.

Enhanced error/warning tracking and handling was first implemented in DARWIN 3.4. These new schemes clearly document unusual conditions such as negative or zero physical dimensions, a crack larger than its plate, or a crack tip outside of the plate, while avoiding a crash of the code execution.

#### 4.9 STABILITY AND SIGNIFICANCE OF RESIDUAL STRESSES IN FATIGUE.

Some components contain residual stresses (RS) that were established prior to placing the component into service and which remain in place during the service life. These RS do not cycle as the applied loads cycle, and so they do not directly influence the amplitudes of the in-service cyclic loading. They do influence the mean or maximum value of the load in each cycle, and therefore they can have a major influence on fatigue.

Residual stresses can arise from many sources. Some RS are an inherent byproduct of the manufacturing process (e.g., welding). Sometimes additional steps are added to the manufacturing process for the specific purpose of inducing beneficial compressive RS at fatigue critical locations. Shot peening and related surface treatments such as laser peening, low plasticity burnishing, and deep rolling are common examples of this approach. Cold expansion of holes is also widely employed.

The conventional wisdom is that RS have relatively little influence on fatigue crack nucleation, but potentially a significant influence on FCG. The influence on FCG may be especially pronounced when the fatigue cracks are small and the driving force for FCG is near the grow/no-grow threshold. The effect of RS on stress-life behavior is complex. To the extent that the S-N curve is driven by crack nucleation behavior, the effects may be small, but to the extent that the S-N curve is driven by crack growth (including microcracks), residual stress effects may be large.

However, one of the biggest complications is that the initial RS inherent in, or induced by, the manufacturing process may not remain stable throughout the service life. The RS can relax and redistribute due to a variety of mechanisms. A single applied load that causes yielding in a region of RS (due to the superposition of residual and applied loads of the same sign) will result in changes in the RS upon removal of the applied load. Repeated cyclic loading can cause gradual changes in the RS over time, even if no single fatigue cycle induces local yielding. Exposure to elevated temperatures can also relax RS. Finally, extension of a fatigue crack through an initial residual stress field can cause significant changes in the RS under some conditions.

#### 4.9.1 Literature Survey.

A broad literature survey has been conducted of the current understandings of significant residual stress issues for fatigue lifetime, and the full text of the survey is provided in Appendix O. The survey focused explicitly on the stability of surface and near-surface residual stress fields under fatigue conditions, including redistribution and relaxation due to static mechanical load, repeated cyclic loads, thermal exposure, and crack extension. The implications of the initial and evolving residual stress state for fatigue behavior were addressed, with special attention to FCG. Brief attention was given, where appropriate, to the major approaches to FCG life analysis proposed and practiced in the literature.

The literature survey was based on a comprehensive (but not exhaustive) bibliography assembled over a period of several years and currently containing well over 300 citations.

This literature survey was not a definitive critical review. No attempt was made to evaluate the relative merits of the different explanations and models proposed, and no attempt was made to provide clear answers on important issues, beyond reporting the preponderance of the published opinions.

The scope of the survey was very broad. Primary attention was given to the RS resulting from four major classes of manufacturing operations: peening and related surface treatments, cold expansion of holes, welding, and machining. Special attention was given to aircraft gas turbine

engine materials and applications. However, materials and applications related to other products such as aircraft structures, welded steel structures, automotive components, and machinery have also been included, because the technical insights and quantitative models may be relevant to gas turbine engines.

#### 4.9.2 Observations and Conclusions.

A great deal has been observed, measured, modeled, and learned during the past fifty years about the stability of RS. Definitive explanations, and models are not yet available for all relaxation phenomena. Nevertheless, a critical reading of the literature leads naturally to a series of general observations and conclusions that should provide a solid foundation for further study, model development, and practical implementation.

First of all, it is clearly important to discern and separate the different relaxation phenomena: thermal effects, static mechanical load effects, cyclic load effects, and crack extension effects. The specific mechanisms are different for each of these different effects, and the various effects can superimpose. For example, the first cycle of fatigue loading may induce static relaxation effects, while subsequent load reversals can induce cyclic relaxation effects. A failure to discern and separate these different effects can lead to some confusion. Separation of the different phenomena facilitates simpler and more accurate modeling of each effect, and these simple models can often be superimposed.

The available literature provides insight into the significance of the various relaxation phenomena. For example, thermal relaxation effects do not appear to be extremely large for most practical applications. Some academic studies subjected materials to temperatures greater than their normal operating envelope and observed substantial relaxation, but relaxation at normal operating temperatures tended to be moderate.

Static relaxation effects appear to be relatively easy to identify and characterize based on knowledge of the initial residual stress field and the applied service loading. In general, compressive loading tends to relax beneficial compressive residual stress fields in proportion to the magnitude of the applied loading. Tensile loading typically has no effect on compressive RS unless the applied loads are extremely large.

Many of the pronounced cyclic relaxation effects identified in the literature appear to be static effects on the first loading cycle (e.g., compressive loads relaxing compressive peening RS). Once these static effects are set aside, the remaining true cyclic relaxation tends to be gradual and moderate unless the applied fatigue stress amplitudes are large.

The effects of crack extension on tensile residual stress fields are relatively easy to identify and understand. The effects of crack extension on compressive fields are not so clear and require further study.

No effort was made in this survey to perform a quantitative evaluation of the models proposed to characterize or predict residual stress stability. However, some general observations are in order. Simple thermal activation models have been developed to treat thermal relaxation effects, but their generality and truly predictive nature has not yet been established. It should not be difficult to formulate a general treatment of static relaxation based on simple mechanics arguments, but

this does not appear to have been done yet outside of idealized profiles or finite element models. Empirical models may be useful for focused, well-characterized cyclic relaxation problems. The more general numerical models proposed for cyclic relaxation are encouraging but require some further detailed study to evaluate their practicality. Tractable models have been proposed for relaxation of tensile residual stresses due to crack extension, but no well-established theory has yet been laid out for crack extension effects on compressive fields.

The available evidence suggests that, in practical engineering applications, induced RS due to cold expansion, peening, or related manufacturing techniques rarely relax fully to zero. Although some relaxation commonly occurs due to one or more mechanisms, so that final residual stress fields are rarely the same as the initial fields, some significant fraction of the initial RS often remains at the end of the relevant fatigue exposure. Static effects appear to be the most deleterious, and these should be easily predictable in most cases. Most of the severe degradation of RS reported in the literature appears to be attributable to unrealistically severe thermal or mechanical loading conditions.

Characterizing and employing the correct residual stress field is essential for accurate life modeling. It is clear that residual stress effects on S-N lifetimes and FCG lives can be very substantial. A life prediction based on an incorrect assumption about RS may be seriously in error. In view of the uncertainties associated with RS, appropriately conservative assumptions may be in order.

Established methods for modeling FCG in residual stress fields using weight function stress intensity factors and superposition techniques appear to provide satisfactory accuracy in many cases. Special attention must be given to stress ratio effects, and appropriate crack closure methods may be satisfactory for this purpose. Several complicating issues may require further attention, including the multi-dimensionality of stress fields, non-elliptical crack shapes, and crack face contact.

Finally, it is important to note that the effects of peening and related techniques, cold expansion, welding, and machining on fatigue behavior are not limited to residual stress effects, and this is especially true for S-N behavior. The same manufacturing processes that induce RS can also influence the surface quality, microstructure, and material condition, all of which may independently influence fatigue life.

## 5. PROBABILISTIC INTEGRATION DESIGN CODE AND DEVELOPMENT.

The DARWIN software was originally developed during TRMD Phase I to predict the risk of fracture associated with rare inherent anomalies in titanium aircraft engine rotors and disks. New capabilities were developed under TRMD Phase II to address anomalies associated with surface damage, as well as inherent anomalies in other materials that may occur more frequently than the hard alpha anomalies associated with titanium. In addition, a number of new capabilities were developed to improve the efficiency and accuracy of the probabilistic computations. A concise overview of the major DARWIN enhancements developed during TRMD Phase II is presented in this chapter and summarized by DARWIN version number in table 5-1. Additional details are provided in several appendices referenced where appropriate. Complete details are available in the DARWIN electronic help system (see section 5.5).

TABLE 5-1. SUMMARY OF DARWIN ENHANCEMENTS DEVELOPED UNDER TRMD-II

Version	Description
3.3	Internet distribution of software and manuals
3.4	Inspection transition, Monte Carlo confidence bounds
3.5	Restart, element subdivision, zone refinement
4.0	1D surface damage, anomaly aspect ratio, GUI plot export
4.1	Importance sampling confidence bounds, deterministic user-defined initial anomaly size, electronic help system, report generation, GUI database converter
4.2	PC and Linux versions, execute analysis code from GUI
5.0	Mission mixing, 3D surface damage, stress/temp multipliers
5.1	Parallel/batch processing, finite element filtering, execute ANS2NEU from GUI, support for additional 3D finite elements
5.2	3D bivariant stress visualization, linked shop visit times, keyword support
6.0	Probabilistic treatment of general inherent anomalies, crack formation module, 3D anomaly modeling, production inspection, sensitivity analysis

### 5.1 ENHANCEMENT OF DARWIN FOR SURFACE ANOMALIES.

Recent aircraft engine accident investigations have revealed that uncontained engine failures can be attributed to anomalies that are introduced by abusive machining practices. Industry experience suggests that surface damage can occur in bolt holes, and this topic is currently under investigation by the AIA RISC committee. Under the TRMD-II program, DARWIN was enhanced to address anomalies associated with surface damage. In contrast with inherent anomalies that may be present anywhere within a component, surface damage is usually present only on the surfaces of machined features. New capabilities were developed to define zones in terms of physical features (with a focus on cracks occurring at bolt holes), and to predict the risk of fracture associated with multiple features.

### 5.1.1 User Specified Surface Damage (1D Analysis).

The stress concentrations associated with bolt holes can have a significant influence on stress gradients, particularly near the surface of a component. The stress gradient modeling capability developed under TRMD-I for materials with rare inherent anomalies was based on values extracted from 2D finite element models and does not adequately address stress concentrations. A new capability was developed allowing the analyst to enter temperature and one-dimensional (1D) stress gradient values via tabular input. A new surface zone editor was also created to allow the analyst to specify the crack geometry and other zone-specific features.

### 5.1.2 3D Finite Element-Based Surface Damage (3D Analysis).

Three-dimensional (3D) finite element models (FEM) are often used to predict the stresses associated with complex geometries such as bolt holes. A capability was developed to extract stresses and temperatures from 3D FEM for application to surface damage-based risk assessment. As shown in figure 5-1, DARWIN was enhanced to allow the analyst to visualize a 3D FEM and select the location of a surface damage anomaly. DARWIN identifies the principal stress plane associated with the anomaly, and prepares a 2D image of the FEM normal to the principal stress plane. The 2D image can be used to assign zone properties using techniques developed previously for rare inherent anomalies. A number of 3D finite element types are supported by this capability, as indicated in table 5-2.

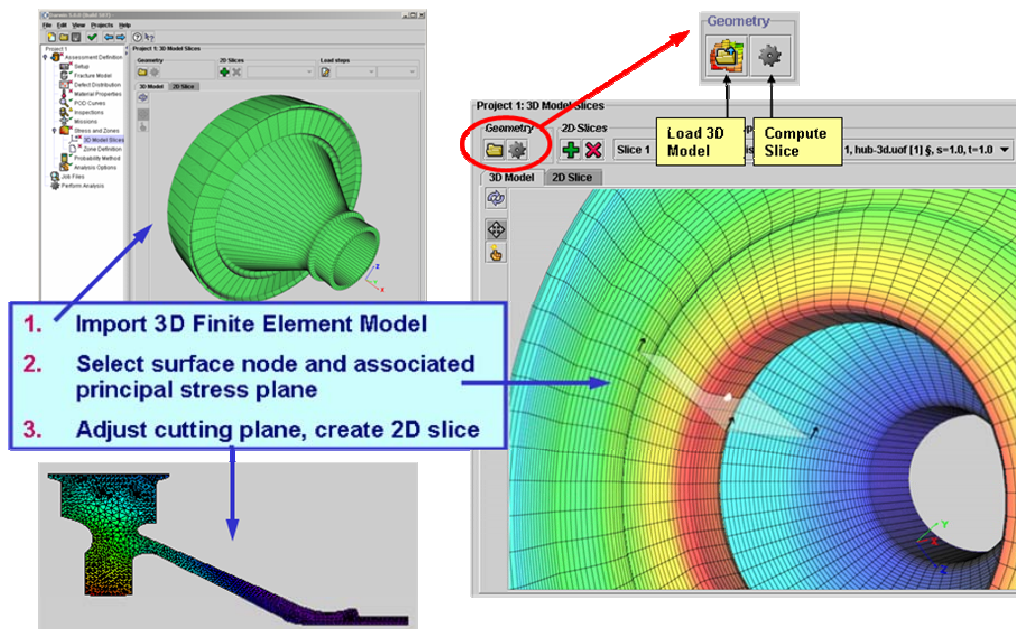


FIGURE 5-1. 3D SURFACE DAMAGE ANALYSIS CAPABILITY LINKED DIRECTLY TO A 3D FINITE ELEMENT MODEL

TABLE 5-2. SUMMARY OF 3D ELEMENT TYPES SUPPORTED IN DARWIN

ANSYS Element	Shape	SIESTA Type
Solid45	Brick	BRI8
	Prism	BRI8
Solid92	Tetrahedron	TETS N10
Solid95	Brick	VANS N20
	Prism	VANS N20
	Tetrahedron	VANS N20
	Pyramid	VANS N20

5.2 ENHANCEMENT OF DARWIN FOR GENERAL INHERENT ANOMALIES.

A number of new concepts were introduced in DARWIN to support risk assessment of materials with multiple anomalies. The risk assessment equations for zones and discs were modified to account for materials with potentially large numbers of anomalies. A crack formation module was developed to allow users to implement and execute OEM specific crack formation algorithms in conjunction with DARWIN. Additional parameters were introduced to provide 3D modeling of anomalies and associated production inspections.

5.2.1 Probabilistic Approach.

The risk computations in DARWIN were developed for materials with relatively low anomaly occurrence rates, such that a disk has at most one significant anomaly. Since some materials may exhibit higher anomaly frequencies, modifications to the risk computations were implemented to account for multiple (i.e., unlimited) significant anomalies in a disk for both the Monte Carlo and Importance Sampling probabilistic methods (and associated confidence bounds). Details regarding the probabilistic treatment of multiple anomaly materials are presented in Appendix P.

5.2.2 Adaptive Optimal Sampling Methodology.

A methodology was developed to improve the computational efficiency of the probabilistic computations associated with general inherent materials. The methodology, described in Appendix Q, focuses on variance reduction of sampling-based series system reliability predictions based on optimal allocation of Monte Carlo samples to individual failure modes. It is demonstrated for a simple series system, in which it is shown that the variance of the system failure probability is reduced compared to a uniform sampling approach, due to the reduced variances in the failure probabilities associated with the weakest members. The adaptive optimal sampling methodology is also illustrated for a gas turbine engine disk modeled using several methods to estimate the failure probability in each zone prior to optimal sampling. It is shown that the computational accuracy of the method does not appear to depend on the initial failure probability estimate, whereas the computational efficiency is highly dependent on the initial failure probability estimate.

### 5.2.3 User-Supplied Crack Formation Module.

Rare inherent anomalies in titanium alloys generally exhibit negligible crack formation lives; fatigue cracks nucleated at anomalies can begin growing almost immediately when the component enters service. However, for anomalies in other materials, the crack formation life may be non-negligible and must be considered in the risk computation to avoid over-conservatism. Several OEMs have developed methods to predict anomaly crack formation life, but these methods are proprietary and cannot be shared with other users. A Crack Formation Module (CFM) was therefore introduced in DARWIN to allow users to link OEM-specific crack formation algorithms with DARWIN (figure 5-2). The CFM and associated data are developed and maintained by the individual OEMs. During run time, DARWIN communicates with the CFM to obtain the crack formation life associated with an anomaly with specified temperature and applied stress values.

The CFM is executed as a separate program that receives input from DARWIN. The following data are passed from DARWIN to the CFM: (1) anomaly global coordinates and distance to the nearest free surface of the fracture mechanics plate, (2) anomaly dimension ( $a$ ,  $c$ ) in the crack plane, (3) six components of stress at the anomaly location for each load pair, and (4) temperature at the anomaly location for each load pair. The following data are passed from the CFM to DARWIN: (1) crack formation life for entire history, and (2) crack dimensions at the end of crack formation life.

Linking two independent computer programs together is a nontrivial task, particularly when multiple platforms and associated operating systems must be supported. One approach is to use a FORTRAN link algorithm, but this often requires the sharing of source code. Another approach is to execute one program from another via a system call, but the computation time associated with this approach can be significant due to the excessive file read/write operations associated with passing information between the programs. As an alternative approach, an application program interface (API) can be used that allows two programs to share information without the need for ASCII input/output files. A Formation API was developed that links DARWIN with the CFM, allowing the two programs to be compiled separately. During run time, data is passed between DARWIN and the CFM via the Formation API. This approach provides efficient data exchange rates without the requirement to share source code.

### 5.2.4 3D Anomalies.

The anomaly distribution architecture in previous versions of DARWIN was based on the single degree-of-freedom distributions for rare anomalies associated with titanium materials (described in AC 33.14-1) and surface damage (currently under development by RISC). In order to address materials with generalized inherent anomalies, additional parameters were introduced to provide three-dimensional geometry modeling of anomalies using six degrees of freedom (length, two aspect ratios, and three orientation angles). Each of the six degrees of freedom can be modeled as a random variable using several parametric formats (e.g., exceedance curve, lognormal, deterministic).

The anomaly distributions published in the Advisory Circular (AC 33.14-1) quantify the number of anomalies present following a specific production inspection. A capability was added to DARWIN allowing the user to specify the parameters of the anomaly distribution independent of the production inspection, and to specify a probability of detection (POD) for production inspection for anomaly distributions that do not have a pre-specified production inspection.

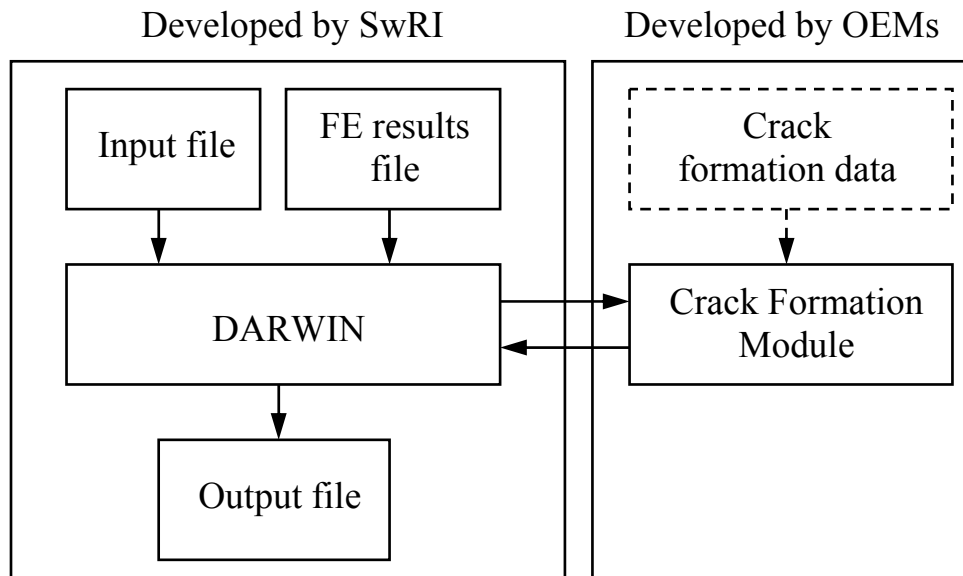


FIGURE 5-2. ARCHITECTURE LINKING THE USER-SUPPLIED CRACK FORMATION MODULE TO DARWIN

### 5.3 GENERAL DARWIN ENHANCEMENTS.

#### 5.3.1 Probabilistic Methods.

A number of probabilistic enhancements were developed to improve the overall efficiency and accuracy of the risk assessment computations, including optimal sampling, importance sampling, and probabilistic confidence bounds. A number of enhancements were also developed to provide the engineer with additional information regarding the influences of design variables on overall risk, such as probabilistic sensitivities and conditional failure analysis.

##### 5.3.1.1 Confidence Bounds.

Confidence bounds for Monte Carlo simulation and Importance Sampling were introduced in DARWIN versions 3.5 and 4.1, respectively. For a specified number of samples, the Importance Sampling confidence bounds are narrower than those associated with Monte Carlo simulation, indicating a more accurate solution. These bounds provide an estimate of the accuracy associated with sampling-based probabilistic methods. Further details on the confidence bounds in DARWIN are provided in Appendix R.

#### 5.3.1.2 Importance Sampling.

The DARWIN Importance Sampling method was enhanced to provide improved efficiency and accuracy. A complete description of the DARWIN importance sampling method, including a summary of recent enhancements, is provided in Appendix S.

#### 5.3.1.3 Probabilistic Sensitivities.

The probability of fracture is influenced by several random variables that are described in both empirical and parametric terms. Complete analytical expressions were developed that describe the sensitivity of the probability of fracture to changes in various parameters associated with the random variables. Further details are provided in Appendix T.

#### 5.3.1.4 Optimum Number of Samples per Zone.

A technique was developed to reduce the variance associated with the probabilistic computations for titanium materials. The technique, described in Appendix U, provides an optimal allocation of Monte Carlo samples to individual zones. It is shown that reallocation of samples based on risk contribution factors or an optimal approach can significantly reduce the total number of samples required for a specified accuracy. In addition, a hybrid approach is presented in which optimal sampling is combined with a semi-automated zone refinement procedure. This approach is illustrated for an aircraft rotor disk in which it is shown that zone refinement influences mean disk risk, whereas optimal sampling influences disk risk variance.

#### 5.3.1.5 Conditional Failure Analysis.

When the DARWIN importance sampling method is used, the ranges of random variables associated with failure must be identified to efficiently quantify the influence of inspection. This information can be reviewed using a conditional failure analysis (CFA) approach that provides valuable information to the engineer for improvement of component design, and helps to validate the mathematical models and probabilistic input distributions associated with reliability computations. A CFA technique is presented in Appendix V that is based on generation of conditional failure samples obtained during computation of component reliability. It provides a graphical description of the failure region that can be used for failure analysis.

#### 5.3.2 Zone Discretization.

During the TRMD-I program, a zone-based probabilistic approach was developed for risk assessment of rare inherent anomalies that (1) provided a conservative risk result regardless of the number of zones used, and (2) converged to a single risk value as the number of zones was increased. The practical implementation of the approach revealed the need for zones smaller than the finite elements defined in 2D FEM, and the need to subdivide zones into subzones. These capabilities were developed under TRMD-II.

### 5.3.2.1 Zone Refinement.

A capability was developed to subdivide zones into two or more subzones (figure 5-3). The size and shape of the subzones are based on the relative values of the stress contours of the original zone, and subzones inherit zone characteristics from the original zone. This capability significantly reduces the human effort associated with zone creation.

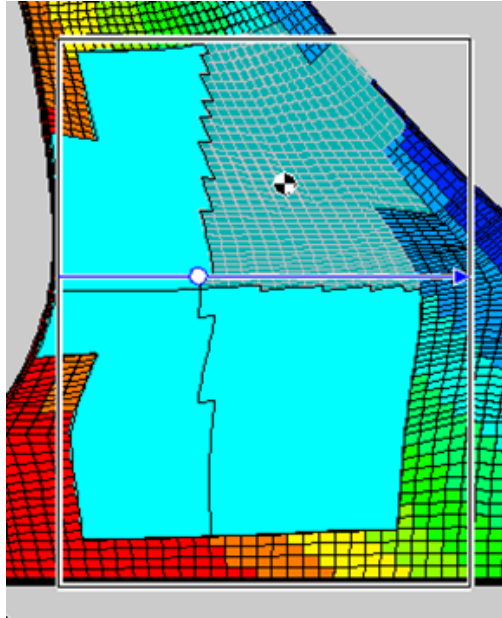


FIGURE 5-3. ILLUSTRATION OF ZONE REFINEMENT CAPABILITY

### 5.3.2.2 Element Refinement.

A zone in DARWIN can be no smaller than a single finite element, but in some cases the original finite element mesh (developed for purposes of stress analysis) is not sufficiently refined for zoning purposes. Therefore, capabilities were developed to further discretize a finite element mesh. As shown in figure 5-4, the capability can be used to define new elements at specific locations that are smaller than those in the original mesh. In addition, as shown in figure 5-5, the capability can be applied to an entire component to define the near-surface “onion skin” region for surface zone modeling. This capability reduces the human time that would be required to re-create finite element models to address specific zone modeling issues. The revised finite element mesh is used only for zoning purposes, and not for additional stress analysis.

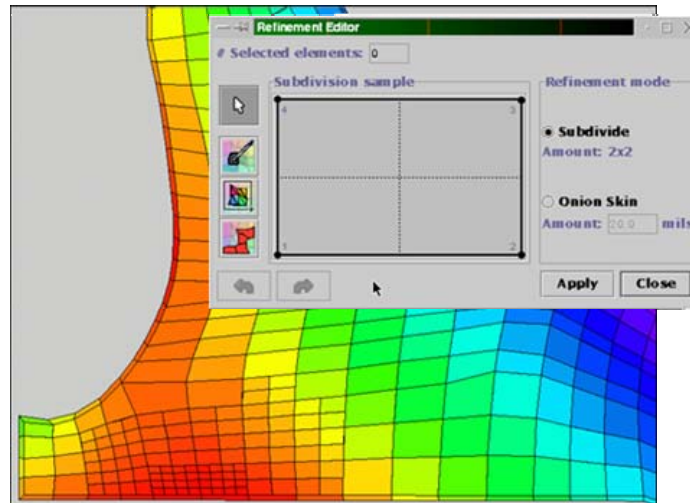


FIGURE 5-4. ILLUSTRATION OF THE ELEMENT SUBDIVISION TECHNIQUE

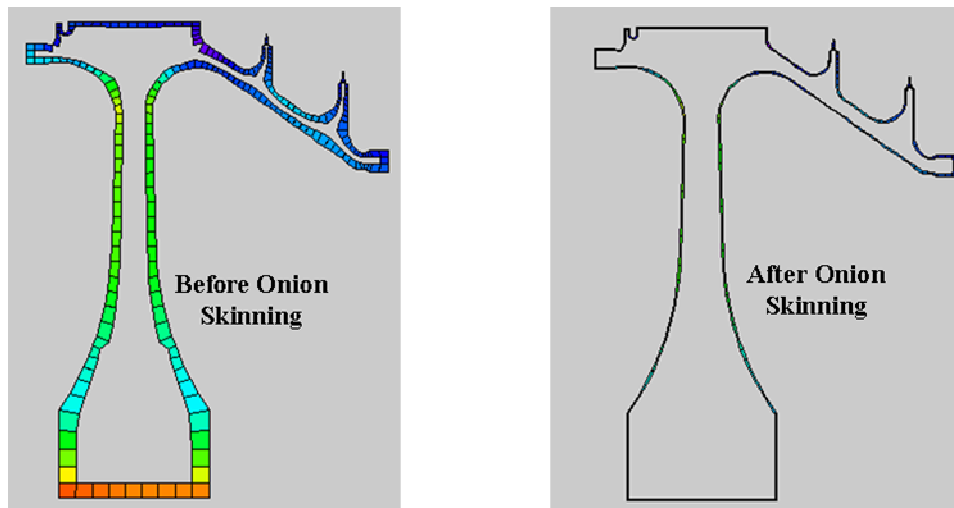


FIGURE 5-5. ILLUSTRATION OF THE ONION SKIN CAPABILITY

### 5.3.3 Inspection.

The inspection capabilities developed under the TRMD-I program were enhanced to provide more realistic treatment of shop visit practices in the following areas: inspection following transition of a subsurface to a surface crack, and linked shop visit times.

#### 5.3.3.1 Inspection for Transitioned Subsurface Cracks.

A variety of inspection methods may be applied to a component during a shop visit inspection, each with an associated probability of detection. When a crack initiates at the subsurface level, an ultrasonic inspection can be used to detect it. However, when a subsurface crack transitions to a surface, it may be more easily detected using a surface inspection method. A capability was developed in DARWIN allowing the analyst to specify different inspection techniques for the pre- and post- transition phases of subsurface crack growth.

### 5.3.3.2 Linked Shop Visit Time.

In previous versions of DARWIN, shop visit (inspection) times were modeled as independent random variables. This approach did not take into account the potential relationship among inspection times (i.e., the dependency of future inspections on the timing of previous inspections). A new capability was added to allow specification of inspection time in terms of a previous inspection. The capability was implemented in DARWIN for both tabular and normally distributed inspections.

### 5.3.4 Mission Mixing.

The fracture risk of rotors and disks is highly dependent on the usage history of an engine. During the design stage, a series of predefined missions are sometimes used to establish the design stresses for engine components. A capability was developed in DARWIN to allow analysts to define multiple missions and to combine them to define the mission mix for risk assessment computations.

#### 5.3.4.1 Stress and Temperature Scaling Factors, Zone Groups.

Several input formats were required to support OEM requirements for importing stress/temperature data, including (a) finite element data for all missions for the entire disk, (b) data from OEM specific regression tools for specified regions of the disk, and (c) combined scaling factors and finite element data for part or all of a component. A capability was implemented in DARWIN allowing the analyst to apply scaling factors to the stresses and temperatures associated with some or all of the load steps in a mission. Zone groups were also introduced to enable analysts to apply scaling factors to specific regions of a component.

#### 5.3.4.2 Mission Sequencing.

A capability was developed in DARWIN allowing the analyst to specify the number and sequence of missions in a mission mix. For crack growth computations, all of the missions are assembled into a single compound mission.

### 5.3.5 Stress Conversion.

The ANS2NEU stress conversion program developed under the TRMD-I program was relatively inefficient, and was limited to command line use on UNIX systems. It was significantly enhanced during the TRMD phase II program, including a new capability to select specific results for use in DARWIN.

#### 5.3.5.1 ANS2NEU Enhancements.

The ANS2NEU program and its companion RDB2UIF program were enhanced to support the PC-based Windows operating systems. These programs are used to translate ANSYS result files to neutral file format for input to DARWIN and previously were only supported for UNIX-based platforms. An interface was also developed to allow users to execute ANS2NEU directly from the DARWIN GUI.

#### 5.3.5.2 Element Filtering.

The ANS2NEU file translation program was enhanced to provide finite element filtering using element selection/extraction capabilities contained within the SIESTA program. It has the capability to include or exclude elements (and associated stress/temperature results) during translation based on specified ranges of Element ID, Material ID, or Load Case. The DARWIN GUI includes an interface allowing the analyst to specify these ranges.

#### 5.3.6 Stress Processing Enhancements.

A new DARWIN capability was developed to read stress and temperature data directly into memory (rather than perform multiple calls to the ANS2NEU program). By eliminating the time previously required for multiple read/write operations associated with ANS2NEU, the computation time associated with stress processing was significantly reduced (roughly 80% reduction). Other improvements such as dynamic array allocation also reduced the memory required to execute the DARWIN program.

#### 5.3.7 Data Management Enhancements.

A number of repetitive operations are often required as part of the design process. Since the computation time associated with risk assessment is nontrivial, data management enhancements were developed to reuse results from previous computations where practical. This consisted of a new restart capability coupled with a new Extensible Markup Language (XML) database.

##### 5.3.7.1 Restart.

A restart capability was developed that applies the results of previous computations to a DARWIN analysis to reduce overall computation time. During execution, restart compares the input information for a previous run to the current analysis for each zone. If the zone input data are identical, the zone risk results are extracted from the output database file (\*.ddb) of the previous run. This feature was developed for stress processing, deterministic crack growth, and risk assessment computations.

##### 5.3.7.2 XML Database.

The standard ASCII results file format developed under TRMD-I was sufficient for limited read/write operations associated with a single execution of DARWIN. However, this file format is inefficient for restart operations because the entire file must be processed for each retrieved data value. A new XML database system was developed under TRMD-II that provides efficient storage and retrieval of results. It uses a hierarchical format based on a series of address statements in which data values are stored and retrieved directly from memory, eliminating the time consuming read/write operations associated with the ASCII file format.

### 5.3.8 PC/Linux Versions of DARWIN.

The stress processing enhancements described in section 5.3.6 eliminated the need for the use of ANS2NEU in DARWIN. This led to the development of PC and Linux versions of DARWIN. The PC version has been verified on a number of Windows platforms (including 95, 2000, NT 4.0, and XP) and Linux platforms (SUSE 8.0). Fees from commercial DARWIN licenses were used to support the additional verification and code development tools associated with the development of these versions.

### 5.3.9 Parallel Processing Capability.

A parallel processing capability was developed that allows DARWIN to be executed simultaneously on multiple computers. During execution of the parallel processing feature, the DARWIN input file is reconfigured as a master and multiple slave files. The master input file contains the information for all zones, and the slave files contain information for a subset of zones. The slave files are distributed to multiple computers and executed to predict the risk associated with individual zones. For disk risk predictions, the master file combines results of the slave files using the restart capability described in section 5.3.7.1.

### 5.3.10 Influence of Finite Element-Based Random Variables.

The variability associated with applied stress values is currently modeled in DARWIN using a stress scatter factor applied to deterministic finite element stress results. However, a number of random variables can influence the finite element stress results (e.g., applied load, boundary conditions, component geometry, and elastic modulus, among others). The influence of these random variables on the disk probability of fracture was explored using a conditional expectation approach [12, 13].

A demonstration prototype was developed using the ANSYS probabilistic design system (PDS) in which a response surface was developed for the probability of fracture in terms of the finite element-based random variables. The mean probability of fracture was computed by applying Monte Carlo sampling to the response surface results. Although the prototype was not implemented in DARWIN, it can be used to quantify the influence of other variables on the probability of fracture for future code planning purposes. Further details are provided in published papers [14, 15].

## 5.4 GRAPHICAL USER INTERFACE (GUI).

The graphical user interface (GUI) preprocesses input data for application to the DARWIN risk assessment code, and postprocesses the results for display to the analyst. The GUI was enhanced significantly to support the DARWIN enhancements described in the previous sections. A number of additional GUI capabilities were developed to improve the interaction with the analyst and to provide hard copy documentation of results. Note that additional enhancements to the DARWIN risk assessment code were required to support many of the capabilities described in this section.

## 5.4.1 Visualization and Polynomial Fitting of Stress Gradients.

### 5.4.1.1 Univariate Stress Gradients.

A GUI capability was developed allowing the analyst to specify the number and spacing of points associated with the stress gradient for inherent anomalies. This provides improved accuracy for risk critical zones.

### 5.4.1.2 Bivariate Stress Gradients.

The bivariate stress intensity factor solutions introduced in Flight\_Life require the analyst to select a univariate or bivariate solution based on the character of the stress field. Therefore, a new capability was developed to provide visualization of the stress field in three-dimensional space (figure 5-6). This allows the user to decide whether a full bivariate analysis is required to model the crack growth behavior associated with the stress field.

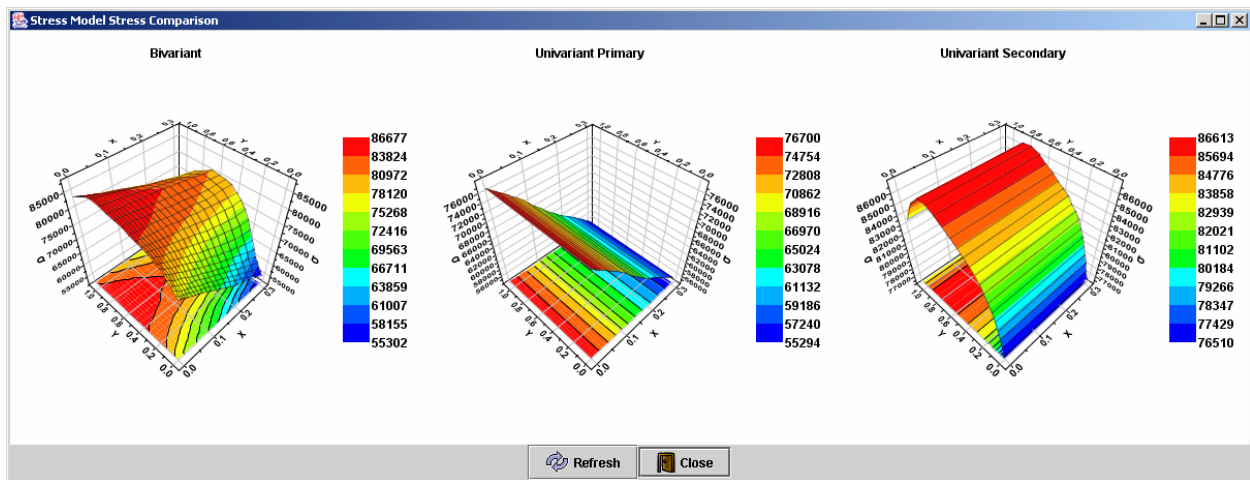


FIGURE 5-6. VISUALIZATION AND POLYNOMIAL FITTING OF BIVARIANT STRESS GRADIENTS

### 5.4.2 Report Generation.

Following execution of the DARWIN risk assessment code, the complete results are available to the analyst in the form of an ASCII results file or GUI displays. Many of the GUI plots can also be exported for use in word processing programs such as Microsoft Word (see section 5.4.4.1). However, these results are not in a condensed format suitable for use in FAA certification reports. A GUI report generation capability was developed to address this need, shown in figure 5-7. In addition, the GUI also provides an analyst report generation option that provides additional plotting options for hard copy reports.

### 5.4.3 GUI Directed Execution of Risk Assessment Code.

The GUI was enhanced to allow the analyst to execute the DARWIN risk assessment code directly from the GUI. The GUI provides a separate window for display of execution parameters. Upon completion, the GUI loads the results file for display of results.

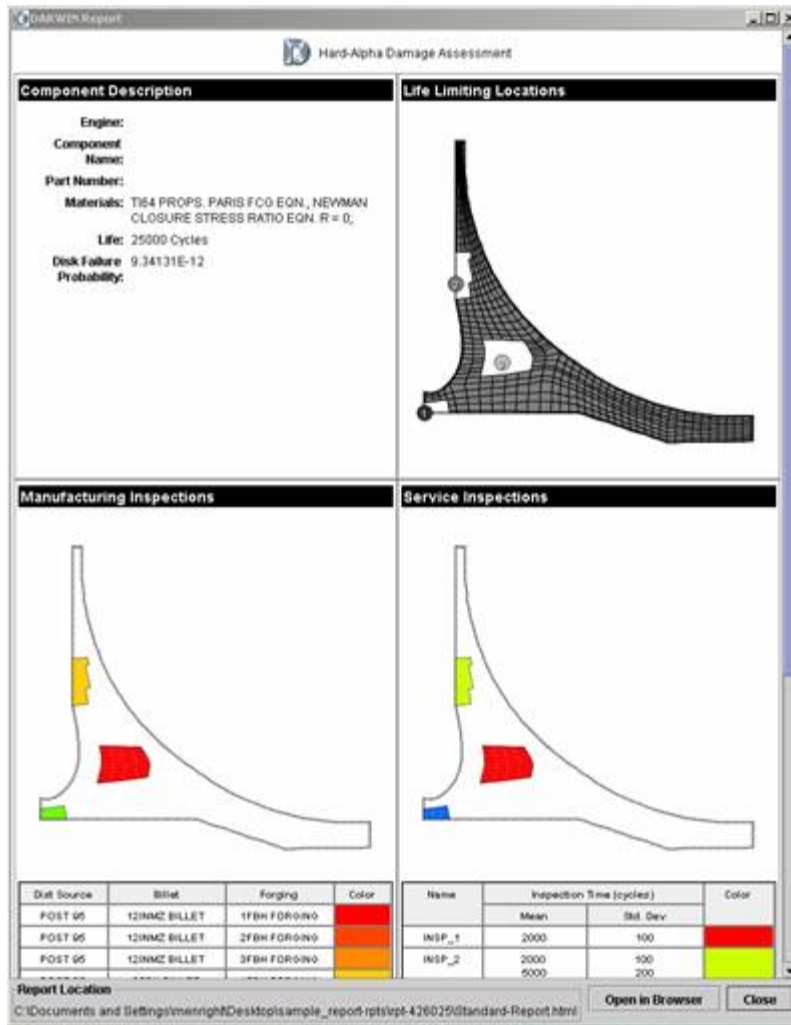


FIGURE 5-7. ILLUSTRATION OF GUI REPORT GENERATION CAPABILITY

#### 5.4.4 Additional Enhancements.

##### 5.4.4.1 Plot Export Capability.

A GUI capability was developed to save a plot image to a file (JPEG format). The plot image can be adjusted by the analyst and can be directly imported into word processing software.

##### 5.4.4.2 Input File Preview.

A capability was developed to allow the analyst to preview data files during the assessment definition stage of analysis. This preview capability is provided for a number of input data files, including anomaly distribution, POD curve, and material properties data.

#### 5.4.4.3 Database Converter.

When developing a commercial software program, backwards compatibility must always be considered to allow analysts to use previously created input/output files in new versions of the code. A database converter was developed that allows the analyst to translate previously created output files for review in new versions of the code. The converter is updated for each major release of DARWIN.

#### 5.4.4.4 Crack Growth Visualization.

In addition to risk predictions, DARWIN also provides complete details regarding the dimensions of the crack over the life of the component. A GUI capability was developed to provide a graphical display of the crack, shown in figure 5-8.

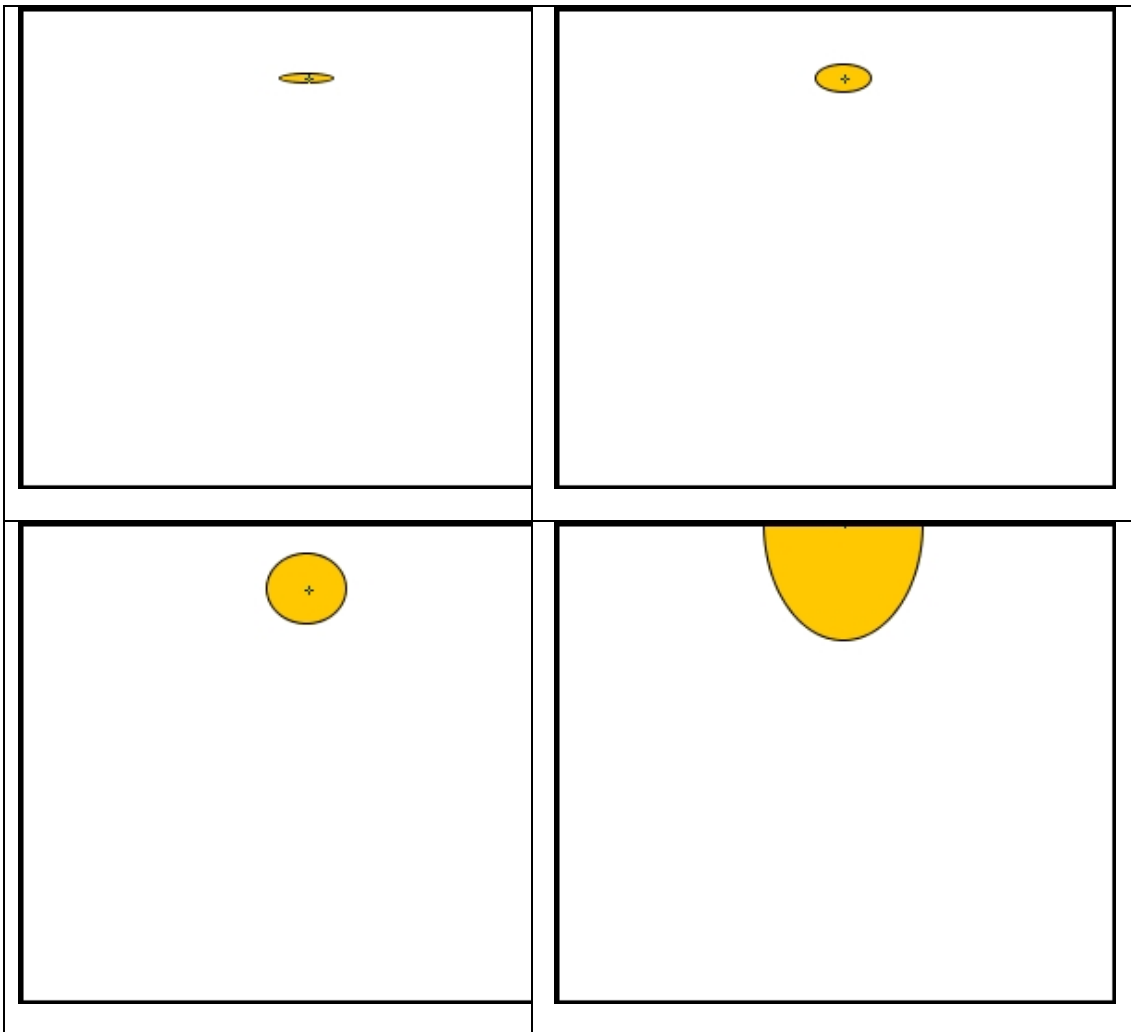


FIGURE 5-8. ILLUSTRATION OF CRACK GROWTH VISUALIZATION CAPABILITY

#### 5.4.4.5 Extract Fracture Mechanics Plate Dimensions Directly From FEM.

For inherent anomalies, the GUI provides a feature that allows the user to define the length, width, and orientation of a rectangular plate that is used for fracture mechanics computations. However, for a 3D surface damage assessment, additional parameters are often required to describe completely the fracture mechanics geometry (e.g., location and radius of hole). A new GUI capability was developed that allows the user to define these additional parameters based on geometry values extracted directly from the 3D finite element model. These parameters are displayed in the GUI and can be manually adjusted as necessary by the user.

#### 5.5 DARWIN ELECTRONIC HELP SYSTEM.

An electronic help system was developed to provide assistance to the analyst. As shown in figure 5-9, the DARWIN user's guide and theory manual were combined into a single electronic document available in web browser format. This allows the analyst to consult the help system for questions related to DARWIN theory, verification, and computational procedures. The enhanced help system includes an index and text search capabilities that apply to all sections (including theory and verification sections). These improvements provide improved documentation for support of existing and new DARWIN features.

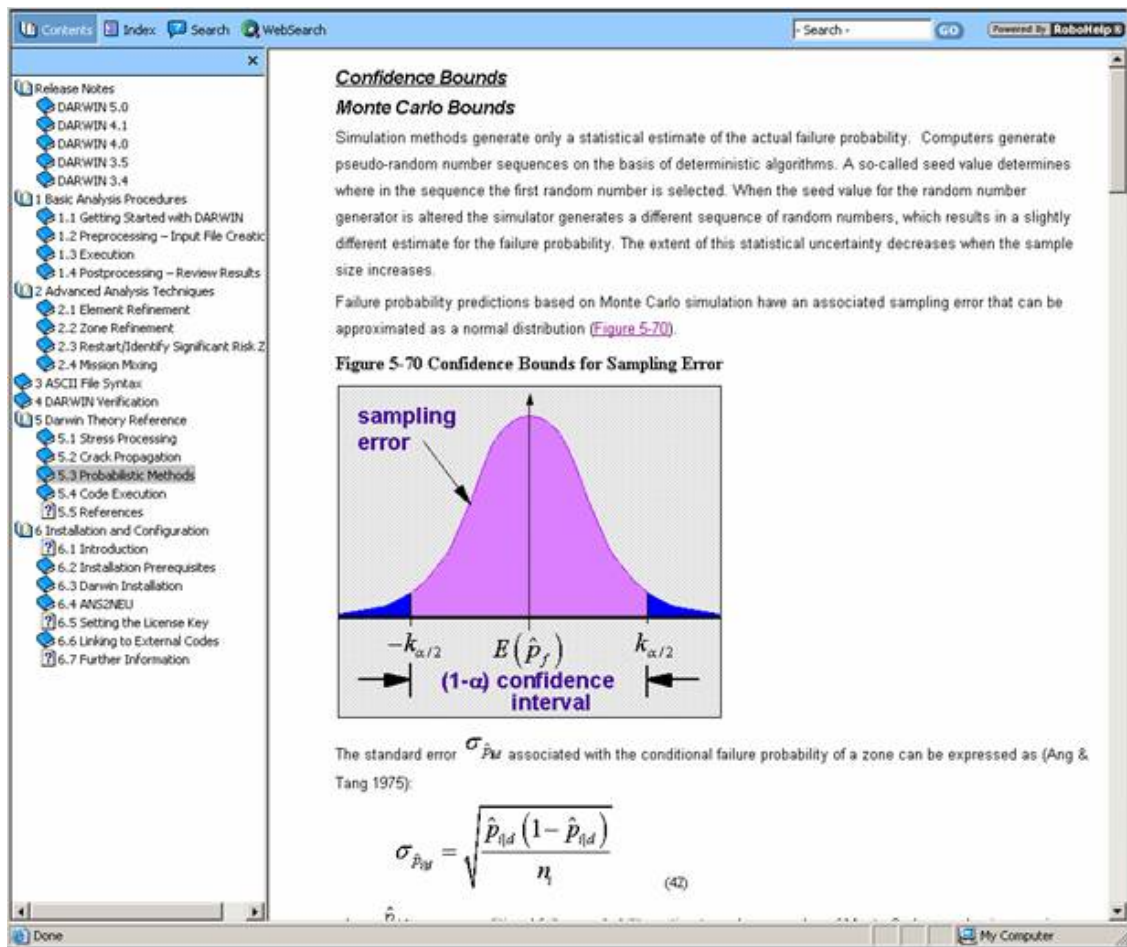


FIGURE 5-9. THE DARWIN ELECTRONIC HELP SYSTEM IN WEB BROWSER FORMAT

## 5.6 OEM EVALUATION OF DARWIN.

The TRMD Steering Committee was instrumental in the development of the DARWIN computer program. In addition to providing algorithms and design guidance, the partner companies also participated in substantial code review efforts to verify the accuracy and usability of the DARWIN software.

### 5.6.1 Quantitative Verification.

Throughout the TRMD-II program, DARWIN was evaluated by each of the four TRMD Steering Committee companies. The evaluations consisted of a series of studies focused on comparison of DARWIN predictions to experimental data, field experience, and OEM in-house code results. These studies included an extensive set of test cases that were exercised by multiple users within each of the four OEM companies. The studies were performed using DARWIN versions 3.3-6.0 on several computer platforms, including SUN, HP, and PC (with a greater emphasis on the PC platform during the final years of the TRMD-II program). OEM evaluation of DARWIN Alpha and Beta versions not only identified a number of bugs that were fixed prior to the production release of the code, but also helped to improve user confidence in the quantitative results.

#### 5.6.1.1 Verification for Inherent Anomalies.

DARWIN verification studies for hard alpha titanium assessed the field experiences of over 50 engine disks of varying levels of maturity. This included various titanium alloys with different disk and hub geometries. The computed probability of fracture predictions representing 2 billion part cycles were combined with representative fleet population and accumulated cycles to predict the number of fractures and finds (HA detection prior to fracture). The probability-of-fracture predictions were reasonably consistent with earlier results used by the AIA Rotor Integrity Subcommittee to set the initial HA defect distributions [8].

A number of studies were performed to compare DARWIN probability of fracture predictions to the results of OEM internal codes. The results of one of these studies, focused on the rotating ring disc geometry defined in AC33.14-1, are shown in figure 5-10. It can be seen that DARWIN results compare very favorably with the risk values computed independently by one manufacturer using their own code and by other OEMs using the DARWIN probabilistic algorithms with their own fracture mechanics modules.

Additional studies assessed the performance of specific algorithms within DARWIN. For example, benchmark testing of the DARWIN rainflow code against an in-house code at Pratt & Whitney has shown agreement between the two codes for test cases with over 6500 load steps. A number of comparisons were made between the Flight\_Life fracture mechanics module and various fracture mechanics codes in use by the manufacturers. The selected results shown in figure 5-11 (based on the ring disc geometry defined in AC 33.14-1) illustrate the close agreement between Flight\_Life and the results obtained by the OEMs.

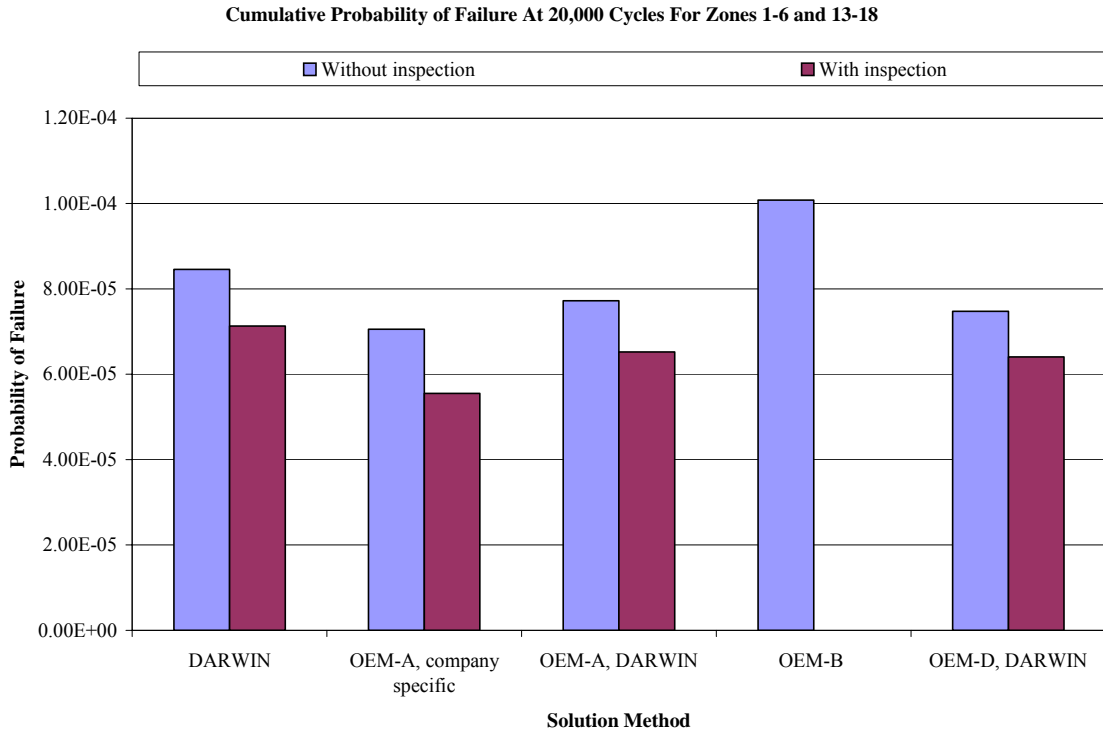


FIGURE 5-10. ILLUSTRATION OF OEM VERIFICATION OF DARWIN FOR INHERENT ANOMALIES

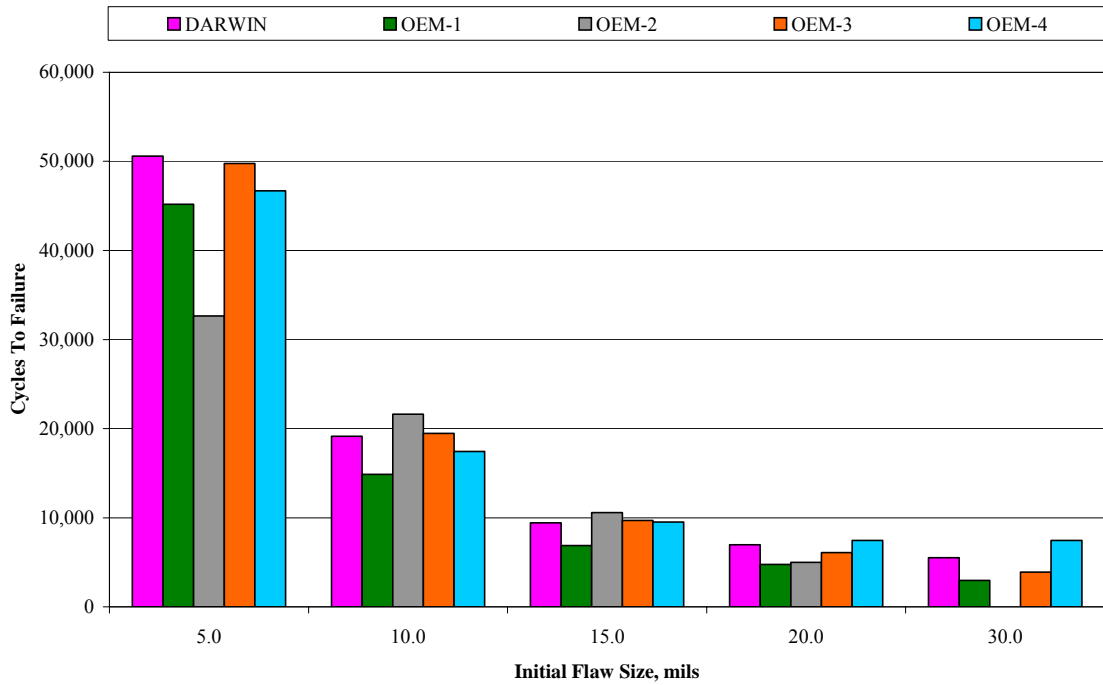


FIGURE 5-11. ILLUSTRATION OF OEM VERIFICATION OF FLIGHT\_LIFE MODULE

### 5.6.1.2 Verification for Induced Anomalies.

Pratt & Whitney conducted an extensive study comparing DARWIN 5.0/5.2 crack growth life predictions to experimental fatigue test results for surface crack, center notch (through thickness edge crack), compact tension, and bolt hole test specimens. Verification of the surface crack specimen was performed for nickel and titanium alloys, and nickel alloys were used for all other specimen types. As shown in figure 5-12, values predicted by DARWIN are in close agreement with the experimental results for both the uniformly stressed surface crack specimens (figure 5-12a) and the center notch specimens (figure 5-12b). For all specimen types, the results are within the 2.5x scatter bands for most of the tests considered.

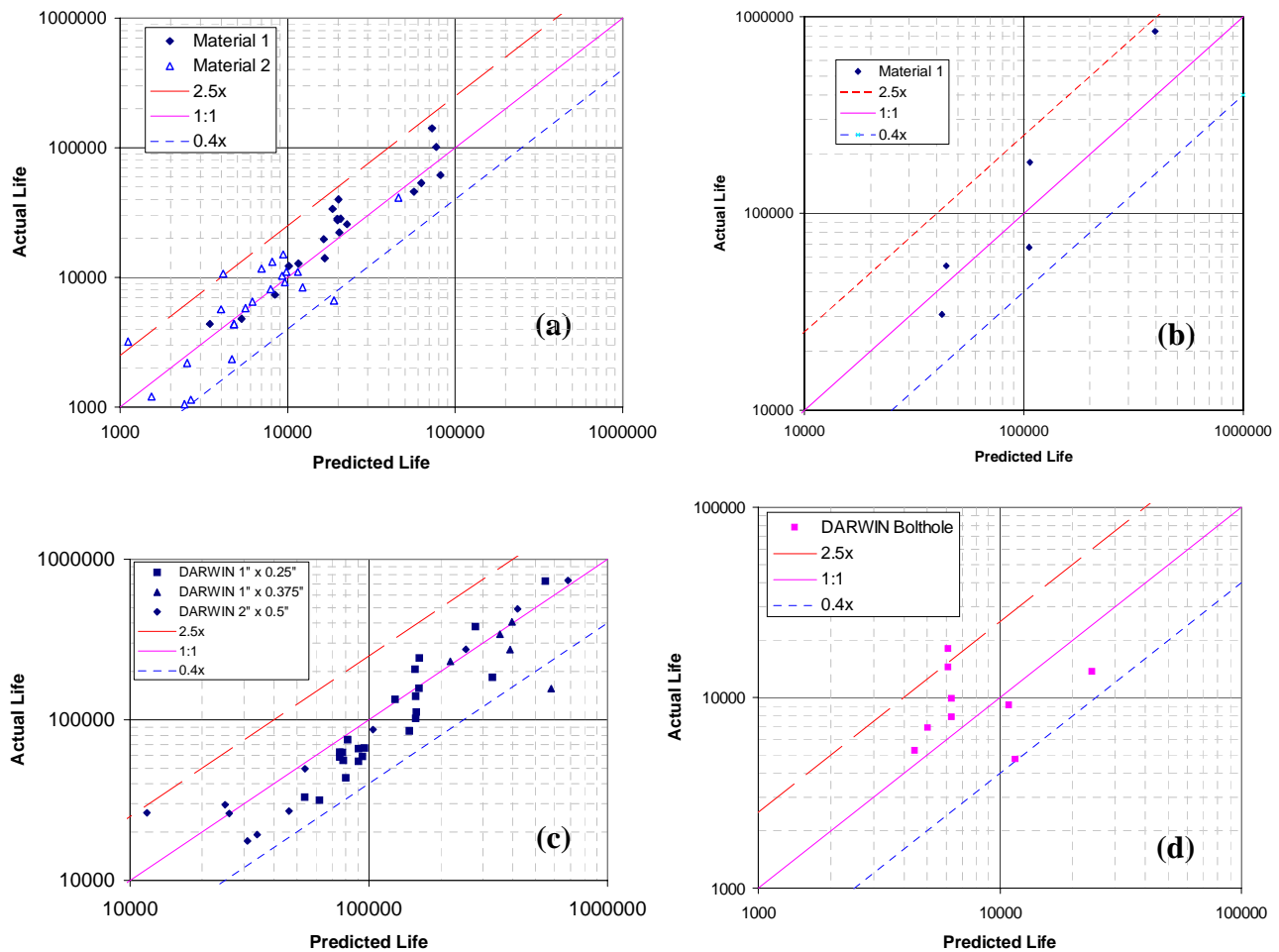


FIGURE 5-12. ILLUSTRATION OF OEM VERIFICATION OF INDUCED ANOMALIES, COMPARING DARWIN LIFE PREDICTIONS TO EXPERIMENTAL RESULTS FOR THE FOLLOWING SPECIMEN CLASSIFICATIONS:  
 (A) SURFACE CRACK, (B) CENTER NOTCH,  
 (C) COMPACT TENSION, AND (D) BOLTHOLE

### 5.6.2 Qualitative Evaluation.

The TRMD Steering Committee performed a series of evaluations to assess the practical use of DARWIN in a design environment. In collaboration with the FAA and the AIA RISC Committee, the Steering Committee identified a number of key enhancements to improve the use of DARWIN as a design and certification tool. Examples include the Standard Report that simplifies the certification process (requested by the FAA, designed by the Steering Committee), the Analyst Report that provides a complete hardcopy summary of results (requested by the Steering Committee), and the linked in-service inspection capability that allows the analyst to specify an inspection in terms of a previous inspection (requested by the Steering Committee). Many additional DARWIN features were improved based on the guidance from the Steering Committee.

### 5.6.3 OEM Review Comments.

Over the course of the TRMD-I and TRMD-II programs, the OEMs provided general feedback regarding their experiences with the DARWIN code. The response was very positive, with several of the OEMs electing to license DARWIN for certification of new engine rotors and disks. Some OEMs use the deterministic fracture mechanics capability in DARWIN to supplement (or replace) their internal fracture codes.

OEM feedback has centered primarily on the efficiency, accuracy, and ease of use associated with DARWIN. The OEMs provided a number of positive comments related to the efficiency of DARWIN, focusing on the reduction of human time and computer time required to perform a certification assessment compared to internal codes. For example, one manufacturer reported that the human time required to complete an assessment was reduced from 40 hours to 8 hours when DARWIN was used instead of an internal code. Several OEMs have reported significant computer speed improvements (for a specified accuracy) associated with use of DARWIN advanced probabilistic methods (i.e., importance sampling, life approximation function) compared to the standard Monte Carlo simulation approach. Recent DARWIN enhancements such as zone/element refinement and finite element filtering were noted as substantial human/computational efficiency improvements.

The OEMs also provided a number of positive comments related to the overall ease of use of DARWIN. Several manufacturers mentioned that the graphical user interface was very easy to understand, and that new users could quickly learn to use it with minimal training. The OEMs also mentioned that the DARWIN electronic help system was well-documented and provided substantial assistance to both new and experienced users of the code. In addition, the extension of DARWIN to the PC facilitated the use of DARWIN by a wider group of engineers.

## 6. TECHNOLOGY TRANSFER.

### 6.1 PROGRESS REPORTS AND REVIEW MEETINGS.

Regular communication with the FAA and the gas turbine engine industry facilitated effective oversight of the research program as well as timely transfer of important new results. Written reports included brief monthly progress reports and substantially longer periodic interim progress reports, which were issued to coincide with program review meetings. These one-day program review meetings with the FAA were typically held two or three times per year, with frequency and specific schedules directed by the FAA. The program Steering Committee conducted a one-day or two-day working meeting in conjunction with each program review meeting, and occasionally conducted independent working meetings of one or two days duration. A representative (usually the Chairman) of the Steering Committee presented a short status report on program activities at each meeting of the Rotor Integrity Sub-Committee (generally held three times per year). Once per year, the SwRI Program Manager or one of the SwRI co-Principal Investigators attended the RISC meeting and made the TRMD presentation. The Steering Committee often held a working meeting in conjunction with this particular RISC meeting.

### 6.2 DARWIN TRAINING WORKSHOPS.

Workshops were conducted in order to train DARWIN users and FAA staff on the theory and functionality of the DARWIN software. A major workshop was conducted at SwRI on May 3-5, 2005. The scope of this workshop included DARWIN capabilities for titanium hard alpha, surface damage, and generalized inherent anomalies. The first day was an executive overview and software demonstration with 34 people in attendance, including six FAA staff as well as representatives from the USAF, NASA, Transport Canada, Central Institute of Aviation Motors (Russia), and eleven gas turbine engine companies. The second and third days of the workshop were devoted to hands-on DARWIN training, with 26 in attendance for some or all of the training. A course outline is provided in Table 6.1.

Other training workshops with more limited scope were conducted on an as-needed basis throughout the program. One engine company licensing DARWIN sent an engineer to SwRI for a full week of training, while another engine company licensee arranged one day of training at their facility for about thirty employees. Two members of the SwRI DARWIN team conducted three days of training for about fifteen engineers at the Defence Science and Technology Organisation (DSTO) facility in Melbourne, Australia. They also presented one day of DARWIN training for about fifteen NAVAIR and USAF personnel as part of a three-day short course on "Probabilistic Analysis and Design for High Performance Computing" at Patuxent River, Maryland. The presentation costs and any travel expenses for these workshops were funded by sources other than the FAA. Some Steering Committee members also provided internal training workshops for employees of their company.

TABLE 6-1. AGENDA FOR DARWIN SHORT COURSE (MAY 3-5, 2005)

**Tuesday, May 3**

<u>Time</u>	<u>Subject</u>
7:45 - 8:15	Registration
8:15 - 8:30	Welcome
8:30 - 8:45	FAA Opening Remarks
8:45 - 9:00	Introduction & Training Agenda
9:00 - 9:45	RISC Overview
9:45 - 10:00	Break
10:00 - 10:45	Probabilistic Damage Tolerance Analysis Process
10:45 - 11:15	TRMD Overview
11:15 - 12:00	DARWIN Overview
12:00 - 1:00	Lunch
1:00 - 3:00	Use of DARWIN for Titanium Inherent Anomalies
3:00 - 3:15	Break
3:15 - 4:00	Use of DARWIN for General Inherent Anomalies
4:00 - 5:00	Use of DARWIN for Surface Damage

**Wednesday, May 4**

<u>Time</u>	<u>Subject</u>
8:00 - 9:45	Titanium Inherent Anomalies: Hands-On Example Problem
9:45 - 10:00	Break
10:00 - 11:45	Titanium Inherent Anomalies: Hands-On Example Problem (cont'd)
11:45 - 12:45	Lunch
12:45 - 1:45	Stress Processing: Options and Exercises
1:45 - 2:45	Zone Creation: Options and Exercises
2:45 - 3:00	Break
3:00 - 4:00	Fracture Mechanics: Options and Exercises
4:00 - 5:00	Efficient Risk Assessment: Options and Exercises

**Thursday, May 5**

<u>Time</u>	<u>Subject</u>
8:00 - 10:00	Surface Damage: 1D Hands-On Example Problem
10:00 - 10:15	Break
10:15 - 12:00	Surface Damage: 3D Hands-On Example Problem
12:00 - 1:00	Lunch
1:00 - 2:00	Data Preparation Exercises
2:00 - 3:00	General Inherent Anomalies Exercises
3:00 - 3:15	Break
3:15 - 4:15	Zone Refinement Exercises
4:15 - 5:00	Parallel & Batch Processing Exercises

**6.3 CONFERENCE PRESENTATIONS AND JOURNAL ARTICLES.**

Important results from this research program were disseminated to a much broader audience in the gas turbine engine community or the international technical community in disciplines such as fracture mechanics or reliability through presentations at conferences and symposia or publications in archival technical journals. A complete listing of these presentations and publications is provided in Appendix W.

#### 6.4 TECHNOLOGY TRANSFER TO OTHER GOVERNMENT AGENCIES.

Royalty-free DARWIN licenses have been provided to engineers at the NASA Glenn Research Center (Cleveland, Ohio), Air Force Research Laboratory (Dayton, Ohio), Naval Air Warfare Center Aircraft Division (Patuxent River, Maryland), and Army Aviation and Missile Research, Development, and Engineering Center (Redstone Arsenal, Alabama).

DARWIN was installed on the SGI Origin system at the Aeronautical Systems Center, Major Shared Resource Center, at Wright-Patterson AFB, Ohio, a computational science facility created as part of the Department of Defense High Performance Computing Modernization Program. The SGI Origin system has a large number of CPUs that can be simultaneously exercised using the parallel processing feature in DARWIN.

SwRI collaborates with NASA through a Space Act Agreement on the development and distribution of the NASGRO<sup>®</sup> analysis software for fracture mechanics and fatigue crack growth. NASGRO shares some functionality with the Flight\_Life fracture mechanics module in DARWIN, and in fact some of the early Flight\_Life SIF solutions were taken from NASGRO. Many of the new Flight\_Life capabilities developed under this grant, including all of the new weight function SIF solutions, have now been inserted into recent versions of NASGRO. NASGRO is used extensively by NASA and NASA contractors as well as the European Space Agency, the FAA (especially by FAA Designated Engineering Representatives for damage tolerance analysis), and many aerospace companies. Industrial NASGRO users in the aircraft, rotorcraft, and gas turbine engine businesses include thirteen major companies comprising the NASGRO Consortium (Airbus, Boeing, Bombardier, Embraer, Hamilton Sundstrand, Honeywell, Israel Aircraft Industries, Lockheed Martin, Mitsubishi Heavy Industries, Northrop Grumman, Siemens Power Generation, Sikorsky, and Volvo Aero) and many other licensees.

The DARWIN code was used as a demonstration platform in SwRI research programs funded by the Air Force Research Laboratory (AFRL) and the Defense Advanced Research Projects Agency (DARPA) [16, 17, 18]. Additional features not included in the FAA/Production version of DARWIN were added to investigate other technical issues. These enhancements included an interface with simulated engine sensor data for rotational speed (and an algorithm to convert speed into local stress values for select features), simple and advanced crack formation models, integration of crack formation and growth to calculate total life, a spectrum editing algorithm to remove small cycles with negligible contributions to damage, and simulations of continuous crack sensor monitoring. The enhancements were used to study issues such as variability in mission profiles and mission histories, on-board engine monitoring for cracks, improved total fatigue life prediction for cracks in steep stress gradients, and physically-informed characterization of fatigue life variability. The larger goals of this research, all in a military context, included the feasibility of prognosis systems to improve reliability and forecast readiness, as well as the potential for engine rotor life extension.

## 7. INDUSTRIALIZATION OF DARWIN SOFTWARE.

At the request of the industry and FAA, an infrastructure was developed to support the formal use of DARWIN by engine companies for official FAA and company purposes. This industrialization activity addresses formal software configuration management, code licensing and distribution, and user support. The supporting infrastructure includes a source code repository, automated software verification procedures, bug-tracking software, user manuals, an on-line help system, and a web site.

### 7.1 AUTOMATED SOFTWARE VERIFICATION.

An automated verification procedure was developed to confirm that the DARWIN risk assessment code performs as intended following a major code change. The procedure is used to compare the results of a number of verification output files immediately before and after a change is implemented in the Fortran source code. A comparison results file is created that highlights values that do not fall within specified tolerance values. These highlighted values are used to identify and fix bugs that occasionally occur during the code development stage.

The automated verification procedure consists of a (platform specific) script file and a text extraction program called SCOUT (SCanning Outfile Utility). The script file extracts the DARWIN source code, verification examples, and previous verification results from the CVS repository (described below). The script file compiles the DARWIN code and then executes it for each of the verification examples. SCOUT extracts the data from the DARWIN output files, compares it to the previous verification results, and identifies any results that do not fall within specified tolerance values. This process is repeated for all supported computer platforms (Sun, SGI, HP, LiNuX, and PC).

### 7.2 SOFTWARE REVISION MANAGEMENT.

The development of commercial software requires the interaction of many engineers that serve in a variety of roles (e.g., programmer, reviewer, end user). As the software is continuously enhanced, a number of different versions may exist that are in various stages of development. A revision management system is necessary to keep track of the changes to each version.

A revision management system called CVS (Concurrent Version System) was identified and implemented for DARWIN to address the issues associated with multiple programmers and versions. CVS provides a directory structure similar to an electronic file manager that serves as a repository for source code. It provides a framework that allows multiple programmers to access and share source code, and it records all changes to the code. CVS can also support multiple versions of the code using a technique called "branching." CVS requires a relatively small amount of memory because it stores only the original source code and line-by-line changes to the source code.

CVS has the capability to store most file types including ASCII text, word processing documents, and binary files (e.g., executable programs). It is used to store a variety of information associated with the DARWIN software, including verification example problems and results, programmer's documentation, and user manual documents, among others.

### 7.3 INTERNET DISTRIBUTION OF DARWIN.

An Internet web site ([www.darwin.swri.org](http://www.darwin.swri.org)) was developed for electronic distribution of DARWIN. It serves as a repository for the software and manuals, and provides resources for attracting new users, as described below.

#### 7.3.1 Internet Distribution of Software.

In the past, commercial software was often distributed exclusively in electronic media format (i.e., magnetic tape, CD-ROM). This practice was relatively expensive due to the costs associated with creation and shipment of the media. In addition, this approach required the redistribution of the media to address any changes to the software (including minor bug fixes).

To address these issues (and others), an Internet site was created for the distribution of the DARWIN software (Internet address: [www.darwin.swri.org](http://www.darwin.swri.org)). This site provides the DARWIN executable program for all releasable versions (Alpha, Beta, Production) of the code on all supported computer platforms (Sun, SGI, HP, LiNuX, PC). Internet distribution provides users with instant access to DARWIN following a bug fix or other code change, without the expense associated with the creation and shipping of electronic media. Internet distribution of the software and manuals is password-protected, secure, and restricted to authorized users from the TRMD Steering Committee, AIA RISC Committee, and DARWIN Licensees.

#### 7.3.2 Electronic Distribution of Manuals.

Distribution of the DARWIN user manual is also provided by the DARWIN web site. The manual is distributed on the web site as PDF (portable document format) files. It is also distributed with DARWIN software as an electronic help system that can be accessed directly from the DARWIN graphical user interface (GUI).

#### 7.3.3 Resources for New Users.

The DARWIN web site also provides valuable information to potential new users. The site provides background information about DARWIN and the TRMD project, including downloadable PDF copies of all the public presentations, published papers, and major reports generated under TRMD-I and TRMD-II. In addition, a capability is provided to allow potential new users to download an evaluation version of the code and manuals for a time-limited trial period. Over the period of the TRMD-II program, over 200 evaluation copies were provided to potential new users from government, private industry, and universities.

### 7.4 USER SUPPORT.

New users often have questions regarding the use and limitations of the computer code. Experienced users occasionally report software bugs that need to be fixed. An infrastructure was developed to address these issues, as described below.

User support to Steering Committee and RISC members for Alpha and Beta (pre-production) versions of DARWIN and for TRMD-II users of production versions was funded by the TRMD-II

program. User support to licensees for commercial use of production versions of DARWIN was funded by licensing fees (see Section 7.5).

#### 7.4.1 Live User Support.

A help desk was created providing live support to users via telephone, email, and Internet. This allows users to report bugs and to obtain the status on bug resolution, and it also provides general assistance to all licensed users.

#### 7.4.2 Video Tutorials.

An on-line tutorial was developed as a training aid for new users. The tutorial consists of a PowerPoint presentation with embedded video sessions that describe the primary menus of the DARWIN GUI. The tutorial is available to the general public via the DARWIN web site.

#### 7.4.3 Automated Bug Tracking Software.

A bug tracking system was implemented to ensure efficient tracking and resolution of reported software bugs. The system consists of the Bugzilla<sup>®</sup> automated bug tracking system, developed by the Mozilla Foundation. Bugzilla was adapted to address the primary software categories associated with DARWIN. Additional features were added to improve the efficiency of bug tracking, including a capability to automatically send bug reports directly to code developers via email. It serves as a repository for all bugs, including placeholders for desired enhancement and new features.

### 7.5 SOFTWARE LICENSING.

Technology transfer of DARWIN to engine companies and other organizations for official use in both production and research settings is accomplished through a formal commercial licensing process. License fees collected by SwRI are exclusively used to enhance the DARWIN code and to provide user support for the benefit of engine manufacturers, other licensees, and the FAA.

#### 7.5.1 Software License Agreement.

A software license agreement was created that provides a detailed description of the terms, conditions, and options associated with DARWIN. It serves as a legal document for the commercial distribution and use of the DARWIN software.

#### 7.5.2 Registered Trademark.

A number of trademark applications were filed to ensure that the DARWIN acronym could be used in commercial trade to describe the software developed under the TRMD program, and to prevent the use of this designation by unauthorized persons. The following U.S. registered trademarks were approved by the United States Patent and Trademark Office:

D (logo) DARWIN<sup>®</sup>, DARWIN<sup>®</sup>

In addition, the following European registered trademarks were approved by the Office for Harmonization in the Internal Market, European Union:

D (logo) DARWIN<sup>®</sup>, DARWIN<sup>®</sup>

### 7.5.3 Commercial Licensing Activity.

At this writing, a total of eight commercial licenses have been issued, including six gas turbine engine companies and two foreign government laboratories. The engine companies are based in three different countries, for a total of five countries among the eight existing licenses. The engine company licenses include both single seat and site (company-wide) licenses. Several of the engine companies obtained their first DARWIN license shortly after licensing activity commenced, and have renewed their license each year. Three of the eight total licenses were initiated within the last year of the TRMD-II program. Other prospective licenses are in negotiation at this writing.

In accordance with the terms of the FAA grant agreement, agencies of the U.S. Government are entitled to receive a royalty-free license for DARWIN upon request. Licensing to these agencies is described further in section 6.4.

## 8. SUMMARY AND CONCLUSIONS.

The aircraft engine industry is currently working with the FAA through the Rotor Integrity Sub-Committee of AIA to develop an enhanced life management process, based on probabilistic damage tolerance principles, to address the threat of material or manufacturing anomalies in high-energy rotating components. The enhanced life management process for hard alpha anomalies in titanium rotors is documented in FAA Advisory Circular (AC) 33.14-1, and future revisions to AC 33.14 will address other rotor materials and other anomaly types. The FAA funded a multi-year, multi-disciplinary research program titled “Turbine Rotor Material Design—Phase II” (TRMD-II) to address identified shortfalls in the data and technology required to support and enhance the Advisory Circular and its implementation. The integrated TRMD-II program team, led by Southwest Research Institute and including major engine manufacturers GE Aircraft Engines, Pratt & Whitney, Honeywell, and Rolls-Royce Corporation, developed both enhanced predictive tool capability and supplementary material/anomaly behavior characterization and modeling. The TRMD-II program built on the results and the strong working relationships generated under the previous TRMD-Phase I program. Major accomplishments and conclusions of the TRMD-II program include the following:

1. Sensitivity studies were performed to support a planned update by RISC of the HA anomaly distributions included in AC 33.14-1. These studies incorporated new TRMD-generated technology (vacuum FCG data, the HA forging microcode, and the spin pit and coupon HA fatigue tests) as well as new data and insights from OEM experience in order to identify the variables with the most significant impact on the resulting distributions. The issues and factors identified as being of sufficient significance to be potentially included in future updates include scatter in crack growth life, vacuum crack growth data, an alternative approach to estimate the ingot distribution, five additional years of JETQC data, and the definition of inclusion size (core vs. diffusion zone).
2. In order to better understand the evolution and predict the size of hard alpha anomalies, a mathematical model and computer code were developed to describe the diffusion of nitrogen or oxygen in titanium from an inclusion during metal forming and heat treatment. The code was calibrated with available literature data. For a given melt process and initial anomaly size distribution, the code can be used to predict the maximum expected sizes of undetected (“stealth”) anomalies.
3. Detailed NDE and metallography were performed on the forgings with seeded or natural HA anomalies produced in TRMD-Phase I to validate the DEFORM™ forging microcode developed in TRMD-I. Detailed experimental measurements of core and diffusion zone (DZ) sizes in the forgings were compared with predictions from the direct application of the microcode as well as predictions from a new set of regression equations generated with the microcode. Overall, the agreement between measurements and predictions was good.

4. The HA microcode was used to characterize the nitrogen contents, temperatures, strain rates, and orientations associated with cracking of HA anomalies during the forging operation. The strain required to cause HA cracking was generally found to increase, and damage was found to decrease, with decreasing HA and DZ nitrogen content, increasing temperature, and decreasing strain rate. Studies of three representative forging shapes indicated that ingot-to-billet conversion and component forging would, under commonly used processing conditions, crack all HA with nitrogen contents greater than 4%, which was the lowest HA nitrogen content evaluated.
5. A series of ultrasonic inspections were performed using both conventional and multizone inspection techniques on natural and seeded HA anomalies in final forged shapes, for comparison with inspections on billet and intermediate forged shapes conducted previously in TRMD-I. Based on the inspections conducted, the Multizone #1 FBH inspection was found to detect anomalies more effectively than either Conventional #1 or Conventional #2 inspections, and both synthetic and natural HA inclusions were easier to detect in the billet than in the forgings.
6. The development of the DEFORM forging analysis software to predict bulk residual stresses was evaluated. Comparisons between predicted and experimentally measured residual stresses performed outside the TRMD-II program indicated generally good agreement for several different conditions.
7. Tensile and fatigue tests were performed on high oxygen seeded Ti-17. Results indicated only a small impact of elevated oxygen on tensile and dwell fatigue properties, a slightly higher impact than for Ti-6-4, but a much smaller impact than for Ti-6-2-4-2.
8. Fatigue tests with embedded HA defects were performed on coupon specimens machined from selected seeded forgings in the microcode validation study. The DARWIN Flight\_Life module was used to predict the FCG lifetime of each test, based on the assumptions that crack nucleation life was zero and the initial crack size was equal to the core plus DZ size. The actual total fatigue life observed was nearly always at least twice as long the calculated FCG life.
9. The coefficient of thermal expansion of bulk HA with different nitrogen contents was measured experimentally. These results were employed in detailed stress, damage, and fracture mechanics analyses to evaluate the potential effects of thermally-induced residual stresses on fatigue crack initiation and growth at synthetic HA inclusions. These residual stresses appear to be significant for embedded defects at higher nitrogen contents and lower applied stresses, but not significant at lower nitrogen contents and higher applied stresses.
10. Spin pit tests were performed with material from the TRMD-I forgings containing embedded natural and synthetic HA anomalies. Post-test fractography and metallography were performed, and the spin disks were also nondestructively inspected periodically during the test. NDE results were provided to the Engine Titanium Consortium. Test lives were compared with Flight\_Life analyses, indicating that initial flaw sizes more nearly corresponded to core sizes than DZ sizes.

11. Vacuum FCG data were generated at representative temperatures and stress ratios for one titanium rotor alloy (coarse-grained Ti-6-2-4-2), two nickel rotor alloys (IN 718 and Waspaloy), and a powder metallurgy nickel alloy (Udimet 720).
12. Several mults of Waspaloy with sonic indications were obtained from a nickel melter. The mults were inspected ultrasonically, forged, and then reinspected. Some of the original indications could not be located again following forging. Some remaining indications were selected for machining into coupon specimens for future fatigue testing.
13. Thermo-mechanical FCG data for IN 718 were generated with simple diagnostic stress-temperature histories. Simple stress rainflow analysis methods employing isothermal data from the temperature at the maximum stress time point were shown to exhibit a slightly nonconservative bias.
14. Twelve different new or enhanced stress intensity factor (SIF) solutions were developed for the Flight\_Life fracture mechanics analysis module. A robust new weight function (WF) SIF formulation was developed to accommodate general bivariant stress distributions on the crack plane. Highly accurate new WF SIF solutions were developed for select crack geometries under univariant and bivariant stressing using state-of-the-art 3D boundary element analysis to generate the reference solutions. Novel strategies were developed to increase the computational speed of select SIF solutions. Other Flight\_Life improvements included an enhanced Walker interpolation scheme, an improved shakedown module, and first-order plastic corrections to the SIF for instability analysis.
15. A broad survey was conducted of the scientific and technical literature on the stability and significance of surface and near-surface residual stresses in fatigue, based on a comprehensive bibliography containing over 300 citations. Primary attention was given to the residual stresses resulting from peening and related surface treatments, cold expansion of holes, welding, and machining, with special attention to gas turbine engine materials and applications. Relaxation and redistribution of residual stresses due to thermal exposure, static mechanical loading, cyclic mechanical loading, and crack extension were addressed in the survey.
16. New DARWIN versions were developed to address anomalies associated with surface damage (Versions 4.x and 5.x), as well as different types of inherent anomalies in other materials (Version 6.0).
17. New surface damage capabilities in DARWIN initially focused on bolt hole configurations. Versions 4.x allowed the user to enter temperature and one-dimensional stress gradient values via tabular input. Versions 5.x introduced a sophisticated 3D GUI that enables the user to load and visualize a fully 3D finite element model and stress results, select a surface crack location, slice the 3D model along the principal stress plane at that location, re-mesh the slice to create a 2D stress model, build a 2D fracture mechanics model on the cut plane, and extract the necessary input for the 2D fracture mechanics life calculation.

18. A number of new capabilities were introduced in DARWIN 6.0 to support risk assessment of materials with other types of inherent material anomalies. The risk assessment equations for zones and components were modified to account for materials with potentially large numbers of anomalies. A crack formation module was developed to allow users to implement and execute company-specific crack formation modules in DARWIN. Additional parameters were introduced to support 3D modeling of anomalies and associated production inspections. An adaptive optimal sampling methodology was developed to improve computational efficiency for materials with general inherent anomalies.
19. A number of enhancements in the probabilistic methods were developed to improve the overall efficiency and accuracy of the risk assessment computations, including enhanced importance sampling that can calculate reliability two orders of magnitude faster than Monte Carlo simulation without loss of accuracy, optimal allocation of Monte Carlo samples to individual zones based on relative risk to dramatically reduce the total number of samples required, probabilistic confidence bounds, computation of probabilistic sensitivities, and conditional failure analysis methods. Some of these enhancements have already been implemented in DARWIN, and others will be implemented in future releases.
20. Additional zone discretization methods were developed to improve the efficiency of solution convergence. Capabilities were implemented in DARWIN to automatically subdivide zones into two or more subzones, to subdivide individual finite elements into smaller elements, and to generate a uniform “onion skin” of surface elements.
21. The inspection capabilities in DARWIN were enhanced to provide more realistic treatment of shop visit practices, including inspection following transition of a subsurface to a surface crack, and linked shop visit times.
22. A capability was developed in DARWIN to allow users to define multiple missions and to combine them to define the mission mix for risk assessment computations. Supporting features include stress and temperature scaling factors, zone groups, and mission sequencing.
23. The ANS2NEU module used to convert ANSYS results files to DARWIN input format was significantly enhanced to support PC-based Windows operating systems, to permit ANS2NEU execution directly from the DARWIN GUI, and to provide finite element filtering based on element type, material, or load case.
24. A number of different enhancements were implemented to improve computational efficiency. Stress processing enhancements significantly reduced analysis time and memory requirements. A restart capability was developed that applies the results of previous computations to a DARWIN analysis to reduce overall computation time. A new XML database system was developed to provide improved efficiency for storage and retrieval of results. PC and Linux versions of DARWIN were developed. A parallel processing capability was developed that allows DARWIN to be executed simultaneously on multiple computers, and a batch processing capability was developed that permits execution of multiple DARWIN files in batch mode directly from the GUI.

25. The DARWIN graphical user interface was enhanced significantly to support all of the enhancements cited previously. In addition, new capabilities were implemented for visualization and polynomial fitting of univariant and bivariate stress gradients, generation of standard or custom reports of DARWIN results, execution of the risk assessment code directly from the DARWIN GUI, plot export, input file preview, database conversion, crack growth visualization, and extraction of dimensions directly from finite element models.
26. An electronic help system was developed to provide assistance to the DARWIN user. The DARWIN user's guide and theory manual were combined into a single electronic document available in web browser format and including an index and text search capabilities.
27. The partner gas turbine engine companies participated in substantial code review efforts to verify the accuracy and usability of the DARWIN software. Studies included quantitative comparisons of DARWIN and Flight\_Life predictions to experimental data, field experience, and internal company software results. Company evaluation of Alpha and Beta versions not only identified bugs that were fixed prior to production releases of the code, but also helped to improve user confidence in the quantitative results. Qualitative evaluations assessed the practical use of DARWIN in a design environment and identified key enhancements to improve the use of DARWIN for both design and certification. The partner companies provided regular feedback on accuracy, efficiency, and ease of use.
28. Technology transfer was accomplished through a variety of mechanisms, including regular progress reports and review meetings focused on FAA needs and regular presentations at RISC meetings. A three-day DARWIN training workshop was conducted for 34 people (government and industry) near the end of the program, and other training workshops with more limited scope were conducted on an as-needed basis throughout the program. To date, a total of 23 technical papers resulting from TRMD-II research were presented at conferences and published in conference proceedings, an additional 13 papers were presented at conferences or workshops without formally published proceedings, and 8 papers were published in archival journals. Royalty-free DARWIN licenses were provided to engineers at NASA, AFRL, NAVAIR, and the Army, and DARWIN was installed on a DOD high-performance (parallel) computer system. DARWIN and DARWIN capabilities were employed in significant research projects for NASA, AFRL, and DARPA.
29. At the request of the industry and FAA, an infrastructure was developed for formal software configuration management, code licensing and distribution, and user support for engine companies to employ DARWIN for official FAA and company purposes. This infrastructure includes a source code repository with revision management system; automated software verification procedures; a web site for Internet distribution of software, manuals, published papers, and information for prospective users; live user support; video tutorials; and bug-tracking software. The code is currently licensed by six different engine manufacturers and two foreign government laboratories. License fees collected by SwRI are exclusively used to enhance the DARWIN code for the benefit of engine manufacturers and the FAA.

## 9. REFERENCES.

1. "Aircraft Accident Report: United Airlines Flight 232, McDonnell Douglas DC-10-10, Sioux Gateway Airport, Sioux City, Iowa, July 19, 1989," National Transportation Safety Board, NTSB/AAR-90/06, 1990.
2. McClung, R.C., Lawless, B.H., Gorelik, M., Date, C., Gill, Y., and Piascik, R.S., "Fatigue Crack Growth of Titanium Rotor Alloys in Vacuum And Air," *Fatigue Behavior of Titanium Alloys*, TMS, pp. 211-218, 1999.
3. Chan, K.S., Perocchi, L., and Leverant, G.R., "Constitutive Properties of Hard Alpha Titanium," *Metallurgical and Materials Transactions A*, Vol. 31A, pp. 3029-3040, 2000.
4. Chan, K.S., "Constitutive Relations for Inelastic Deformation and Damage Accumulation in Hard Alpha Titanium," *ASME Transactions, Journal of Engineering Materials and Technology*, Vol. 123, pp. 281-286, 2001.
5. McKeighan, P.C., Perocchi, L.C., Nicholls, A.E., and McClung, R.C., "Characterizing the Cracking Behavior of Hard Alpha Defects in Rotor Grade Ti-6-4 Alloy," *Fatigue Behavior of Titanium Alloys*, TMS, pp. 349-356, 1999.
6. Wu, Y.-T., Enright, M.P., and Millwater, H.R., "Probabilistic Methods for Design Assessment of Reliability with Inspection," *AIAA Journal*, Vol. 40, pp. 937-946, 2002.
7. Leverant, G.R., McClung, R.C., Wu, Y.-T., Millwater, H.R., Riha, D.S., Enright, M.P., Chell, G.G., Chan, K.S., McKeighan, P.C., Gorelik, M., Fischer, C., Lehmann, D., Green, K., Bartos, J., Howard, N., and Srivatsa S., "Turbine Rotor Material Design," DOT/FAA/AR-00/64, Final Report to Federal Aviation Administration, Grant No. 95-G-041, 2000.
8. Sub-Team to the Aerospace Industries Association Rotor Integrity Sub-Committee, "The Development of Anomaly Distributions for Aircraft Engine Titanium Disk Alloys," *Proc. 38th AIAA/ASME/ASCE/AHS/ASC Structures, Structural Dynamics, and Materials Conference*, pp. 2543-2553, 1997.
9. McKeighan, P.C., Nicholls, A.E., Perocchi, L.C. and McClung, R.C., "Sensing Crack Nucleation and Growth in Hard Alpha Defects Embedded in Ti-6Al-4V Alloy," *Nontraditional Methods of Sensing Stress, Strain and Damage in Materials and Structures: Second Volume, ASTM STP 1323*, G.F. Lucas, P.C. McKeighan and J.S. Ransom, Eds., American Society for Testing and Materials, West Conshohocken, PA, 2001.
10. Li, S., Mear, M.E., and Xiao, L., "Symmetric Weak-Form Integral Equation Method for Three Dimensional Fracture Analysis," *Computer Methods in Applied Mechanics and Engineering*, Vol. 151, 435-539, 1998.
11. *NASGRO Reference Manual*, Version 4.1, NASA Johnson Space Center and Southwest Research Institute, 2003.

12. Ayyub, B.M., and Chia, C.-Y., "Generalized Conditional Expectation for Structural Reliability Assessment," *Structural Safety*, Vol. 11, pp. 131-146, 1992.
13. Melchers, R.E., *Structural Reliability Analysis and Prediction*, John Wiley & Sons, 2001.
14. Momin, F.N., Millwater, H.R., Osborn, R.W., and Enright, M.P., "Application of a Conditional Expectation Response Surface Approach to Probabilistic Fatigue," *Proc. 9th ASCE Specialty Conference on Probabilistic Mechanics and Structural Reliability*, ASCE Paper PMC2004-204, Albuquerque, New Mexico, 2004.
15. Momin, F.N., Millwater, H.R., Osborn, R.W., and Enright, M.P., "Applications of the Generalized Conditional Expectation Method for Enhancing a Probabilistic Fatigue Design Code," Paper AIAA-2005-2146, *Proc. 46th AIAA/ASME/ASCE/AHS/ASC Structures, Structural Dynamics, and Materials Conference, Non-Deterministic Approaches Forum*, Austin, Texas, 2005.
16. McClung, R.C., Enright, M.P., Millwater, H.R., Leverant, G.R., and Hudak, S.J., Jr., "A Software Framework for Probabilistic Fatigue Life Assessment of Gas Turbine Engine Rotors," *Journal of ASTM International*, Vol. 1, Paper JAI11563, 2004. Also published in *Probabilistic Aspects of Life Prediction, ASTM STP 1450*, W. S. Johnson and B. M. Hillberry, Eds., ASTM International, West Conshohocken, PA, 2004, pp. 199-215, 2004.
17. Hudak, S.J., Enright, M.P., McClung, R.C., Francis, W.L., and Millwater, H.R., "A Probabilistic Analysis of the Benefits of In-Service Fatigue Damage Monitoring for Turbine Engine Prognosis," Paper AIAA-2004-1953, *Proc. 45th AIAA/ASME/ASCE/AHS/ASC Structures, Structural Dynamics, and Materials Conference*, Palm Springs, California, 2004.
18. Enright, M.P., Hudak, S.J., Jr., McClung, R.C., and Millwater, H.R., "Probabilistic-Based System for Prognosis of Fatigue in Aircraft Engine Components," AIAA Paper 2003-8014, *Proc. 44th AIAA/ASME/ASCE/AHS/ASC Structures, Structural Dynamics, and Materials Conference*, Norfolk, Virginia, 2003.